PEOPLE'S DEMOCRATIC REPUBLIC OF ALGERIA
Ministry of Higher Education and Scientific Research
University of Amar Telidji - Laghouat

Faculty of Technology
Department of Electrical Engineering

PhD Thesis in Electrical Engineering
Discipline: Analysis and Control of Energy Systems and Electrical Systems
Option: Control Systems

BAROUD Zakaria

Modelling and Observation of PEM Fuel-Cell Systems:
Application to the Automobile Transport Field

Prof. **LEFKAIER Ibn Khaldoun**	*Chair*	University of Amar Telidji, Laghouat, Algeria
Prof. **BENALIA Atallah**	*Supervisor*	University of Amar Telidji, Laghouat, Algeria
Prof. **OCAMPO-MARTINEZ Carlos**	*Co-supervisor*	Universitat Polètecnica de Catalunya, Barcelona, Spain
Prof. **GUESMI Kamel**	*Examinator*	University of Ziane ACHOUR, Djelfa, Algeria
Prof. **BOUKHETALA Djamel**	*Examinator*	National Polytechnic School, Algiers, Algeria
Prof. **AMEUR Aissa**	*Examinator*	University of Amar Telidji, Laghouat, Algeria

2017-2018

To my parents

To my brothers & sisters

To the memory of my lovely nephew khalil

Acknowledgements

First and foremost, I offer my respect and sincere gratitude to my advisor, **Prof. BENALIA Atallah**, whose encouragement and patience, as well as academic experience, have been very helpful to me. I appreciate his vast expertise and knowledge in many areas. I would also like to express my respect and sincere gratitude to my co-advisor, **Prof. OCAMPO-MARTINEZ Carlos** from *Institut de Robòtica i Informàtica Industrial (CSIC-UPC), Universitat Politècnica de Catalunya*, for his suggestions and collaboration during the course of my studies.

Besides my advisors, I wish to express my profound thanks to my doctoral committee: **Prof. LEFKAIER Ibn khaldoun**, **Prof. GUESMI Kamel**, **Prof. BOUKHETALA Djamel**, and **Prof. AMEUR Aissa** for their insightful comments and valuable efforts. Great thanks to my colleague **BOUGRINE Mohamed** for engaging in many productive discussions and his valuable suggestions.

The support and encouragement of my colleagues at **LACoSERE laboratory** have been indispensable, and I would like to express my appreciation to all of them (especially to **BENMILOUD Mohammed**, **BOUGRINE Mohamed**, **GAZZAM Noureddine** & **AMEUR Iyad**). I very much enjoyed exchange of ideas and thoughts, and all the fun moments together.

And finally, I would like to extend my deepest gratitude to my beloved parents, who have been a constant source of emotional, moral and financial support throughout my life. I must not forget to thank my brothers & sisters for encouragement and love during the different stages of my research.

BAROUD

Laghouat, July 2, 2018

مُلَـــخَّص

فِي الوقت الحاضر، تُعتبرُ خليّة الوقود ذات غشاء التّبادل البروتوني (PEMFC) واحدة من أكثر البدائل كفاءة لإنتاجِ طاقة صديقة للبيئة. خلايا الوقود ذات غشاء التّبادل البروتوني هي أجهزة كهروكيميائية تنتج الكهرباء، الماء و الحرارة باستخدام الهيدروجين و الأوكسجين. إضافة إلى ذلك، تمتلك خلايا الوقود الهيدروجينية مزايا عديدة و متعددة: كالكفاءة العالية، الوزن المنخفض، التلوث المنعدم و درجة تشغيل حرارية منخفضة مقارنة بأجهزة توليد طاقة أخرى. أمَّا بالنسبة لتطبيقاتها، فإنها تستعمل في مجالات واسعة، كتشغيل الحافلات و السيارات و توليد الطاقة الكهربائية على مستوى البنوك و المستشفيات في حالة إنقطاع التيّار الكهربائي. يُعتبَر التّحكم في خلايا الوقود، من خلال توفير التّدفق اللاّزم و الكافي للهيدروجين و الأوكسجين لها، واحدًا من أهمِّ الجوانب التي يعمل الباحثون على تطويرها و تحسينها.

يهتّم الجزء الأول من الأطروحة بالتّحكم في نظام إمداد الهواء لخلايا الوقود. الهدف من التّحكم هو التّنظيم السّريع والفعّال للأوكسجين المستنزف في قناة الكاثود من أجل تجنُّبِ كلاًّ من ظاهِرَتيْ النَّقص الفادح و الفَرْط الزَّائد في الأوكسجين. لقد تمّ معالجة هذه المشكلة باستخدام إستراتيجيتيْ تحكم. الإستراتيجيَّة الأولى، معروفة باسم التَّحكم الغامض الهجين، والتّي بدورها تتشكل من معدِّلَيْن جزئيَيْن: معدّل غامض (FLC) ، معدّل (PID) مضبوط ذاتيًا. أمَّا الإستراتيجية الثانيَّة، معروفة باسم التَّحكم باستخدام وضع الإنزلاق (SMC) . تمَّ التَّحقق من أداء خلايا الوقود مع هذيْن المعدليْن من خلال محاكاة حاسوبيَّة بإستعمال ماتلاب. إلا أنَّ، مهمّة التّحكم ليست متاحة لأن كِلا الإستراتيجيتيْن تتطلَّبانِ معرفة القِيمة الدَّقيقة لنسبة الأوكسجين داخل خلايا الوقود، وهذا يعني أنه يجب إستخدام المزيد من الأجهزة لقياس نسبة الأوكسجين داخل الخلايا ممَّا يعني زيادة تعقيد النِّظام الكُلي من جهة وزيادة التكلفة من جهة أخرى.

قدَّم الجزء الثَّاني من الأطروحة إستراتيجيَّة تحكم تستند إلى الملاحظة (Observability) (أيْ حساب نسبة الأوكسجين داخل قناة الكاثود)، تعتمد هذه الإستراتيجيَّة على تقنية التَّفاضل الجبْرِي لحساب نسبة الأوكسجين وتقنية التَّحكم المتزحلق للمحافظة على نسبة الأوكسجين المُثْلى مهما كانت ظروف عمل خلايا الوقود. تمّ تحليل أداء هذه الإستراتيجيَّة من خلال عمليات محاكاة باستخدام الحاسوب. أظهرت النَّتائج أن الإسترتيجيَّة المقترحة قدَّرتْ و عدّلت في وقت متهِي و بشكل صحيح نسبة الأوكسجين في قناة الكاثود.

الكلمـــات المفتاحيـــة:
خلايا الوقود ذات غشاء التَّبادل البروتوني، نسبة الأوكسجين، التَّحكم الغامض، التَّحكم باستخدام وضع الإنزلاق، الملاحظ الجبري، التَّفاضل العددي.

Abstract

Nowadays, the Proton Exchange Membrane Fuel Cell (PEMFC) are considered as one of the most efficient solutions for energy production to face both serious environmental pollution and energy crisis around the world. PEMFC are electrochemical devices that produce electricity, water, and heat from hydrogen and oxygen. Moreover, the PEMFC, also called Solid Polymer Fuel Cell (SPFC), are used in a wide range of applications, with advantages such as high efficiency, low weight, low pollution and low operation temperature, features that allow fast starting times in the PEMFC systems. However, for applications that require the tracking of rapid load changes, such as transport applications, the PEMFC must be able to follow rapid load changes and also able to be adapted to varying operating conditions. As a result, advanced control strategies must be integrated to ensure that the flows entering the PEMFC stack are sufficient and well-conditioned.

The first contribution of thesis is interested in the control of the PEMFC air supply system. The control objective is to regulate fast and efficiently the oxygen depleted in the cathode channel in order to avoid both oxygen starvation and saturation phenomena. This problem has been addressed using two controllers. The first control strategy, known as hybrid fuzzy PID control, is separated into three parts: fuzzy control, fuzzy-based self-tuned PID control, and fuzzy selector. The second control strategy, known as Second-Order Sliding-Mode (SOSM) twisting control, used an off-line tuning procedure to tune the controller parameters. Their performances are validated through extensive computer simulations. However, this is a challenging task because both two control strategies require knowing the exact value of Oxygen Excess Ratio (OER), which depends on internal variables such as the air pressure in the supply manifold and the partial pressures of both oxygen and nitrogen in the cathode. This means they should be used further sensors for measurements that increase both the overall system complexity and the cost while decreasing the efficiency of the fuel-cell system. Therefore, observers using only the measurements of available states become a cheaper and attractive solution.

The second contribution of thesis presented an algebraic-observer-based output-feedback controller, which is based on both algebraic differentiation and sliding-mode control approaches. At first, an algebraic estimation approach is used to reconstruct the OER based on a robust differentiation method. Then, the SOSM twisting controller presented in the first part of the thesis was adopted. The performance of the proposed algebraic-observer-based output-feedback controller is analyzed through simulations. Results show that the proposed approach properly estimates and regulates the OER in finite time.

Keywords:

PEM Fuel-Cell systems, Oxygen Excess Ratio (OER), Fuzzy-Logic control, Second-Order Sliding-Mode, twisting algorithm, algebraic observer, numerical differentiation.

Résumé

Aujourd'hui, les piles à combustible du type PEM (Membrane Échangeuse de Protons) sont présentées comme l'une des solutions les plus efficaces pour la production d'énergie propre, ceci serait une solution à moyen et long terme pour le problème de la pollution environnementale et à la crise énergétique mondiale. La pile à combustible est un dispositif électrochimique qui produit de l'électricité, de l'eau et de la chaleur à partir d'une simple combinaison entre l'hydrogène et l'oxygène. De plus, les piles à combustible du type PEM, également appelées piles à combustible à polymère solide, sont utilisées dans de nombreuses applications, avec des avantages tels qu'un rendement élevé, forte densité d'energie et de puissance, une faible pollution et une faible température de fonctionnement, qui permettent des démarrages rapides dans les systèmes piles à combustible. Cependant, pour les applications qui nécessitant le suivi de changements de charge rapides, tels que les applications de transport, la pile à combustible doit pouvoir suivre les changements de charge rapides et aussi être capable de s'adapter aux conditions de fonctionnement variables. En conséquence, des stratégies de contrôle avancées doivent être intégrées, via des systèmes auxiliaires, pour s'assurer que les flux entrant dans la pile sont suffisants et bien conditionnés.

La première contribution de la thèse s'intéresse au contrôle du système d'alimentation en air dans la pile à combustible. L'objectif du contrôle est de réguler rapidement et efficacement l'oxygène consommé dans le canal cathodique afin d'éviter à la fois les phénomènes de manque et de saturation d'oxygène. Ce problème a été résolu en utilisant deux stratégies de contrôle. La première stratégie de contrôle, appelée contrôle hybride PID-flou, est séparée en trois parties: contrôle flou, contrôle PID auto-ajusté basé sur la logique floue et un sélecteur flou. La deuxième stratégie de contrôle, connue sous le nom de SOSM twisting contrôle, utilise une procédure d'ajustement hors ligne pour régler les paramètres du contrôleur. Leurs performances sont validées par de nombreuses simulations. Néanmoins, ceci est une tâche difficile car les deux stratégies de contrôle nécessitent de connaître la valeur exacte du rapport d'excès d'oxygène (OER), qui dépend de variables internes. Cela signifie qu'ils devraient utiliser d'autres capteurs pour les mesures qui augmentent à la fois la complexité globale du système et le coût, tout en diminuant l'efficacité du système pile à combustible. Par conséquent, les observateurs utilisant uniquement les mesures des états disponibles deviennent une solution moins chère et attrayante.

La deuxième contribution de la thèse propose un observateur algébrique et un contrôleur par retour de sortie, basé sur des approches de différenciation algébrique et de mode glissant. Dans un premier temps, une approche d'estimation algébrique est utilisée pour reconstruire l'OER sur la base d'une méthode de différenciation robuste. L'observateur proposé est connu par sa convergence en temps fini et son faible temps de calcul par rapport aux autres observateurs présentés dans la littérature. Ensuite, le SOSM twisting contrôle présenté dans la première partie de la thèse a été adopté. Les performances de cette commande, basé sur l'observateur algébrique, sont analysées par des simulations. Les résultats montrent que l'approche proposée estime et régule correctement l'OER en temps fini.

Mots-clés:

Système pile à combustible, rapport d'excés d'oxygène, commande par logique floue, commande par mode glissant d'ordre deux, algorithme de twisting, observateur algébrique, differentiation numérique.

Contents

Abstract **ii**

List of Figures **vi**

List of Tables **viii**

Nomenclature **x**

General Introduction **1**

1 Fuel-Cell Systems: An Overview **7**

1.1 Introduction . . . 7
1.2 Fuel-cell history: 1839 to today . . . 7
1.3 Advantages and disadvantages of fuel-cell systems . . . 11
1.4 Types of fuel cells . . . 12
1.5 Fuel-cell applications . . . 12
1.5.1 Transportation applications . . . 14
1.5.2 Stationary applications . . . 15
1.5.3 Portable applications . . . 15
1.6 Proton exchange membrane fuel cells . . . 15
1.7 PEMFC systems for automobile . . . 18
1.8 PEM fuel-cell structure . . . 18
1.9 Fuel-cell system . . . 20
1.9.1 Air supply . . . 20
1.9.2 Hydrogen supply . . . 21
1.9.3 Heat and temperature . . . 21
1.9.4 Water management . . . 21
1.9.5 Power management . . . 22
1.9.6 Control . . . 22
1.10 Control challenges . . . 22
1.10.1 Air supply control . . . 22
1.10.2 Hydrogen supply control . . . 23
1.10.3 Water and heat management . . . 23

1.10.4 Membrane degradation . . . 24
1.11 Summary . . . 24

2 PEMFC Air Supply System Model **25**
2.1 Introduction . . . 25
2.2 Review on fuel-cell system modelling . . . 25
2.3 PEMFC steady-state model . . . 27
2.3.1 Nernst open circuit voltage . . . 28
2.3.2 Activation loss . . . 30
2.3.3 Ohmic loss . . . 30
2.3.4 Concentration loss . . . 31
2.3.5 Fuel-cell terminal voltage . . . 31
2.4 PEMFC air supply dynamic model . . . 33
2.4.1 Air compressor model . . . 33
2.4.2 Supply manifold model . . . 35
2.4.3 Cathode flow model . . . 36
2.5 Dynamic model with four states . . . 38
2.5.1 System inputs and outputs . . . 38
2.5.2 System performances . . . 39
2.6 Steady-state analysis . . . 39
2.7 Dynamic simulation . . . 40
2.8 Summary . . . 43

3 Advanced Control Strategies for PEMFC Air Supply Systems **44**
3.1 Introduction . . . 44
3.2 Control problem formulation . . . 45
3.3 Review on PEMFC air supply system control . . . 46
3.4 Hybrid fuzzy PID controller design . . . 47
3.4.1 PID controller . . . 47
3.4.2 Fuzzy Logic controller . . . 48
3.4.3 Fuzzy-based Self-Tuned PID controller . . . 50
3.5 HFPID controller simulation results . . . 55
3.5.1 Performance results . . . 55
3.5.2 Sensibility analysis . . . 60
3.5.3 Comparative study . . . 60
3.6 Twisting controller design . . . 61
3.7 Twisting controller simulation results . . . 64
3.7.1 Performance results . . . 65
3.7.2 Comparative study . . . 66
3.8 Summary . . . 66

4 Observer-Based Output-Feedback Control for PEMFC Air Supply Systems **67**
4.1 Introduction . . . 67
4.2 Review on PEMFC system observation . . . 68
4.3 Problem statement . . . 69
4.4 Algebraic observer design . . . 70
4.4.1 Algebraic observability . . . 70
4.4.2 Numerical differentiator . . . 71
4.5 Observer-based output-feedback control for PEM-FC air supply system . . . 72
4.6 Simulation results . . . 73
4.6.1 Test 1. Nominal performance . . . 74
4.6.2 Test 2. Parameters uncertainties . . . 76
4.6.3 Test 3. Noise rejection . . . 78
4.6.4 Test 4. Comparative results . . . 79
4.7 Summary . . . 81

Concluding Remarks **82**

A PEMFC System Model Parameters **84**
A.1 PEMFC steady-state model parameters . . . 84
A.2 Dynamic model parameters . . . 86

References **88**

List of Figures

1.1 William Robert Grove and his gas voltaic battery diagram [Fuel Cell Norway ANS., 2006]. 8
1.2 Francis T. Bacon and his fuel-cell prototype [Spiegel, 2017]. 8
1.3 PEMFCs being installed in a Gemini 7 spacecraft [FuelCellToday., 2017a]. 9
1.4 The alkaline fuel-cell system as used on the space shuttles [FuelCellToday., 2017a]. 9
1.5 Fuel-cell vehicles. 10
1.6 Fuel-cell different applications. 14
1.7 Illustration of PEMFC principle [Spiegel, 2011]. 16
1.8 Fuel-cell polarization curve for 353.15 K. 17
1.9 Fuel-cell structure [Pukrushpan et al., 2002b], ... 18
1.10 Fuel-cell system architecture including the different sub-processes [Pukrushpan et al., 2004c], 20

2.1 Voltage drops due to different types of losses in fuel cell, ... 32
2.2 Fuel-cell system scheme. 34
2.3 z_2 performance curve for different stack currents. 40
2.4 Static feedforward control for fuel-cell system. 41
2.5 Dynamic simulation results of the fuel-cell system model for a series of input stack-current changes. 42

3.1 Model setup scheme. 45
3.2 Structure of PID controller. 48
3.3 Structure of fuzzy controller. 49
3.4 Membership functions of the FLC. 50
3.5 Fuzzy self-tuning PID controller structure. 50
3.6 Structure of the fuzzy tuner. 51
3.7 Membership functions of fuzzy tuner. 52
3.8 Proposed hybrid fuzzy PID controller structure. 53
3.9 Membership functions of the fuzzy supervisor. 54
3.10 Stack-current variation. 56
3.11 Response of OER for different control strategies. 56
3.12 Stack-voltage variation for different control strategies. 56
3.13 Zoomed plot of OER variations. 57
3.14 Regulation of OER with changing reference. 58

3.15 Control signal components. 59
3.16 Output of the fuzzy supervisor. 59
3.17 Sensibility analysis. 60
3.18 Comparative study. 61
3.19 SOSM twisting control system. 62
3.20 Performance results: Twisting controller. 65
3.21 Response of OER for Twisting and HFDPID controllers. 66

4.1 Algebraic observer-based output-feedback control for PEMFC air supply system. 73
4.2 Stack-current variation. 75
4.3 Test 1: Performance results. 76
4.4 Test 2: Parameters uncertainties. 78
4.5 Test 3: Noise rejection. 79
4.6 Test 4: Comparative results. 81

List of Tables

1.1 Summary of fuel-cell types [Spiegel, 2011] 13
1.2 Summary of PEMFC components [Spiegel, 2011, Gold, 2017] 19

2.1 Change in Gibbs free energy of hydrogen fuel-cell at various temperatures [Larminie et al., 2003] 29

3.1 Linear rule base for FLC. 49
3.2 Fuzzy rules for FSTPID -proportional action- 52
3.3 Fuzzy rules for FSTPID -integral action- 52
3.4 Fuzzy rules for FSTPID -deravative action- 52
3.5 Linear rule base for fuzzy supervisor 54
3.6 Performance index comparison and time-domain specifications. 58

4.1 Variation of system parameters 76

A.1 Steady-state model parameters 85
A.2 Constants of the PEMFC system model 86
A.3 Dynamic model parameters 87

Nomenclature

Abbreviations

AFC	Alkaline Fuel Cell
APCWREF	Adaptive Predictive Control with Robust Filter
CHP	Combined Heat and Power
DMFC	Direct Methanol Fuel Cell
FCHV	Fuel-Cell Hybrid Vehicle
FL	Fuzzy Logic
FSTPID	Fuzzy-based Self-Tuned PID
HFPID	Hybrid Fuzzy PID
HIL	Hardware in the Loop
IAE	Integral Absolute Error
ICE	Internal Combustion Engine
IFC	International Fuel Cells
ISE	Integral Squared Error
ITAE	Integral Time-weighted Absolute Error
KF	Kalman Filter
LPV	Linear Parameter-Varying
LQR	Linear Quadratic Regulator
MCFC	Molten Carbonate Fuel Cell
MEA	Membrane Electrode Assembly
OER	Oxygen Excess Ratio
PAFC	Phosphoric Acid Fuel Cell
PID	ProportionalIntegralDerivative
PEMFC	Proton Exchange Membrane Fuel Cell
SOFC	Solid Oxyde Fuel Cell
SOSM	Second-Order Sliding-Mode

Subscripts

act	activation
a	air
ca	cathode
cp	compressor
cm	compressor-motor
conc	concentration
d	derivative
D	discharge
ff	feed-forward
H_2	hydrogen
in	inlet
i	integral
max	maximum
m	membrane
net	net
N_2	nitrogen
ohm	ohmic
out	outlet
opt	optimal
O_2	oxygen
p	proportional
rct	reacted
sat	saturation
st	stack
v	vapour
H_2O	water vapour

General Introduction

The development of new clean energies is a major challenge of the 21^{st} century, on one hand, to face environmental issues and, on the other hand, to have alternatives to fossil fuels. Among these, hydrogen is considered as one of the best alternative to fossil fuels due to potential for zero local pollution and its high net energy density[1]. Fuel cells using hydrogen can be deployed in many areas such as transport, portable and stationary applications because of high efficiency, compactness, and reliability [Fergus et al., 2016, Bagotsky, 2012]. Fuel cells are electrochemical devices that convert the chemical energy of the fuel directly into electricity, heat and water [Ehsani et al., 2017].

Fuel cells can be used for many transportation applications including automobiles, buses, scooters and bicycles. Compared to Internal Combustion Engine (ICE) technology, the fuel cells offer a more pleasant driving behaviour and provide a higher efficiency. At a nominal driving speed (48.28 km/h), the efficiency of a fuel-cell system using direct hydrogen from natural gas is more efficient than that of a conventional ICE [Suh, 2006]. The fuel type most often used is compressed hydrogen. The most common type of fuel cell used for transport applications are the Proton Exchange Membrane Fuel Cells (PEMFC). This is due to their low temperature of operation (typically 333.15-353.15 K), which allows fast startup. Moreover, these fuel cells have high power density, small volume, solid electrolyte, long life, as well as low corrosion [Barbir, 2012]. In addition, the fuel cells can produce power continuously and this makes it more efficient also than a battery [O'hayre et al., 2016]. However, there are still many problems to be solved before considering their development and commercialization on large scale so far. The topic of this thesis deals with the control problem within the fuel-cell system vehicles in order to improve its lifetime and increase its efficiency.

In fact, fuel-cell systems are complex devices, they are including five main interconnected sub-processes: air supply sub-process to the cathode, hydrogen supply sub-process

[1]Net energy density (including average engine/motor efficiency) for diesel is 3.2 kWh/kg, for gasoline 2.8 kWh/kg and hydrogen 2.0 kWh/kg [Suh, 2006].

to the anode, heat and temperature sub-process, water management sub-process, and power management sub-process. For applications that require the tracking of rapid load changes, such as transport applications, the PEMFC must be able to follow rapid load changes and also able to adapt with varying operating conditions. Thus, perfect controllers must be integrated, via a series of actuators auxiliary systems, to ensure that the flows entering the PEMFC stack are sufficient and well-conditioned, without overlook maintaining the desired operating temperature.

Whereas this thesis focuses on the PEMFC air supply system control, which has a great influence on the whole system efficiency. Indeed, one of the most important challenges in PEMFC system control is to ensure sufficient amount of oxygen in the cathode, (i.e. avoid *oxygen starvation and saturation* phenomena), when current is suddenly drawn from the fuel-cell stack. The PEMFC air supply system is generally composed of a motor and compressor, which supplies air to the cathode. Furthermore, the compressor consumes the most power which can reach 20 % of the power provided by the fuel-cell system [Pukrushpan et al., 2004c]. Given these facts, the control of the compressor-motor is needed. The first aim of this thesis is to develop a control system on one hand to optimize the net power provided by the fuel-cell system by forcing the Oxygen Excess Ratio (OER) to its optimum value, and on the other hand, to protect the fuel-cell system.

Nevertheless, the control of the compressor-motor requires the knowledge of the precise value of OER. Unfortunately, it depends on internal variables such as the partial pressures of oxygen and nitrogen in the cathode channel and the air pressure in the supply manifold. This means they should be measured by using extra sensors that increase both the cost and the overall system complexity while decrease the accuracy of the PEMFC system. For these reasons, the second aim of this thesis is to design a sensorless control in order to estimate and regulate the OER within the PEMFC system.

Next, the main developed results in control and observation design for the PEMFC air supply system will be presented.

Developed results

This thesis is interested in the energy optimization and the protection of the PEMFC system.

The main scientific contributions of this thesis include:

- A Hybrid Fuzzy-PID (HFPID) controller is designed to regulate the OER during fast current transitions. The proposed strategy is separated into three parts: fuzzy-logic

control, fuzzy-based self-tuned PID control and fuzzy supervisor. The fuzzy supervisor is used to switch the control model between fuzzy-based self-tuned PID and fuzzy logic controllers. This control system has good response time and robustness.

- An algebraic observer-based output feedback controller has been designed for regulating the OER of a PEMFC air supply system at an optimal setpoint value. The algebraic observer design provides a finite-time converging OER reconstruction based on a robust differentiation method. The proposed controller, which uses the estimated OER, is based on one of the Second-Order Sliding-Mode (SOSM) variety algorithms. In this thesis, a twisting algorithm is adopted, which is depending only on few parameters. These parameters were calculated during an off-line tuning procedure.

  These contributions can be adapted and extended for other hybrid power systems, which consist of a renewable energy source, a fast-dynamic energy storage system and a long-term energy storage system.

Thesis Overview

The thesis is divided into four chapters:

- **Chapter 1** presents an overview of the basic principles of fuel cells and fuel-cell systems in order to clarify the structural notions of thesis main topic study. First, it shows a brief history of the discovery and evolution of fuel cells, as well as different types of fuel-cell systems. Second, the chapter provides a detailed description of the fuel-cell system in order to understand its operation. Finally, a literature review of the principal control challenges within the PEMFC systems, such as air supply control, hydrogen supply control, water and temperature management, and membrane degradation is discussed to make our contribution as clear as possible.

- **Chapter 2** presents a summary review on fuel-cell system modelling. Then, a presentation of a PEMFC steady-state model is given. This model is useful for calculating the PEMFC stack voltage. Then, a presentation of a reduced dynamic model is done. Finally, both steady-state and dynamic analysis of the PEMFC system is performed in order to define the optimal value of the air flow setpoint, termed OER, that results in the maximum net power. It is important to note that the dynamic model presented in this chapter is used as a base model in the other chapters of this thesis.

- **Chapter 3** gives a brief survey of existing control methods for PEMFC air supply system. Next, this chapter presents two controllers in order to regulate the OER during

fast current transitions and uncertainties in the system parameters. The first proposed control strategy, known as hybrid fuzzy PID control, separated into three parts: fuzzy control, fuzzy-based self-tuned PID control and fuzzy supervisor. The second proposed control strategy, known as SOSM twisting control, used an off-line tuning procedure to tune the twisting controller parameters. Then, the designed control strategies are applied to the model of the PEMFC air supply system and the simulation results for stack-current changes, model uncertainties, and comparative study are presented. At the end of this chapter, a comparative study of both two controllers performances is presented.

- **Chapter 4** provides a brief review on PEMFC air supply system observation. Following, this chapter presents an algebraic observer-based output feedback controller for regulating the OER of a PEMFC air supply system at an optimal setpoint value. At first, an algebraic estimation approach is used to reconstruct the OER through estimation of their relevant states in real time, from the measurement of the supply manifold air pressure, based on a robust differentiation method. Then, the SOSM twisting controller presented in Chapter 3 is adopted to control the estimated OER. The performance of the proposed algebraic-observer based output-feedback controller is analyzed through simulations for different stack-current variations, for parameter uncertainties, and for noise rejection. Results are shown that the proposed approach properly estimates and regulates in finite time the OER.

The concluding remarks and the perspectives of this work are finally presented.

Scientific Publications

Journal papers

- **Z. Baroud**, A. Benalia, C. Ocampo-Martinez (**2018**) "Robust Fuzzy Sliding Mode Control For Air Supply on PEM Fuel Cell System", in: *International Journal of Modelling, Identification and Control*, Vol.29, No. 4, **2018**, pp.341–351.

- **Z. Baroud**, M. Benmiloud, A. Benalia, C. Ocampo-Martinez (**2017**) "Novel hybrid fuzzy-PID control scheme for air supply in PEM fuel-cell-based systems", in: *International Journal of Hydrogen Energy*, 42 (15), **2017**, pp.10435–10447.

- **Z. Baroud**, A. Benalia, C. Ocampo-Martinez (**2016**) "Air flow regulation in fuel cells: An efficient design of hybrid fuzzy-PID control", in: *Electrotehnica, Electronica, Automatica (EEA)*, 64 (4) (**2016**) pp.28–32.

International conference papers

- **Z. Baroud**, A. Benalia, C. Ocampo-Martinez (**2017**) "Nonlinear Observer Design for PEM Fuel-Cell Systems using First-Order Sliding Mode Techniques", in: *The IEEE International Conference on Automatic Control, Telecommunications and Signals (ICATS)*, **2017**, Annaba, Algeria.

- **Z. Baroud**, N. Gazzam, A. Benalia, C. Ocampo-Martinez (**2016**) "Algebraic Observer Design for PEM Fuel Cell System", in: *The IEEE International Conference on Modelling, Identification and Control (ICMIC)*, **2016**, Algiers, Algeria.

- **Z. Baroud**, M. Benmiloud, A. Benalia (**2015**) "Fuzzy self-tuning PID controller for air supply on a PEM fuel cell system", in: *The IEEE International Conference on Electrical Engineering (ICEE)*, **2015**, Boumerdes, Algeria.

- **Z. Baroud**, M. Benmiloud, A. Benalia (**2015**) "Sliding mode controller for breathing subsystem on a PEM fuel cell system", in: *The IEEE International Conference on Control and Engineering Information Technology (CEIT)*, **2015**, Tlemcen, Algeria.

- **Z. Baroud**, M. Benmiloud, A. Benalia (**2015**) "Modelling and Analysis of Proton Exchange Membrane Fuel Cell System", in: *The International Conference on Information Processing and Electrical Engineering (ICIPEE)*, **2015**, Tebessa, Algeria.

- **Z. Baroud**, A. Benalia (**2014**) "Dynamic Modeling of PEM Fuel Cell Dedicated for transport application", in: *The 3rd International Seminar on New and Renewable Energies (SIENR)*, **2014**, Ghardaia, Algeria.
- **Z. Baroud**, A. Benalia (**2014**) "Steady-State Modeling and Performance Analysis of PEM Fuel Cell System", in: *The First Day of Automatic Theory and its Applications (JEAA)*, **2014**, Laghouat, Algeria.

Chapter 1

Fuel-Cell Systems: An Overview

> *“ The greatest truth is honesty, and the greatest falsehood is dishonesty. ”*
>
> Abu Bakr

1.1 Introduction

The purpose of this chapter is to present an overview on the basic principles of fuel cells and fuel-cell systems in order to clarify the structural notions of thesis main topic study. First, it presents a concise history of the discovery and evolution of fuel cells, as well as different types of fuel-cell systems. Second, the chapter provides a detailed description of the fuel-cell system in order to understand its operation. Finally, a literature review of the principal control challenges within the PEMFC system, including water and temperature management, energy optimization, and system degradation is discussed to make thesis contribution as clear as possible.

1.2 Fuel-cell history: 1839 to today

As early as 1839, Sir William Grove (often referred to as the ”Father of the Fuel Cell”) was discovered the fuel-cell principle. He conducted a series of experiments which ultimately proved that electric current could be produced from an electrochemical reaction between hydrogen and oxygen using pairs of platinum electrodes (Figure 1.1(b)) half immersed in sulfuric acid and half enclosed in oxygen and hydrogen [Larminie et al., 2003]. The actual term fuel cell was first used in 1889 by Ludwig Mond and Charles Langer, who attempted to make a working fuel cell using air and coal gas [Vielstich et al., 2009].

(a) Sir William Grove (1811-1896)

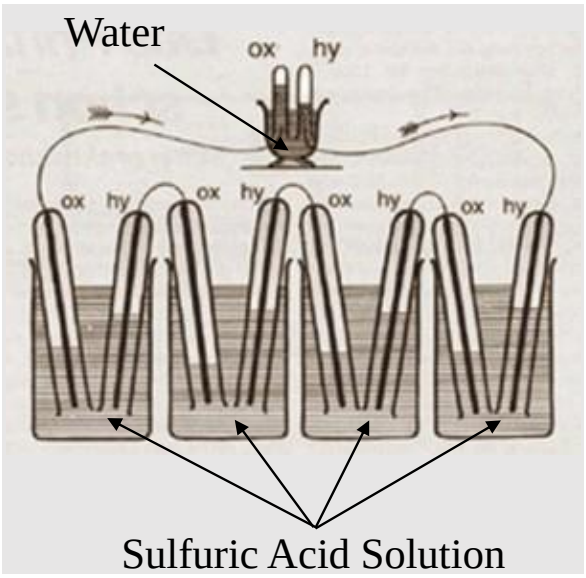

(b) Fuel-cell principle

Figure 1.1: William Robert Grove and his gas voltaic battery diagram [Fuel Cell Norway ANS., 2006].

In 1932, engineer Francis T. Bacon modified Mond's and Langer's equipment to develop the first hydrogen-oxygen cell using non-corrosive alkaline electrolytes and inexpensive nickel electrodes to the catalysts. But, it was not until 1959 that Bacon demonstrated a five-kilowatt alkaline fuel cell (Figure 1.2) that could power a welding machine [FuelCellToday., 2017a].

Figure 1.2: Francis T. Bacon and his fuel-cell prototype [Spiegel, 2017].

During the early 1960s NASA, in collaboration with General Electric, developed Bacon fuel-cell prototype for use on space missions. The researcher Willard Thomas Grubb at General Electric had credited with the invention of the first PEMFC. Grubb's PEMFC using platinum as a catalyst on the membranes. This fuel cell (Figure 1.3) was further developed in cooperation with NASA, and was used in the Gemini space programme of the mid-1960s [FuelCellToday., 2017a].

International Fuel-Cells (IFC) developed a 1.5 kW Alkaline Fuel Cell (AFC), as shown in (Figure 1.4), for use in the Apollo space missions in 1968. The fuel cell provided electrical power as well as drinking water for the crew. IFC subsequently developed a 12 kW AFC, used to give onboard power on all space shuttle flights [UniversityofCambridge., 2018].

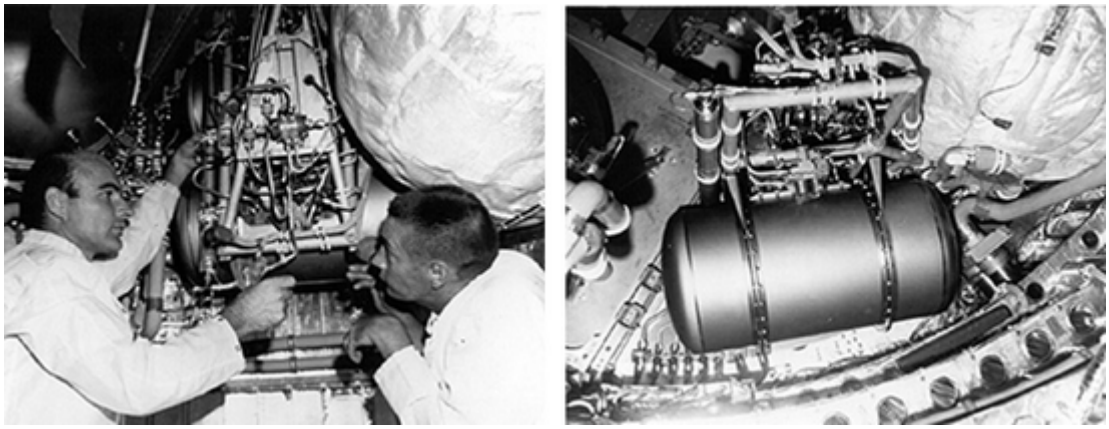

Figure 1.3: PEMFCs being installed in a Gemini 7 spacecraft [FuelCellToday., 2017a].

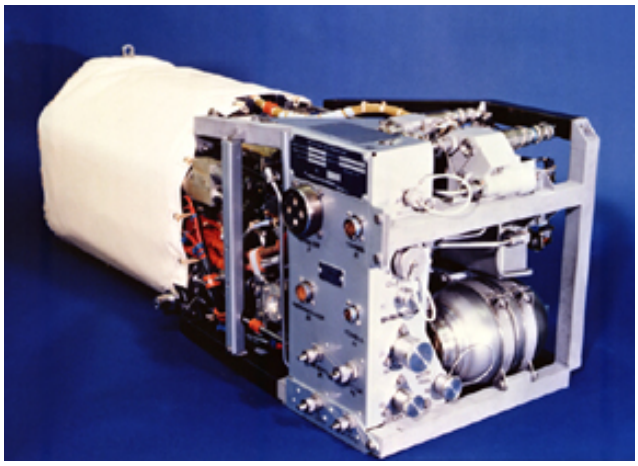

Figure 1.4: The alkaline fuel-cell system as used on the space shuttles [FuelCellToday., 2017a].

In 1970s, the oil crisis and air pollution prompt governments, businesses and consumers to develop alternative energy including fuel cells. These problems accelerated searches in the united states than in Europe and Japan. The researches carried out during this period will be essentially basic and will aim to develop and improve the various components of the fuel cell. In 1970, Du Pont developed the Nafion membrane, which serves the electrolyte of the PEMFCs.

In 1980s, the US Navy used fuel-cell technology for some submarines. Where highly efficient, zero-emission, near-silent running offered considerable operational advantages. In spite of some successes, fuel cells are still considered costly, of short life with a volume and a weight too large to be inserted in a vehicle. In 1983 the Canadian company Ballard started working on the development of PEMFCs, and was poised to become a major player in the manufacture of stacks and systems for stationary and transport applications in later years. In 1986, the company developed the first Ballard fuel-cell stack operating on pressurized air.

Figure 1.5: Fuel-cell vehicles.

From the 1990s to the early 2000s, attention turned particularly to PEMFC and Solid Oxid Fuel Cell (SOFC) technology. In 1993, First fuel-cell bus presented by Ballard in Vancouver, Canada. In 1994, Daimler-Benz designed the first vehicle (NeCar 1) in Europe featuring fuel cell. Fuel-cell stack used was from Ballard Power Systems company, had power of 50 kW. Honda has manufactured its FCX Concept vehicle utilizing a 100 kW hydrogen fuel cell, which started road testing in Japan in 2002. Similarly, both Toyota and Nissan have been developing vehicles with hybrid fuel-cell power system, some of which have been evaluated on north american roads (Figure 1.5) [FuelCellToday., 2017b].

These are only a few examples of the many fuel-cell vehicles under development and/or evaluation in recent years. As prices continue to drop on fuel cell technology and hydrogen becomes more available, expect to see fuel-cell energy replace traditional power sources in coming years from micro fuel cells to be used in cell phones to high-powered fuel cells for transport and stationary applications.

1.3 Advantages and disadvantages of fuel-cell systems

The main advantages of fuel-cell systems are as follows [Rabbani, 2013]:

- High energy efficiency compared with other energy conversion devices. The fuel-cell efficiency varies between 40 % and 70 % without taking into account the system auxiliaries (pumps, heat exchanger, compressor, humidifier and converter) that reduce these values.

- Various operating temperatures. fuel cells have a wide operating temperature range depending on their types. This makes it possible to cover several areas of applications. For example, low-temperature fuel cells are used for portable applications that do not need the heat produced. On the other hand, high temperature fuel cells are more suitable for stationary applications where the heat generated is used to hot the water.

- No pollutants produced. Fuel cells working on pure hydrogen produce nothing, while those using methanol or ethanol produce small amounts of CO_2, CH_4 and CO.

- Fuel cells are silent during operation. Only certain components such as compressors, pumps and the ventilation system produce a slight noise.

- Fuel cells are low maintenance because they have no moving parts.
- Fuel cells do not need to be recharged, and they provide power instantly when supplied with fuel.

Some disadvantages of fuel-cell systems include the following:

- Fuel cells are currently costly due to the need for materials with specific properties. There is an issue with finding low-cost replacements. This includes the need for platinum and Nafion material.
- Short life of the fuel-cell components, especially the membrane. At present, the life of the PEMFC for transport applications is generally limited to a few thousand hours (between 3000 h and 5000 h for cars) [Haddad, 2009].
- Fuel reformation technology can be costly, heavy and needs power in order to run.
- If another fuel besides hydrogen is fed into the fuel cell, the performance gradually decreases over time due to catalyst degradation and electrolyte poisoning.

1.4 Types of fuel cells

There are many fuel-cell types, classified mainly by the type of materials used for the electrolyte. The principal ones include the Alkaline Fuel Cell (AFC), Proton Exchange Membrane (PEM) Fuel Cell, Direct Methanol Fuel Cell (DMFC), Phosphoric Acid Fuel Cell (PAFC), Molten Carbonate Fuel Cell (MCFC), and Solid Oxide Fuel Cell (SOFC). All these fuel-cell types are described in Table 1.1.

A fuel-cells operating characteristics help define its application, such as operating temperature, cell material and type of fuel used. It is known that lower temperature PEMFCs and DMFCs are very suitable to power passenger vehicles, while higher temperature MCFCs and PAFCs are suitable to be used in stationary applications.

1.5 Fuel-cell applications

Fuel cells have been researched and developed for use in any application, from houses to cars to mobile phones [Sheila, 2012], because of their flexibility in sizes (Figure 1.6). The use of fuel cells can be categorized into three broad power applications: Transport, stationary, and portable power applications. More detail on each application is given in this section.

Table 1.1: Summary of fuel-cell types [Spiegel, 2011]

Fuel-Cell Type	*Fuel*	*Mobile Ion*	*Electrolyte*	*Operating Temperature*	*Main Applications*
Alkaline (AFC)	Pure H_2	OH^-	KOH	323.15-473.15 K	Space program (historical)
Proton Exchange Membrane (PEMFC)	Pure H_2 (tolerates CO_2)	H^+	Solid polymer (e.g., Nafion)	303.15-373.15 K	Vehicles and mobile power
Direct Methanol (DMFC), formic acid (DFAFC), and other liquid fuels	Methanol, formic acid, other alcohols	H^+	Solid polymer (e.g., Nafion)	293.15-363.15 K	Portable electronics
Phosphoric Acid (PAFC)	Pure H_2 (tolerates CO_2,$\sim$ 1 % CO)	H^+	Phosphoric acid	493.15 K	$\sim$ 200 kW CHP systems
Molten Carbonate (MCFC)	H_2, CH_4, other hydrocarbons (tolerates CO_2)	CO_3^2	Lithium and potassium carbonate	923.15 K	Medium-to large-scale stationary combined heat and power (MW capacity)
Solid Oxid (SOFC)	H_2, CH_4, other hydrocarbons (tolerates CO_2)	O^{2-}	Solid oxide (e.g., yttria-stabilized zirconia)	773.15-1273.15 K	All-size stationary combined heat and power systems (2-kW to multi-MW capacity)

Figure 1.6: Fuel-cell different applications.

1.5.1 Transportation applications

The transport market is at the origin of the development of the fuel-cell technology to solve the problems of increasing oil prices and climatic degradation. Fuel-cell vehicles have an advantage over diesel vehicles because they have zero emissions. Compared to the ICE technology, the fuel cells offer a more pleasant driving behaviour and provide a higher efficiency. Fuel cells can be used for many transportation applications including automobiles, buses, scooters and bicycles. The fuel type most often used is compressed hydrogen. The most common type of fuel cell used is the PEMFC. In recent years, car manufacturers have developed many prototypes of cars operating with fuel cells. The most advanced of them are: DaimlerChrysler with NECAR and F-Cell, Honda with FCX, Toyota with FCHV, General Motors with Hydrogen, BMW with CleanEnergy, Ford with Focus FCV and P2000, Nissan with Xterra, Renault with FEVER, PSA with H2O, Volkswagen with Touran HyMotion, and finally Audi with A2H2. Fuel-cell buses have been running in British Columbia, California, Amsterdam, Barcelona, Hamburg, London, Luxembourg, Madrid, Porto, Stockholm, and Stuttgart [Spiegel, 2017].

1.5.2 Stationary applications

Fuel cells for stationary applications have been used commercially for over twenty years. In stationary applications, the fuel cell is often used to power houses that are not connected to the grid or to provide power when the grid is down. These fuel cells are also used for Combined Heat and Power (CHP). CHP units or fuel-cell cogeneration system are sized between 0.5 kW and 10 kW, use either PEMFC or SOFC technology. CHP units enable decentralized electricity generation and heat at the consumers home. So, by making use of this heat energy, for example to produce hot water, the overall efficiency of the system increases. As in Japan and South Korea, Residential CHP units have been deployed extensively with more than 10,000 cumulative units by the end of 2010 providing home power and heating. The manufacturing of these units is predominately located in the USA and Japan [FuelCellToday., 2017b].

1.5.3 Portable applications

Portable fuel cells are lightweight, long-lasting, portable power sources that are built into devices that are designed to be moved. Some of these devices include military applications, mp3 players, cameras, laptops, battery chargers, radios, toys etc. Portable fuel cells are being developed in a wide range of sizes ranging from less than 5 W up to 500 kW. In addition, portable fuel cells typically replace or augment battery technology and exploit either PEMFC or DMFC technology. These two fuel cells are characterized by their low operating temperature (between 333.15 and 353.15 K), which reduces thermal management problems. Fuel cells will power a device as long as there is fuel supplied to it [Spiegel, 2017].

1.6 Proton exchange membrane fuel cells

Among the several different types of fuel cells, hydrogen PEMFCs are, without doubt, the most extensively used for transport applications. This is due to their low temperature of operation (typically 333.15-353.15 K), which enables fast startup. Moreover, these fuel cells have high power density, small volume, solid electrolyte, long life, as well as low corrosion [O'hayre et al., 2016, Larminie et al., 2003].

Fuel cells are electrochemical devices that convert chemical of fuel energy directly into electricity. Water and heat are also produced if hydrogen is used as fuel. A PEMFC consists of a negatively charged electrode (anode), a positively charged electrode (cathode), and an electrolyte membrane made of persulfonic acid groups with a Teflon-like

chains. The electrolyte membrane has a property that allows positive ions (protons) to pass through while blocking electrons. Both the anode and cathode contain a platinum catalyst to speed up the electrochemical process. Hydrogen fuel passes over the anode, and with the help of catalyst, separates into electrons and protons. Protons flow from the anode to the cathode through the electrolyte membrane while the electrons flow to the cathode over an external circuit network, thus creating electricity. In the cathodes surface the oxygen reacts with hydrogen protons and electrons to form water and produce heat, as shown in Figure 1.7.

The basic chemical reactions of PEMFC are the following:
Anode:

$$2H_2 \quad \rightarrow \quad 4H^+ + 4e^- \tag{1.1}$$

Cathode:

$$O_2 + 4H^+ + 4e^- \quad \rightarrow \quad 2H_2O \tag{1.2}$$

Overall:

$$2H_2 + O_2 \quad \rightarrow \quad 2H_2O + Electricity + Heat \tag{1.3}$$

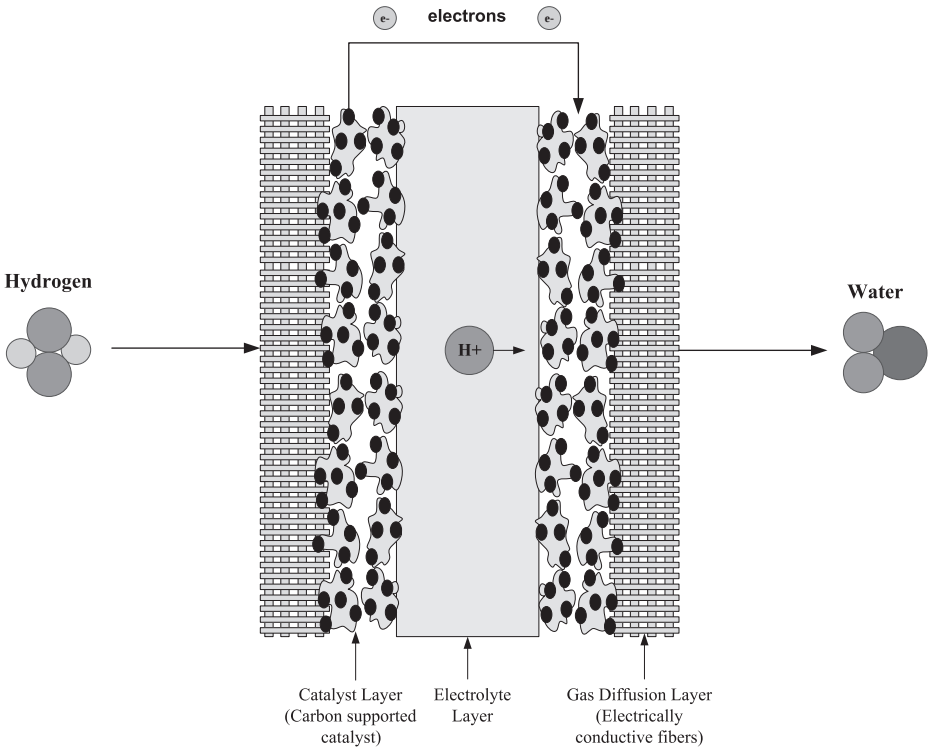

Figure 1.7: Illustration of PEMFC principle [Spiegel, 2011].

Reactants, hydrogen and oxygen, are transported by diffusion and/or convection to catalyst site on electrodes where the electrochemical reactions take place. Products, water and waste heat, must be continuously evacuated and may present critical problems for PEMFCs.

Fuel cells continue producing electricity as long as reactants are supplied. The voltage produced from single fuel cell is between 0 volt to 1 volt [Haddad, 2009] depending on the type of fuel cell, the fuel used, the cell size, the temperature and pressures at which operates, etc. The voltage is proportional to the number of cells connected together. To get higher voltage, multiple cells are stacked in series. The total stack voltage is the number of cells multiplied by the average cell voltage. Typical characteristics of fuel cells are normally given in the form of a polarization curve, shown in Figure 1.8, which is a plot of fuel-cell voltage versus cell current density (current per unit cell active area). The difference between actual voltage and the ideal voltage of the fuel-cell represents the loss in the cell. As shown in Figure 1.8, as more current is drawn from the fuel cell, the voltage decreases, due to fuel-cell electrical resistance, inefficient reactant gas transport and low reaction rate.

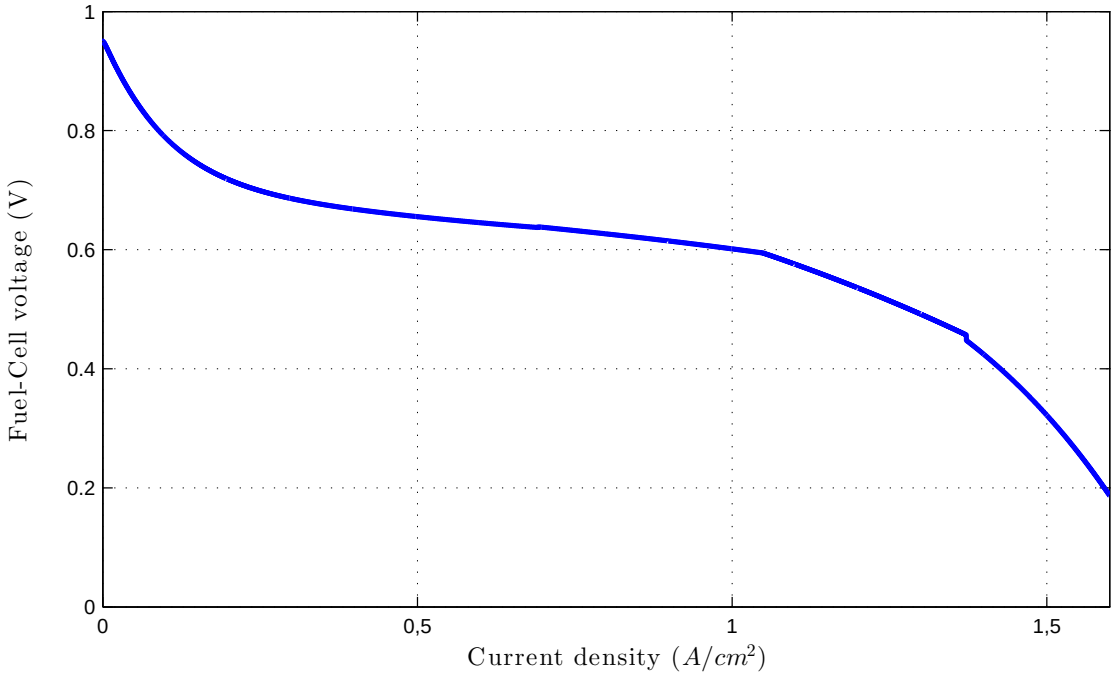

Figure 1.8: Fuel-cell polarization curve for 353.15 K.

1.7 PEMFC systems for automobile

PEMFCs have given the greatest potential for automotive applications. The compact design of the PEMFC system can achieve a high energy, i.e., an effective ratio between energy and weight. The low operating temperature (typically 333.15-353.15 K) and the quick startup make the PEMFC system well-appropriate for transport applications. Moreover, the PEMFC system efficiency falls above 50 % in comparison to ICE, which is around 30 % (gasoline) - 40 % (Diesel) efficient [Meyers and Darling, 2006]. Also, the fuel-cell technology has low noise and vibration operation, even during rapid accelerations and in some cases, is found to be 50 % lower than the corresponding ICEs [Bessarabov, 2011]. In respect, fuel cells also contribute to the environmental protection because the direct hydrogen fuel-cell vehicles release only water vapour.

1.8 PEM fuel-cell structure

To form PEMFC stack, multiple of individual cells, are stacked in series between flow field plates and only one set of end plates (Figure 1.9). Each cell within the stack consists of membrane electrolyte assembly (MEA), backing and catalyst layers, flow fields and current collectors, and sometimes gaskets for sealing/preventing leakage of gases between anode and cathode.

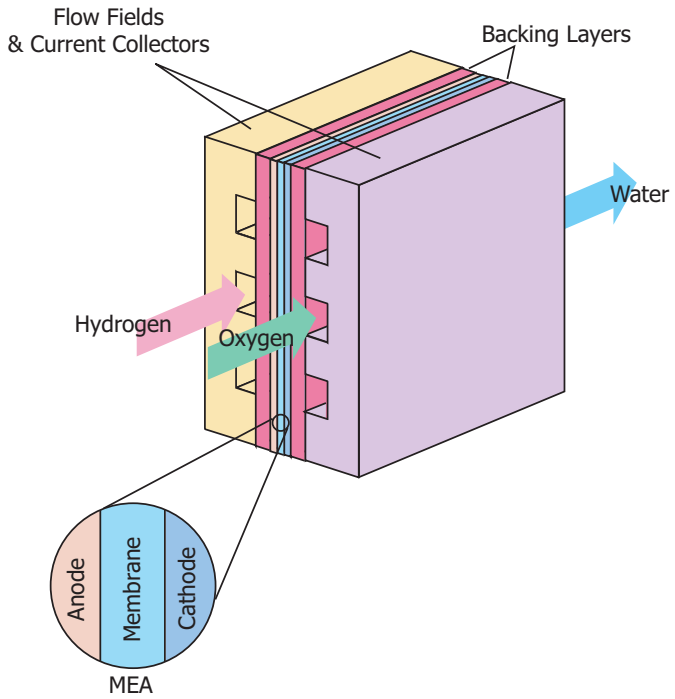

Figure 1.9: Fuel-cell structure [Pukrushpan et al., 2002b],

The MEA, which is typically less than a millimeter thick, consists of a PEM sandwiched between two electrodes (anode and cathode). Electrodes, where the electrochemical reactions take place, made from a highly conducting material such as porous graphite. A platinum catalyst layer is applied to the surface of both electrodes in order to help increase the rate of reaction. The MEA is deposited between two porous substrate carbon called backing layers, which is typically a carbon fiber paper. The main purpose of the backing layers is ensuring effective diffusion of reactant gases from flow field plates to the catalyst site on the MEA. The outer surface of the backing layers is pressed against the flow field plates, also called collectors or separators, which have many functions such as, ensuring electrical connection between individual cells of the stack, and separating gases among adjacent cells [Gold, 2017].

Table 1.2 explains and summarizes the composition of each component and what its role in the PEMFC.

Table 1.2: Summary of PEMFC components [Spiegel, 2011, Gold, 2017]

Component	*Description*	*Common Types*
Proton exchange membrane	Enables hydrogen protons to travel from the anode to the cathode.	Persulfonic acid membrane (Nafion 112, 115, 117)
Catalyst layer	Breaks the fuel into protons and electrons. The protons combine with the oxidant to form water at the fuel-cell cathode. The electrons travel to the load.	Platinum/carbon catalyst
Backing layers	Allow fuel/oxidant to travel through the porous layer, while collecting electrons.	Carbon cloth or Toray paper
Flow fiels plates	Distribute the fuel and oxidant to the backing layer.	Graphite, stainless steel
Gaskets	Prevent fuel leakage, and helps to distribute pressure evenly.	Silicon, Teflon
End plates	Holds stack layers in place.	Stainless steel, graphite, polyethylene, PVC

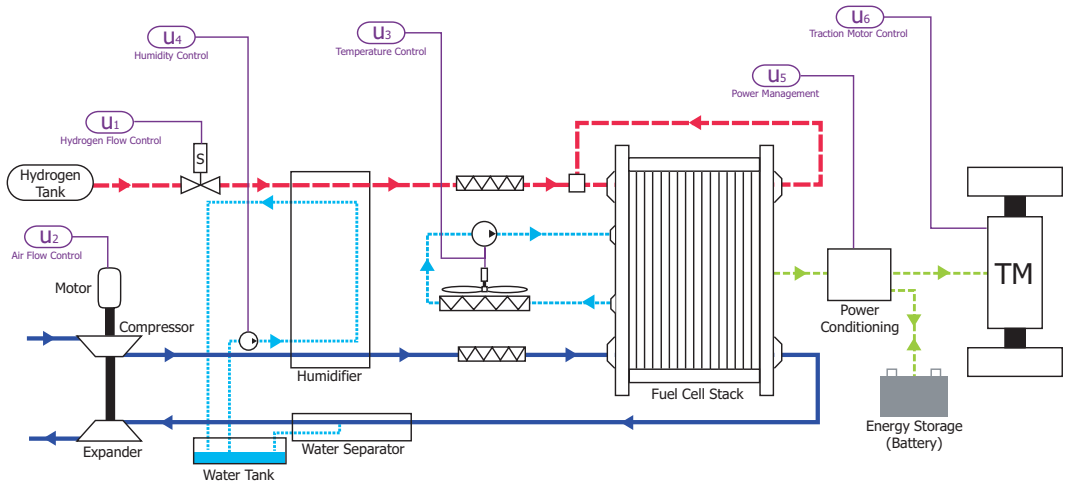

Figure 1.10: Fuel-cell system architecture including the different sub-processes [Pukrushpan et al., 2004c],

1.9 Fuel-cell system

In order to operate the stack and function as system, it is necessary to integrate it with other various auxiliary sub-processes, also referred to as balance-of-plant, to form a fuel-cell system [Pukrushpan et al., 2002b]. Figure 1.10 presents the main sub-processes and interconnections required for a pressurized fuel-cell stack. The precise configuration will depend to a large extent on the type of fuel-cell technology used, but in general, the PEMFC system includes several main sub-processes: air supply sub-process to the cathode part, hydrogen supply sub-process to the anode part, heat and temperature sub-process, water management sub-process, power management sub-process, and control sub-process [Pukrushpan et al., 2002b].

1.9.1 Air supply

The air supply sub-process consists of air flow loop in the cathode part. The air can be supplied by means of a compressor, a fan or a compressed air source, although the latter is mostly used in submarines applications and laboratory settings. Fans are generally used in low-pressure systems that are supplying directly by atmospheric air, with oxygen accounting for 21 % of the air. Whereas an air compressor may be used for pressurized systems. Moreover, air compressors give autonomy and flexibility to the system, allowing precise control of working pressures. Several types of compressors can be used, such as: centrifugal compressor, twin screw compressor, lobe compressor, etc. In any case, both

compressors and fans require electrical power and thus becoming part of losses or parasitic loads, which reduce the amount of energy available to external loads [Laghrouche et al., 2013].

1.9.2 Hydrogen supply

The hydrogen supply sub-process is generally composed of a pressurized tank with pure H_2 connected to the anode through a pressure-reduction valve and a pressure-controlled valve. hydrogen flow loop in the anode part. Although hydrogen is the most abundant element on earth, it is not often present in its molecular form, but is always associated with other chemical elements, such as water and hydrocarbons [Basualdo et al., 2012]. In current applications of fuel-cell systems, two types of hydrogen sources are used: (i) pure hydrogen may be produced from other fuels and then stored, as part of the , in a high-pressure reservoir (300 to 700 bar) [Matraji, 2013], or (ii) by integrating hydrogen generation as a sub-process of fuel-cell system [Basualdo et al., 2012]. There are several processes for generating hydrogen from hydrocarbon fuels, such as steam reforming, partial oxidation, and autothermal reforming, which is a combination of steam reforming and partial oxidation [Basualdo et al., 2012].

1.9.3 Heat and temperature

The heat and temperature sub-process includes the fuel-cell stack cooling system and the reactant heating system. The thermal management of the fuel cell is critical since the performance depends strongly on the temperature. As chemical reaction between oxygen and hydrogen occurred, heat is generated in the fuel cell. In addition, the compressed air gas leaving the compressor also has a high temperature. These two reasons contribute to increase the stack temperature. The PEMFC is designed to operate at the temperature around 353.15 K [Matraji, 2013]. Therefore, a cooling system, using a fan or a water refrigeration subsystem, is required to control the temperature inside the fuel-cell system [Kunusch et al., 2012].

1.9.4 Water management

Water content is as important as temperature, and both magnitudes are closely related. The objective of the water management sub-process is to maintain an effective hydration of the polymer membrane and an adequate amount of liquid water. This objective can be achieved by controlling the relative humidity of the reacting gases, as well as their individual pressures and temperatures.

Both air and hydrogen must be humidified before entering the fuel-cell stack with humidifiers. For proper operation, a minimum threshold of membrane humidity is essential in order to ensure a good chemical reaction and fluent ionic conductivity through the membrane [Pukrushpan et al., 2002a]. Particularly, the membrane must neither dry nor flooded, as otherwise it causes high polarization losses and reduces the fuel-cell life. A 20-40 % drop in voltage can occur if there is no proper humidification control [Pukrushpan et al., 2004b].

1.9.5 Power management

The power management sub-process controls the electricity produced by the fuel-cell stack in order to satisfy the load requirements in terms of voltage, power quantity and transients. If no energy storage devices are used, the full load can be viewed as a disturbance to the fuel-cell system and no power management sub-process is necessary. However, hybridization of fuel-cell system with another energy storage device, like batteries or supercapacitors, allowing apply the power management sub-process within the fuel-cell system. For this purpose, DC/DC converters should be connected between all power sources and external load to conditioned the power (voltage) required by the load. Finally, characteristics of the power management sub-process depend on the load requirements, which vary with application [Sheila, 2012].

1.9.6 Control

This sub-process implements a strategy to control the system operating parameters, e.g., flow rates, temperature, pressure, etc. It also communicates with the load and other electrical components of a system. It is typically composed of sensors, actuators, controllers, processors, etc.

1.10 Control challenges

To achieve high efficiency and a long life cycle of the fuel-cell system, the reactant gas supply and water and heat sub-processes need to be properly controlled both during steady-state and transient operations. [Matraji, 2013] described the main challenges related with fuel-cell control as follows:

1.10.1 Air supply control

One of the most important problems in fuel-cell systems control is to guarantee sufficient oxygen supply during abrupt changes in the load demand. If the oxygen flow is too

low, undesirable hot spots appear in the membrane, and output power decreases because of the lack of reactants, a situation called cathode starvation. On the other hand, if oxygen flow is too high, an excessive amount of water is pushed to the cathode outlet, which in turn results in membrane drying, which affects its ionic resistance. Besides, an increase of the air flow results in higher power demand to the compressor that supplies it, reducing the overall system performance. Thus, an efficient control system must be capable of regulating air flow properly, avoiding irreversible damages to the membrane and delivering enough oxygen to meet the electric power demand in a reliable and efficient way. According to [Pukrushpan et al., 2004a], the optimum net power is reached for an Oxygen Excess Ratio (OER) between 2 and 2.5. The goal is therefore to maintain an optimal OER.

1.10.2 Hydrogen supply control

The hydrogen supply control aim is to feed the fuel-cell system with hydrogen at the same pressure as air independently of the hydrogen consumed, which is proportional to the current load [Andrew, 1996]. It is important to reduce the pressure difference across the membrane in order to avoid damaging it. When pressurized hydrogen is used, the hydrogen flow in the anode are adjusted by a servo valve. Since the valve is fast, it is supposed that the hydrogen flow is regulated by a simple proportional controller based on the feedback difference pressure between anode and cathode [Pukrushpan et al., 2004c]. Usually, a purge valve is installed at the output of the anode to evacuate the excess water. The purge valve can also be employed to reduce the anode pressure quickly in case of necessity. It is important to note that the hydrogen supply control problem is important when the hydrogen production is made using an Internal fuel processor system with a relatively slow transitory response [Pukrushpan et al., 2005].

1.10.3 Water and heat management

The problem of water management is to maintain a constant hydration coefficient of the membrane. The latter is sensitive to drying and drowning [Basualdo et al., 2012]. These two constraints slow down the rate of passage of gases and degrade the membrane. It is experienced experimentally that an excess of water degrades the electrical output power of the fuel-cell system [Gold, 2017, Spiegel, 2011], and a lack of hydration reduces its life. It should be noted that poor water management can create a voltage drop of 20 % to 40 % [Bagotsky, 2012].

PEMFCs are temperature sensitive during operation. High temperature accelerates

the chemical reaction and thus improves the performance of the system [O'hayre et al., 2016]. But as soon as this air is injected into the fuel-cell system, it will also cause the drying of the membrane, so we have to find the ideal operating temperature. The hydration problems of the system are dependent on water management and temperature management, as treated in [Gold, 2017, Spiegel, 2011].

1.10.4 Membrane degradation

Another issue which deserves special attention is membrane degradation. In some applications, fuel cells are fed with pure hydrogen, which is stored in a high-pressure tank. The oxygen, when supplied, is supplied with compressed air [Larminie et al., 2003]. During operation, it is essential to keep the difference between the pressure of the anode and that of the cathode less than 0.5 bar. This difference can deform the membrane and reduce the lifespan of fuel cells. For this, the pressures in the cathode and in the anode, are set at a given pressure. By keeping the pressure high, the battery will not run out of oxygen in the cathode when the charge is changed [Sheila, 2012]. This also increases the power provided by the fuel cell. For this reason, a control system must be put in place to control the pressures at the entrance to the anode and the cathode.

This thesis is interested in the optimization of energy and the protection of the fuel-cell system. The goal is to develop a control system on the one hand, to optimize the net power provided by the fuel-cell system by forcing the OER to its optimum value, and on the other hand to protect the fuel-cell system, the membrane and the compressor. In addition, this control system will have to answer two imperatives: the response time and the robustness.

1.11 Summary

Fuel cells are electrochemical devices that allow production of electrical energy from hydrogen or other fuels with high efficiency and low emission. The fuel-cell technology is promising in the area of stationary, transportation and portable applications. This chapter covered the fundamental principles of fuel cells and fuel-cell systems, their operation and applications. A good understanding of these concepts is essential in appropriate designing fuel-cell systems model, which is the focus of the following chapter. The next chapter will present the static and dynamic modelling of PEMFC air supply system.

Chapter 2

PEMFC Air Supply System Model

> *No amount of guilt can change the past, and no amount of worrying can change the future.*
>
> Umar ibn al-Khattab

2.1 Introduction

As it was introduced in Chapter 1, The objectives of PEMFC system control are to reduce the fuel consumption while preventing performance deterioration, oxygen starvation and, eventually, irreversible damage in the polymeric membranes. However, the PEMFC system has several variables to be regulated in a specific way such as the amount of hydrogen at the anode, the amount of air injected by the compressor into the cathode, the quantity of water produced, the temperature generated by the chemical reaction and the energy provided by the fuel-cell system. These sub-processes are strongly interconnected, this makes the whole system highly nonlinear and difficult to control. In this context, fuel-cell system models suitable for nonlinear control strategies design are required.

2.2 Review on fuel-cell system modelling

The models developed in the literature can be organized into three main categories, namely, fuel-cell performance models, steady-state fuel-cell system models, and dynamic fuel-cell system models. The main purposes of the first two categories of models are to design the fuel-cell components and to determine the fuel-cell operating points [Baroud and Benalia, 2014]. While these models are not proper for control purposes; they obtain the

polarization characteristics of the fuel-cell system, which are defined by a relationship betweeen voltage and current of the fuel-cell system for fixed fuel-cell parameters [Pukrushpan et al., 2004c]. In most models, the current of the fuel-cell system is considered as an input to the system, and the electrical voltage of the fuel-cell system is considered as an output [Töpler and Lehmann, 2015].

The last two decades has recognized the development of many dynamic fuel-cell system models, only a few are suitable for use in nonlinear control design. A suitable model should be capable to predict both steady and transient behaviour of the fuel-cell system in a wide range of operating conditions. It should be noted that only the most relevant models that are proper for control study are cited.

Jurado [Jurado, 2004] has established a linear dynamic model of the SOFC stack that considers only the electrical output power. The model is reduced to transfer functions using identification algorithms in order to simplify it and thus facilitate its control. The linear nature of the model makes the results obtained more critical.

Lachaize et al. [Lachaize, 2004] bring together electrochemical and thermal phenomena. However, they study each part of the cell separately (anode, cathode, and membrane) without taking into account the coupling and the interference between the different phenomena. In addition, the linearization of the model in order to simplify the control makes the results obtained even less precise.

A typical PEM single cell is modelled in detail in Phatapathi et al. [Pathapati et al., 2005]. The model describes the transient behaviour of thermal and fluidic phenomena as well as the effect of the double layer capacitance. The model is then linearized to simplify the study. However, Yerramalla et al. [Yerramalla et al., 2003] have simulated the model in nonlinear and linear form. The results of work [Yerramalla et al., 2003] have shown a major difference between the nonlinear model and its linearized.

Another approach for fuel-cell modelling is the use of equivalent circuits using electrical elements, such as resistances, capacitances or inductances to represent the system behaviour. Qi et al. [Qi et al., 2005] have presented a complete equivalent electrical circuit of a SOFC single cell despite some simplifications taken into account. Their model is completed and improved by a second work integrating the phenomena of heat transfer through the different components of the cell. The problem with this model is not taking into account the influence of the membrane humidification on the ohmic losses.

In Maldonado's model [Maldonado, 2012], problems of membrane drying and water flooding of gas distribution channels are discussed. This model calculates gas consumption by treating water transport through the membrane. It assumes that the active area is

reduced to an interface of zero thickness between the electrode and membrane areas. This hypothesis seems valid only for small cells, which limits the interest of the model.

Kang [Kang, 2015] have developed a model for PEMFC system, this model integrates the dynamic evolution of heat transfer and water transport phenomena. It is based on a simplified approach of a three-dimensional geometric representation of the cell. However, the model does not consider the dynamic evolution of electrical quantities such as the electrochemical potential.

However, many of these models have not been experimentally validated, and there is still a lack of rigorous studies on parameters identification and their association with performance variables. To this end, the model developed by J. Pukrushpan et al. [Pukrushpan et al., 2004c] has been chosen, since it is one of the most complete and accurate models available in the open literature. Pukrushpan et al model incorporates the transient behaviours that are important for analysis and control design. Models of the various auxiliary components, namely a compressor, manifolds, an air cooler, and a humidifier, are associated with the fuel-cell stack model, which is composed of four interacting submodels, namely stack voltage, cathode flow, anode flow, and membrane hydration models. Flow equations, mass continuity, mass and energy balances, electrochemistry relations, water and nitrogen crossovers in membrane and fuel-cell thermodynamics and other physical phenomena are incorporated to create this model. The polarization curve in this model is a function of the stack current, stack temperature, water vapour, hydrogen, and oxygen partial pressures and membrane humidity.

In the remainder of this chapter, a presentation of a PEMFC steady-state model is given. This model is useful for calculating the PEMFC stack voltage. Then, a presentation of reduced dynamic model based on the work of [Gruber et al., 2008] and [Suh, 2006] is done. Finally, a steady-state analysis of the PEMFC system is performed in order to define the optimal value of the air flow setpoint, termed Oxygen Excess Ratio (OER), that results in the maximum net power.

2.3 PEMFC steady-state model

The steady-state model can be used to predict the fuel-cell output voltage v_{fc} according to the current density of the fuel-cell system, cell temperature, reactant and product gas pressures, and membrane humidity [Pukrushpan et al., 2004c]. The fuel-cell voltage expression is calculated on the basis of the Nernst open circuit voltage with activation, ohmic and concentration losses [Pukrushpan et al., 2004c]. The Nernst open circuit

voltage and the three main types of losses in the fuel-cell system are further disscused in the following subsections.

2.3.1 Nernst open circuit voltage

Fuel cells convert directly chemical potential energy into electrical energy through an electrochemical reaction. The electrical energy released from the fuel cell can be calculated from the Gibbs free energy change (ΔG), that is, the difference between the Gibbs free energy of products and the Gibbs free energy of reactants. The change in Gibbs free energy (ΔG), also known as free enthalpy, depends on both temperature and pressure. For the hydrogen/oxygen fuel-cell chemical reaction

$$H_2 + \frac{1}{2}O_2 \rightarrow H_2O, \tag{2.1}$$

the change in the Gibbs free energy ΔG is expressed by [Pukrushpan et al., 2004c]

$$\Delta G = \Delta G^0 - RT_{fc} \ln \left[\frac{p_{H_2} p_{O_2}^{\frac{1}{2}}}{p_{H_2O}} \right], \tag{2.2}$$

where ΔG^0 is change in the Gibbs free energy at standard pressure (1 bar) which in turn varies with the fuel-cell temperature, T_{fc}, in Kelvin. R is the universal constant for ideal gases, p_{H_2} is the hydrogen partial pressure, p_{O_2} is the oxygen partial pressure, and p_{H_2O} is the water vapour partial pressure. Values of changes on the Gibbs free energy, ΔG^0, of the reaction in (2.1) for standard pressure at various reaction temperatures are given in Table (2.1). The value of ΔG^0 is negative which means that the energy is released from the reaction.

If the electrochemical process in the cell were reversible, all of the Gibbs free energy, at a constant temperature and pressure, could be converted to electrical energy and thus, define a standard potential [Pukrushpan et al., 2004c]

$$E^0 = \frac{-\Delta G^0}{\bar{n}F}, \tag{2.3}$$

where E^0 is the ideal cell potential, which is the maximum potential theoretically achievable. $\bar{n}$ is the number of electrons and F is the Faradays constant. The number of electrons for an $H_2 - O_2$ cell reaction is 2, hence (2.3) for ideal fuel-cell potential becomes

$$E^0 = \frac{-\Delta G^0}{2F} \tag{2.4}$$

This potential, E^0, is correct for standard temperature and pressure. However, PEMFCs usually operate at higher temperatures and because Gibbs free energy is a function

Table 2.1: Change in Gibbs free energy of hydrogen fuel-cell at various temperatures [Larminie et al., 2003]

Form of water product	*Temperature K*	ΔG^0 *(kJ/mole)*
Liquid	298.15	-237.2
Liquid	353.15	-228.2
Gas	353.15	-226.1
Gas	373.15	-225.2
Gas	473.15	-220.4
Gas	673.15	-210.3
Gas	873.15	-199.6
Gas	1073.15	-188.6
Gas	1273.15	-177.4

of temperature, it decreases the cell potential to a certain degree. Therefore, using (2.2), the actual theoretical potential of a PEMFC can be written as

$$E = \frac{-\Delta G}{2F} = \frac{-\Delta G^0}{2F} + \frac{RT_{fc}}{2F} \ln \left[\frac{p_{H_2} p_{O_2}^{\frac{1}{2}}}{p_{H_2O}} \right]. \tag{2.5}$$

Potential E in (2.5) is so called the Nernst open circuit voltage of a PEMFC. In practice, the fuel-cell process is not reversible, some of the chemical energy is converted to heat energy, and the Nernst voltage, is smaller than that what (2.5) predicts. In fact, the term $-\Delta G^0/2F$ varies from its reference potential at standard conditions ($E^0 = 1.229$ volts) in accordance with the temperature [Basualdo et al., 2012]

$$\frac{-\Delta G^0}{2F} = 1.229 + (T_{fc} - T_0) \left(\frac{\Delta S^0}{2F} \right), \tag{2.6}$$

where T_0 is the standard temperature (298.15 °K), and ΔS^0 is the entropy change. Thus, (2.6) can be rewritten as

$$\frac{-\Delta G^0}{2F} = 1.229 - \frac{298.15 \times \Delta S^0}{2F} + \left(\frac{\Delta S^0}{2F} \right) T_{fc}. \tag{2.7}$$

Using the standard thermodynamic values regarding entropy changes, (2.7) is further expanded and yields [Basualdo et al., 2012]

$$E = 1.229 - 0.85 \times 10^{-3}(T_{fc} - 298.15) + 4.3085 \times 10^{-5} T_{fc} \left[\ln(p_{H_2}) + \frac{1}{2} \ln(p_{O_2}) \right]. \tag{2.8}$$

When the fuel cell operates, the fuel-cell actual voltage v_{fc} drops from the Nernst open circuit voltage, E, and this drop in voltage is a result of losses, which are proportional to the current drawn by the electric circuit (Figure 2.1(d)). This phenomenon is known as polarization and allows us to identify the PEMFC system operating point. There are three main types of losses: activation loss v_{act}, ohmic loss v_{ohm} and concentration loss v_{conc}. These aspects are more disscused next.

2.3.2 Activation loss

The activation loss or activation overvoltage, shown in Figure 2.1(a), is the voltage required to form and break the chemical bounds, both in the anode and cathode [Liu, 2014]. Also, some amount of voltage is used in electrons transfer, also referred as exchange current density, to and from electrodes. It is worth noting that the reactions at the anode are very quick in comparison to the ones at the cathode, hence anode overvoltage is sometimes ignored [Liu et al., 2006]. Reduction in activation losses can be accomplished by increasing the active surface of the catalysts, raising the temperature and increasing the concentration of reactants. The relation between activation loss and current density can be determined from the Tafel equation [Liu, 2014]

$$v_{act} = \frac{RT_{fc}}{2\bar{\alpha}F} \ln\left(\frac{i}{i_0}\right), \tag{2.9}$$

where the constant $\bar{\alpha}$ is the change transfer coefficient and i_0 is the exchange current density. i is the current density, which is defined as stack current $I_{st}\,(\mathrm{A})$, per cell active area, $A_{fc}\,(\mathrm{cm}^2)$.

$$i = \frac{I_{st}}{A_{fc}}. \tag{2.10}$$

It should be noted that this equation is only exact correct $i > i_0$, which can cause simulation problems. Accordingly, a similar function that is correct for the whole range of i is preferred

$$v_{act} = v_0 + v_a\left(1 - e^{-b_1 i}\right), \tag{2.11}$$

where v_0 is the voltage drop at zero current density, and v_a and b_1 are constants that depend on the temperature and the oxygen partial pressure [Amphlett et al., 1995, Steele and Heinzel, 2011]. The expressions of v_0 and v_a are defined in Appendix A.

2.3.3 Ohmic loss

The ohmic loss, shown in Figure 2.1(b), is due to the resistance of the membrane to the proton transfer, and the resistance of electrodes to the electrons transfer. Ohmic losses can

be overcome by using electrodes with high electronic conductivity and weak membrane thickness which has high proton transference propriety. The formulation of this type of losses is presented below

$$v_{ohm} = iR_{ohm}, \tag{2.12}$$

where R_{ohm} represents the internal electrical resistance of the cell and has a strong dependency on temperature and membrane humidity [Santarelli and Torchio, 2007]. The ohmic resistance of Nafion 117 membrane is a function of the membrane conductivity, σ_m, and membrane thickness, t_m according to the following expression [Mann et al., 2000]:

$$R_{ohm} = \frac{t_m}{\sigma_m}, \tag{2.13}$$

The membrane conductivity, σ_m, is a function of membrane water content, λ_m, and is defined by the following equation [Pukrushpan et al., 2004c]:

$$\sigma_m = (0.005139\lambda_m - 0.00326)\, e^{\left(350\left(\frac{1}{303}-\frac{1}{T_{fc}}\right)\right)}. \tag{2.14}$$

2.3.4 Concentration loss

Concentration losses are important at high current densities and appear when a reduction in the concentration of reactants at the electrode-membrane interface occurred. This drop is even more important if the reactants are not pure and mixed gases are supplied to the fuel cell e.g., air is used instead of oxygen [Larminie et al., 2003]. This loss can be expressed by a semi-empirical expression as,

$$v_{conc} = i\left(b_2 \frac{i}{i_{max}}\right)^{b_3}, \tag{2.15}$$

where b_2, b_3 and i_{max} are constants that depend on the temperature and the partial pressures of reactants. i_{max} is the current density that causes the sudden voltage drop. These constants are settled empirically and is defined in Table A.1 in Appendix A. The concentration loss is shown in Figure 2.1(c).

2.3.5 Fuel-cell terminal voltage

The fuel-cell terminal voltage is equal to the difference between the Nernst open circuit voltage of the fuel-cell system and the different type of losses (activation, ohmic and concentration). The fuel-cell terminal voltage is expressed by the following equation:

$$\begin{aligned} v_{fc} &= E - v_{act} - v_{ohm} - v_{conc} \\ &= E - v_0 - v_a\left(1 - e^{-b_1 i}\right) - iR_{ohm} - i\left(b_2 \frac{i}{i_{max}}\right)^{b_3}. \end{aligned} \tag{2.16}$$

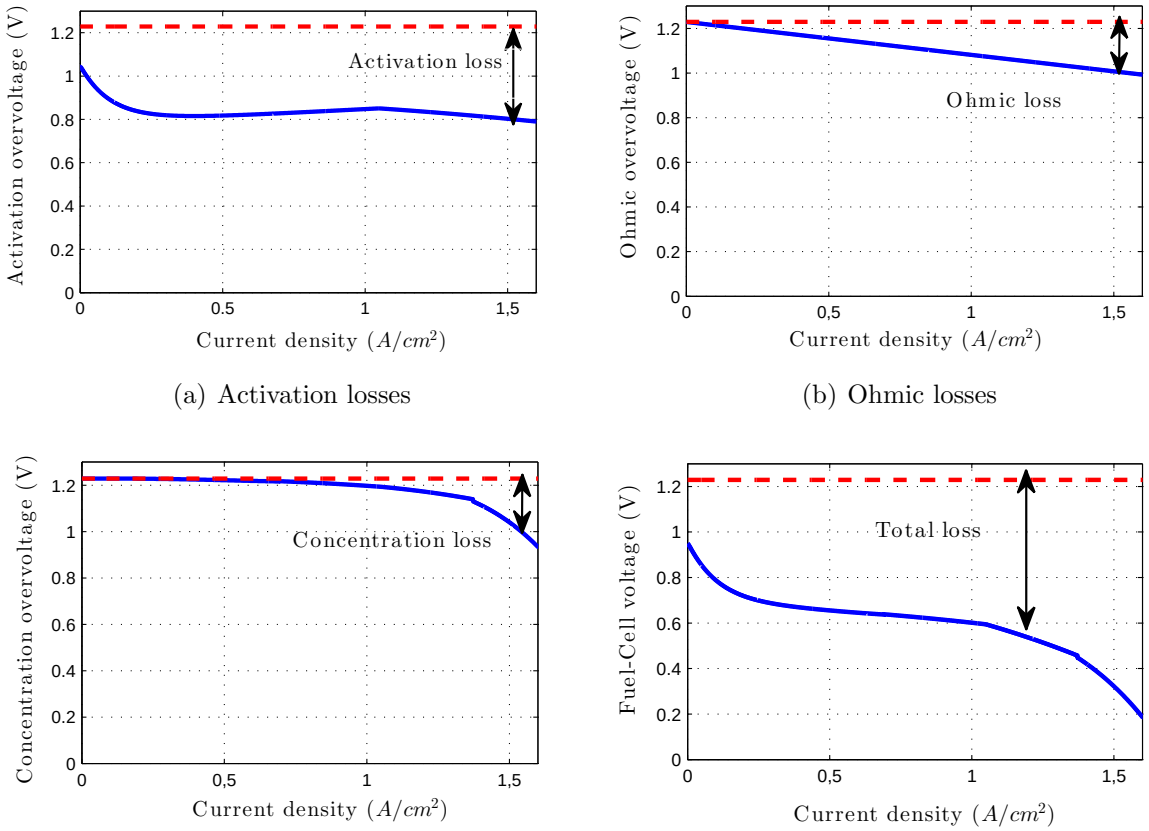

(a) Activation losses

(b) Ohmic losses

(c) Concentration losses

(d) Total losses

Figure 2.1: Voltage drops due to different types of losses in fuel cell,

The resulting PEMFC polarization curve is depicted in Figure 2.1(d). It can be seen that the voltage drop is significantly more at low and high current densities. At low current densities, the activation loss is predominant and at high current densities, the concentration loss is a major cause of losses. The ohmic loss is nothing but cell resistance and hence with increase in cell current the voltage drop increases proportionately (Figure 2.1(b)). All numerical parameters vlues are found in Table A.1 in Appendix A. The stack voltage V_{st} is calculated as the sum of the individual fuel-cell voltages

$$V_{st} = nv_{fc}, \tag{2.17}$$

where n is the number of cells. Thus, the fuel-cell power is calculated as

$$P_{st} = I_{st}V_{st}. \tag{2.18}$$

2.4 PEMFC air supply dynamic model

To concentrate the study on the air (oxygen) supply sub-process, which has a great influence on the whole PEMFC system efficiency, the ninth-order state-space model proposed by Pukrushpan et al. [Pukrushpan et al., 2004c] has been simplified to fourth-order state-space model by [Suh, 2006] under the following assumptions:

- All gases obey the ideal gas law;
- The fuel-cell system is fed by pressurized high-purity hydrogen and the hydrogen supply control is perfect for tracking the anode pressure to the cathode pressure;
- The temperature of the fuel-cell stack, T_{fc}, is well controlled and is maintained constant at 353.15 K;
- The temperature of the flow inside the cathode is equal to the stack temperature;
- The input reactant flows are humidified in a consistent and rapid way;
- The water inside the cathode is only in vapour phase and any extra water in liquid phase is removed from the channels;
- The flooding of the gas diffusion layer is neglected;
- The spatial variations are neglected, it is assumed that the flow channel and the gas diffusion layer are lumped into one volume;
- Humidity and temperature dynamics are neglected because they are slower than the air flow dynamics.

Moreover, experimental validation was performed in [Liu, 2014] through a Hardware In the Loop (HIL) test bench which consists of a physical PEMFC air supply system, based on a commercial twin screw compressor and a real time PEMFC emulator.

2.4.1 Air compressor model

The air compressor consists of a 14 kW turbo-compressor and a direct current motor. It is used to provide air to the cathode side through supply maniflod. The inputs to the model include inlet air pressure $p_{cp,in}$, its temperature $T_{cp,in}$, compressor motor voltage v_{cm} and supply manifold pressure p_{sm}. The inlet air is atmospheric and its pressure and temperature are equal to $p_{atm} = 101325$ Pa and $T_{atm} = 298.15$ K, respectively.

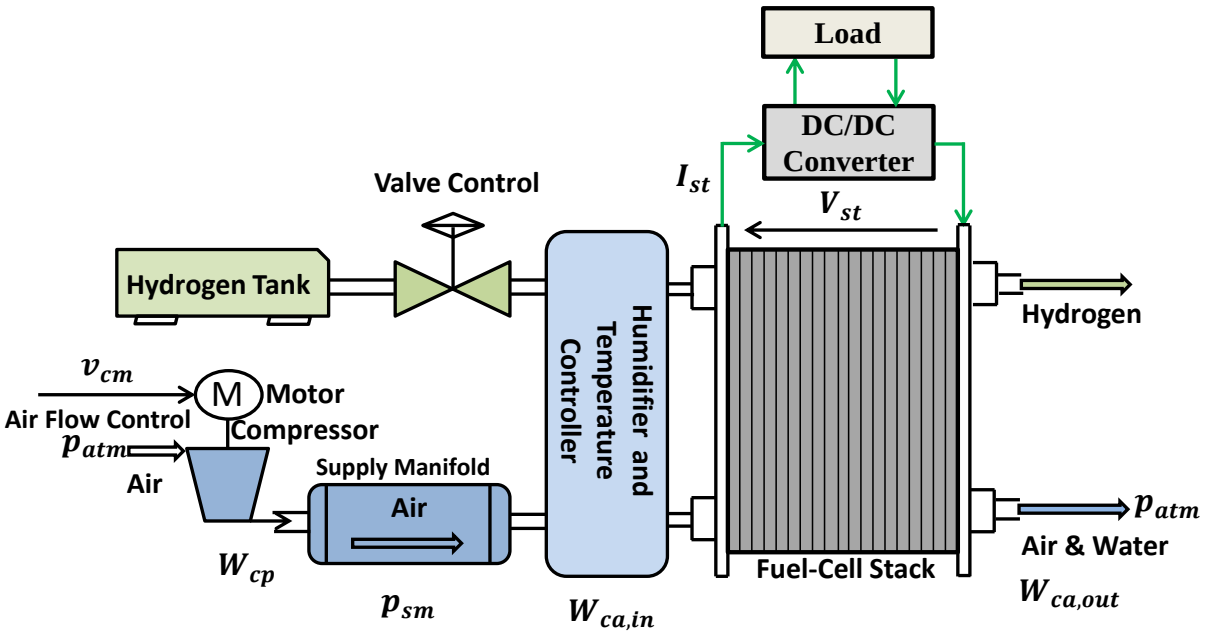

Figure 2.2: Fuel-cell system scheme.

The dynamic state in the model is the rotational speed of the motor shaft in the compressor ω_{cp}, which is presented by the following equation

$$\frac{d\omega_{cp}}{dt} = \frac{1}{J_{cp}}\left(\tau_{cm} - \tau_{cp}\right), \tag{2.19}$$

where J_{cp} denotes the compressor and motor inertia (kg×m^2), τ_{cm} is the compressor motor torque (N×m) and τ_{cp} is the torque needed to drive the compressor (N×m), which

$$\begin{aligned} \tau_{cm} &= \eta_{cm}\frac{k_t}{R_{cm}}\left(v_{cm} - k_v\omega_{cp}\right), \\ \tau_{cp} &= \frac{C_p T_{atm}}{\eta_{cp}\omega_{cp}}\left[\left(\frac{p_{sm}}{p_{atm}}\right)^{\frac{\gamma}{\gamma-1}} - 1\right] W_{cp}, \end{aligned} \tag{2.20}$$

where k_t, R_{cm} and k_v are motor constants, η_{cm} is the motor mechanical efficiency, C_p and γ correspond to the specific heat capacities of the air, η_{cp} is the compressor efficiency and W_{cp} is the compressor mass flow rate. This latter is determined by the rotational speed of the motor compressor and the air pressure in the supply manifold, which has been approximated by the following equation

$$W_{cp} = \frac{W_{cp}^{max}\omega_{cp}}{\omega_{cp}^{max}}\left(1 - exp\left(\frac{-r\left(s + \frac{\omega_{cp}^2}{q} - p_{sm}\right)}{s + \frac{\omega_{cp}^2}{q} - p_{sm}^{min}}\right)\right), \tag{2.21}$$

with exp is the exponential function, $r = 15$, $q = 462.25$ rad^2/(s^{2}Pa), $\omega_{cp}^{max} = 11500$ rad/s, $p_{sm}^{min} = 50000$ Pa, $s = 100000$ Pa and $W_{cp}^{max} = 0.0975$ kg/s.

The compressor motor power P_{cp} is calculated using the compressor torque τ_{cm} and its rotational speed ω_{cp}

$$P_{cp} = \frac{v_{cm}}{R_{cm}} \left(v_{cm} - k_v \omega_{cp} \right). \tag{2.22}$$

This power can be satisfied directly from the fuel cell or from an auxiliary power source, like batteries or supercapacitors.

2.4.2 Supply manifold model

The air supply manifold is associated with pipes and connections between the compressor and the fuel-cell cathode (shown in Figure 2.2). By applying the mass conservation principle, the air pressure dynamic in the supply manifold depends on the inlet flow to the supply manifold W_{cp}, the outlet flow from the supply manifold $W_{sm,out}$ and the compressor flow temperature T_{cp}

$$\frac{dp_{sm}}{dt} = \frac{\gamma R T_{cp}}{M_{a,atm} V_{sm}} \left(W_{cp} - W_{ca,in} \right), \tag{2.23}$$

where V_{sm} is the supply manifold volume, $M_{a,atm}$ is the molar mass of the atmospheric air and T_{cp} is the temperature of the air leaving the compressor, which is calculated based on [Pukrushpan et al., 2004b] with a map of the compressor efficiency η_{cp}, i.e.,

$$T_{cp} = T_{atm} + \frac{T_{atm}}{\eta_{cp}} \left[\left(\frac{p_{sm}}{p_{atm}} \right)^{\frac{\gamma}{\gamma - 1}} - 1 \right]. \tag{2.24}$$

The relationship between the outlet flow of the supply manifold and the pressure drop can be simplified as a linear nozzle equation due to the small pressure difference between the cathode p_{ca} and the supply manifold p_{sm}

$$W_{sm,out} = k_{sm,out} \left(p_{sm} - p_{ca} \right), \tag{2.25}$$

where $k_{sm,out}$ is the supply manifold outlet flow constant, the flow leaving the supply manifold enters the fuel-cell cathode and so, the supply manifold outlet flow $W_{sm,out}$ is referred to being cathode inlet flow $W_{ca,in}$.

2.4.3 Cathode flow model

The cathode mass flow model describes the air flow behaviour inside the cathode. Air is mixture of gases, consisting primarily of 78 % nitrogen, 21 % oxygen, and other gases in less than 1 % like argon, carbon monoxide, carbon dioxide, neon, etc. It will only consider the main gases for the cathode part modelling, that is, nitrogen and oxygen. The model is generated using thermodynamic properties of air and mass conservation principle [Pukrushpan et al., 2004c]. On account of the mass continuity of both oxygen and nitrogen inside the cathode volume and ideal gas law, the partial pressure of both oxygen and nitrogen inside the cathode are yielded as

$$\begin{aligned} \frac{dp_{O_2}}{dt} &= \frac{RT_{fc}}{M_{O_2}V_{ca}}\left(W_{O_2,in} - W_{O_2,out} - W_{O_2,rct}\right), \\ \frac{dp_{N_2}}{dt} &= \frac{RT_{fc}}{M_{N_2}V_{ca}}\left(W_{N_2,in} - W_{N_2,out}\right), \end{aligned} \tag{2.26}$$

where $W_{O_2,in}$ and $W_{N_2,in}$ are, respectively the mass flow rate of oxygen and nitrogen entering the cathode, $W_{O_2,out}$ and $W_{N_2,out}$ are, respectively the mass flow rate of oxygen and nitrogen leaving the cathode, $W_{O_2,rct}$ is the rate of oxygen reacted, V_{ca} is the cathode volume and M_{O_2}, M_{N_2} are, the molar mass of oxygen and nitrogen, respectively.

The inlet mass flow rate of oxygen $W_{O_2,in}$ and nitrogen $W_{N_2,in}$ are calculated from the inlet cathode flow $W_{ca,in}$ as follows:

$$\begin{aligned} W_{O_2,in} &= \frac{x_{O_2,atm}}{1+\omega_{atm}} W_{ca,in}, \\ W_{N_2,in} &= \frac{1-x_{O_2,atm}}{1+\omega_{atm}} W_{ca,in}, \end{aligned} \tag{2.27}$$

where $x_{O_2,atm}$ is the oxygen mass fraction of the inlet air

$$x_{O_2,atm} = \frac{y_{O_2,atm}M_{O_2}}{M_{a,atm}} = \frac{y_{O_2,atm}M_{O_2}}{y_{O_2,atm}M_{O_2} + \left(1-y_{O_2,atm}\right)M_{N_2}}, \tag{2.28}$$

with the oxygen mole fraction $y_{O_2,atm} = 0.21$ for inlet air and the humidity ratio of inlet air ω_{atm} is expressed as

$$\omega_{atm} = \frac{M_v}{M_{a,atm}} \frac{\phi_{atm} p_{sat}\left(T_{fc}\right)}{p_{atm} - \phi_{atm} p_{sat}\left(T_{fc}\right)}, \tag{2.29}$$

where M_v is the molar mass of vapour, ϕ_{atm} is the relative humidify at ambient conditions (its value is set to 0.5) and $p_{sat}\left(T_{fc}\right)$ is the vapour saturation pressure. The saturation pressure p_{sat} depends on the temperature and is determined from the equation given in [Liu, 2005] as

$$\log_{10}\left(p_{sat}\right) = -1.69\times10^{-10}T_{fc}^4 + 3.85\times10^{-17}T_{fc}^3 - 3.39\times10^{-4}T_{fc}^2 + 0.143T_{fc} - 20.92, \tag{2.30}$$

where the saturation pressure p_{sat} is in kPa and the temperature T_{fc} is in Kelvin.

As mentionned above, the cathode inlet flow rate $W_{ca,in}$ is assumed to be similar to the supply manifold outlet flow rate $W_{sm,out}$ (2.25)

$$W_{ca,in} = k_{sm,out}\left(p_{sm} - p_{ca}\right), \tag{2.31}$$

where the cathode pressure p_{ca} is assumed to be spatially invariant, which is given by

$$p_{ca} = p_{O_2} + p_{N_2} + p_{sat}\left(T_{fc}\right), \tag{2.32}$$

where p_{O_2}, p_{N_2} and $p_{sat}\left(T_{fc}\right)$ are respectively, oxygen, nitrogen and vapour partial pressures.

The outlet mass flow rate of oxygen $W_{O_2,out}$ and nitrogen $W_{N_2,out}$ are calculated as a function of the cathode outlet mass flow rate $W_{ca,out}$ as follows:

$$\begin{aligned} W_{O_2,out} &= \frac{x_{O_2,ca}}{1+\omega_{ca,out}} W_{ca,out}, \\ W_{N_2,out} &= \frac{1-x_{O_2,ca}}{1+\omega_{ca,out}} W_{ca,out}, \end{aligned} \tag{2.33}$$

where $x_{O_2,ca}$, $\omega_{ca,out}$ are the oxygen mass fraction, the humidity ratio inside the cathode, respectively, which are defined as

$$\begin{aligned} x_{O_2,ca} &= \frac{y_{O_2,ca} M_{O_2}}{y_{O_2,ca} M_{O_2} + \left(1 - y_{O_2,ca}\right) M_{N_2}}, \\ \omega_{ca,out} &= \frac{M_v}{y_{O_2,ca} M_{O_2} + \left(1 - y_{O_2,ca}\right) M_{N_2}} \frac{p_{sat}}{p_{O_2} - p_{N_2}}. \end{aligned} \tag{2.34}$$

Unlike the inlet flow, the oxygen mole fraction of the cathode outlet flow $y_{O_2,ca}$ is not constant because oxygen is reacted, which is calculated as

$$y_{O_2,ca} = \frac{p_{O_2}}{p_{O_2} + p_{N_2}}. \tag{2.35}$$

Using (2.34) and (2.35), (2.33) can be rewritten as

$$W_{O_2,out} = \frac{M_{O_2} p_{O_2}}{M_{O_2} p_{O_2} + M_{N_2} p_{N_2} + M_v p_{sat}} W_{ca,out}, \tag{2.36}$$

$$W_{N_2,out} = \frac{M_{N_2} p_{N_2}}{M_{O_2} p_{O_2} + M_{N_2} p_{N_2} + M_v p_{sat}} W_{ca,out}. \tag{2.37}$$

The cathode outlet mass flow rate $W_{ca,out}$ is governed by nozzle equations [Pukrushpan et al., 2002b] and is calculated as follows:

$$W_{ca,out} = \frac{C_D A_T}{\sqrt{RT_{fc}}} \sqrt{\frac{2\gamma}{\gamma - 1}} \left(p_{ca}\right) \left(\frac{p_{atm}}{p_{ca}}\right)^{\frac{1}{\gamma}} \sqrt{1 - \left(\frac{p_{atm}}{p_{ca}}\right)^{\frac{\gamma-1}{\gamma}}}, \tag{2.38}$$

where C_D is the discharge coefficient of the nozzle, A_T is the opening area of the nozzle.

The amount of oxygen reacted $W_{O_2,rct}$ is calculated using electrochemistry principles, which is a function of the stack current I_{st}, and written as

$$W_{O_2,rct} \;=\; M_{O_2} \frac{nI_{st}}{2F}. \tag{2.39}$$

2.5 Dynamic model with four states

Equations (2.26), (2.19) and (2.23) can be represented by the following four-state dynamic model

$$\dot{x}_1 = c_1 \left(x_4 - \chi - c_2\right) - \frac{c_3 x_1 \alpha}{c_4 x_1 + c_5 x_2 + c_6} - c_7 w, \tag{2.40a}$$

$$\dot{x}_2 = c_8 \left(x_4 - \chi - c_2\right) - \frac{c_3 x_2 \alpha}{c_4 x_1 + c_5 x_2 + c_6}, \tag{2.40b}$$

$$\dot{x}_3 = -c_9 x_3 - \frac{c_{10}}{x_3} \left[\left(\frac{x_4}{c_{11}}\right)^{c_{12}} - 1\right] y_3 + c_{13} u, \tag{2.40c}$$

$$\dot{x}_4 = c_{14} \left[1 + c_{15} \left[\left(\frac{x_4}{c_{11}}\right)^{c_{12}} - 1\right]\right] \times \left[y_3 - c_{16} \left(x_4 - \chi - c_2\right)\right], \tag{2.40d}$$

where

$$\begin{aligned} \chi &= p_{O_2} + p_{N_2} \;= x_1 + x_2, \\ \alpha &= W_{ca,in} \;= c_{17} \left(\chi - c_2\right) \left(\frac{c_{11}}{\chi - c_2}\right)^{c_{18}} \sqrt{1 - \left(\frac{c_{11}}{\chi - c_2}\right)^{c_{12}}}, \end{aligned} \tag{2.41}$$

and coefficients c_i, for $\{i = 1, \ldots, 24\}$, are defined in Table A.2 in Appendix A. The vector of states $x \in \mathbb{R}^4$ is associated to the oxygen and nitrogen partial pressures in the cathode channel, the rotational speed of the motor shaft in the compressor and the air pressure in the supply manifold, respectively [Gruber et al., 2008]. Then,

$$x \;=\; \begin{bmatrix} p_{O_2} & p_{N_2} & \omega_{cp} & p_{sm} \end{bmatrix}^T. \tag{2.42}$$

2.5.1 System inputs and outputs

The inputs of the fuel-cell system are (i) the compressor motor voltage $u = v_{cm}$ that is considered as a control input, it allows the manipulation of the angular speed of the compressor, and thus, the oxygen supply to the fuel-cell stack, and (ii) the stack current $w = I_{st}$ that is considered as a measurable disturbance of the system.

The vector of the fuel-cell system outputs $y \in \mathbb{R}^3$ is given by

$$y = \begin{bmatrix} y_1 & y_2 & y_3 \end{bmatrix}^T = \begin{bmatrix} p_{sm} & V_{st} & W_{cp} \end{bmatrix}^T, \tag{2.43}$$

where the supply manifold pressure p_{sm}, the stack voltage V_{st} and the compressor air flow rate W_{cp} are given in (2.23), (2.17) and (2.21), respectively.

2.5.2 System performances

The performance variables $z \in \mathbb{R}^2$, with z_1 as net power and z_2 as OER, are given by

$$z = \begin{bmatrix} z_1 & z_2 \end{bmatrix}^T = \begin{bmatrix} P_{net} & \lambda_{O_2} \end{bmatrix}^T. \tag{2.44}$$

The fuel-cell net power z_1 is the difference between the power produced by the stack P_{st} and the power consumed by the compressor P_{cm}. Thus, the net power can be expressed as

$$z_1 \;=\; P_{st} - P_{cm} = \; y_2 w - c_{21} u \left(u - c_{22} x_3\right), \tag{2.45}$$

where the stack power P_{st} and the compressor power P_{cm} are given in (2.18) and (2.22), respectively.

The OER z_2, which is defined by the amount of oxygen provided, denoted by $W_{O_2,in}$, and the amount of oxygen reacted, denoted as $W_{O_2,rct}$, is expressed as

$$z_2 \;=\; \frac{W_{O_2,in}}{W_{O_2,rct}} = \; \frac{c_{23}\left(x_4 - \chi - c_2\right)}{c_{24} w}. \tag{2.46}$$

2.6 Steady-state analysis

The air supply system has a compressor motor voltage as the only control actuator. Two variables considered for the control performance are the fuel-cell system net power, z_1, and the OER, z_2. If the value of z_2 is quite low, even though higher than 1, it is likely to cause *Oxygen starvation*. This phenomenon can cause a short circuit and a hot spot on the surface of the fuel-cell membrane. On the other hand, higher values of z_2 will drive the compressor motor to consume more power and, therefore, towards lower efficiency operating conditions. As a result, it is necessary to state the optimal value of z_2 that maximizes the net power z_1. The relation between the OER and the net power for different stack currents is called the *performance curve* (see Figure 2.3). This curve is obtained from a complete off-line analysis of the open-loop PEMFC air supply system, in light of stack-current changes and a wide range of OER values. The nonlinear model in (2.40) corresponds to a 75 kW high-pressure FC stack fed by a 14 kW turbo compressoor

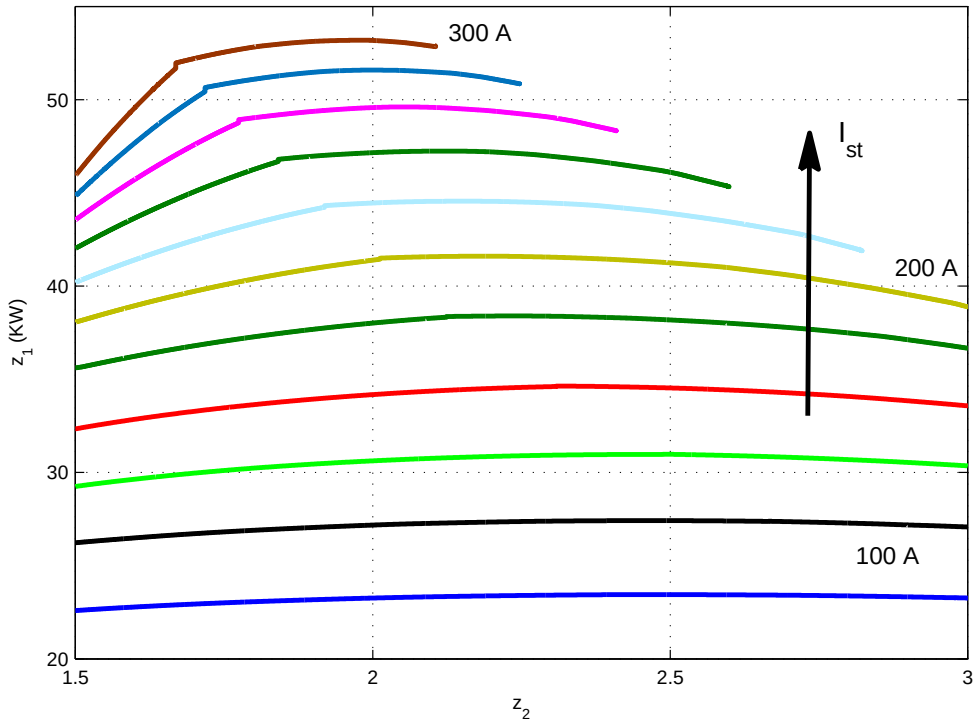

Figure 2.3: z_2 performance curve for different stack currents.

used in Ford P2000 FC electric vehicle. The nominal model parameters are listed in Table A.3 in Appendix A. It can be seen from Figure 2.3 that the maximum net power z_1 is achieved at an OER z_2 between 1.9 and 2.5 for stack-current variations between 100-300 A. However, in order to get the best trade-off between safety and efficiency, it is necessary to regulates z_2 around an optimal value $z_{2,opt} = 2.05$ as discussed in [Kunusch et al., 2012].

2.7 Dynamic simulation

A stack-current changes, depicted in Figure 2.5(a), is applied to the fuel-cell system as a disturbance. The stack current rises up from 100 A to 150 A at t=5 s. Next, after 5 s, it increases by 50 A. This increment stopped when the stack current reaches 250 A. After 20 s, the current falls to 220 A. Finally, at time t=25 s, it increases again from 220 A to 250 A (Figure 2.5(a)). A compressor motor input voltage, shown in Figure 2.5(b), is also applied to the fuel-cell system as a control input. The control input is deduced from a static feed-forward controller based on the measurement of the stack current, as shown in Figure 2.4.

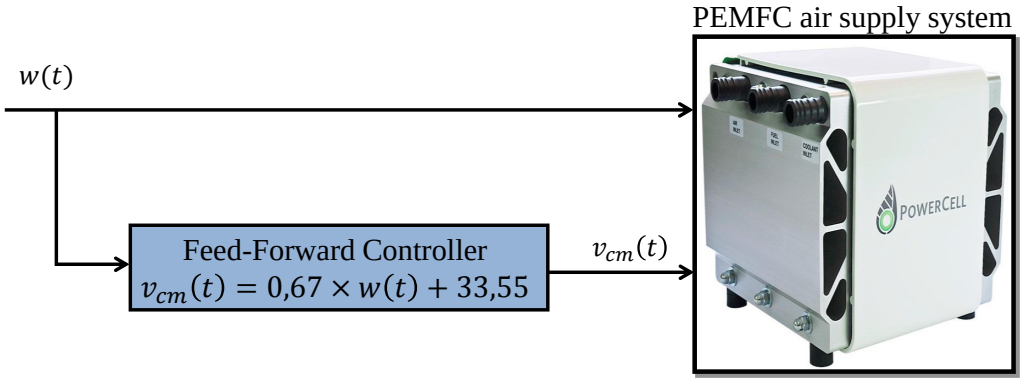

Figure 2.4: Static feedforward control for fuel-cell system.

During a positive current change, the OER drops, as shown in Figure 2.5(e), due to the reduction of oxygen in the cathode channel. This, in turn, causes an important decrease in the stack voltage, as shown in Figure 2.5(c). One can immediately remark from Figure 2.5(b) that the compressor voltage responds instantaneously during the current steps (at 5, 10, 15, 20, and 25 seconds), there is still a transient effect in the stack voltage, and consequently in the stack power and the net power (Figure 2.5(d)), as a result of the transient behaviour in oxygen partial pressure (Figure 2.5(f)).

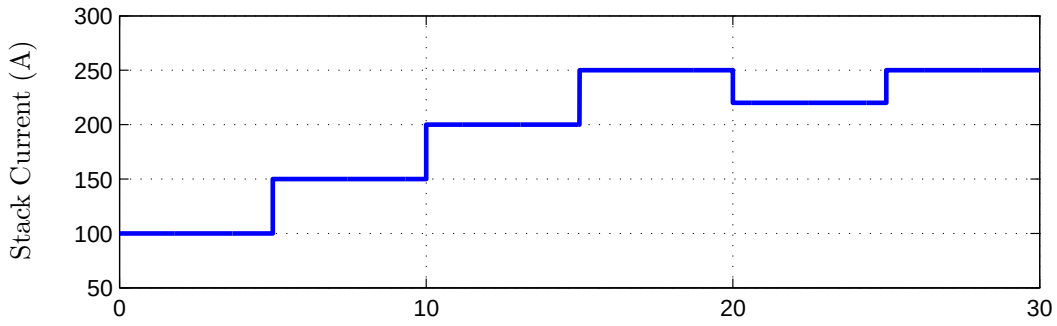

(a) Stack-current

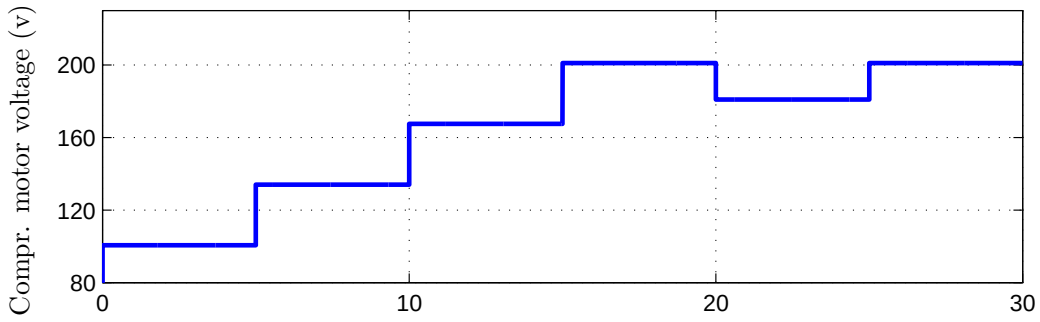

(b) Compressor motor voltage

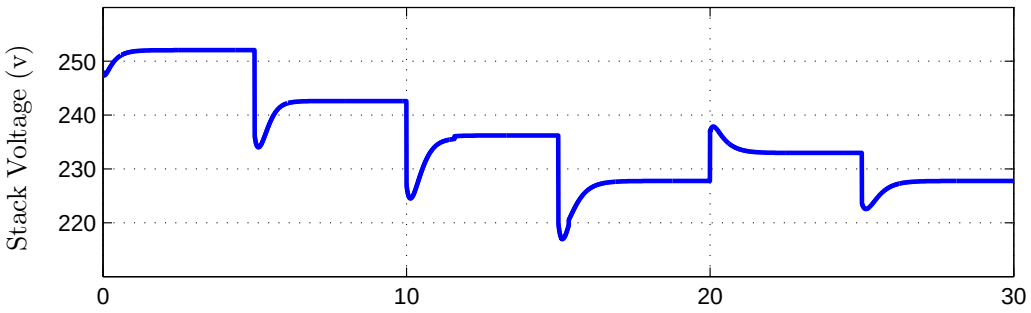

(c) Stack voltage

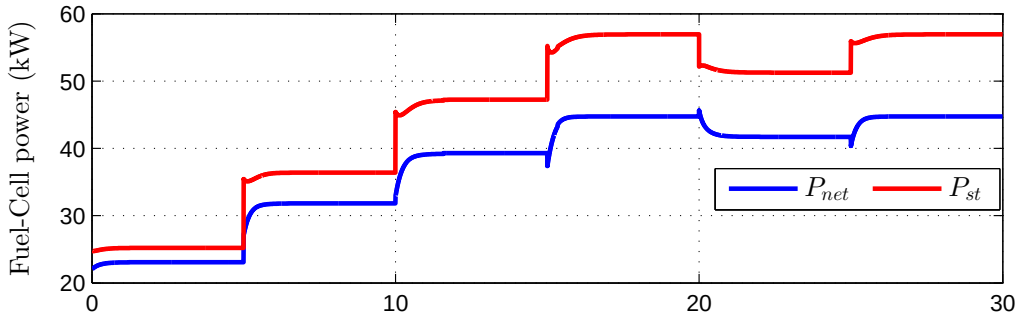

(d) Stack and net power

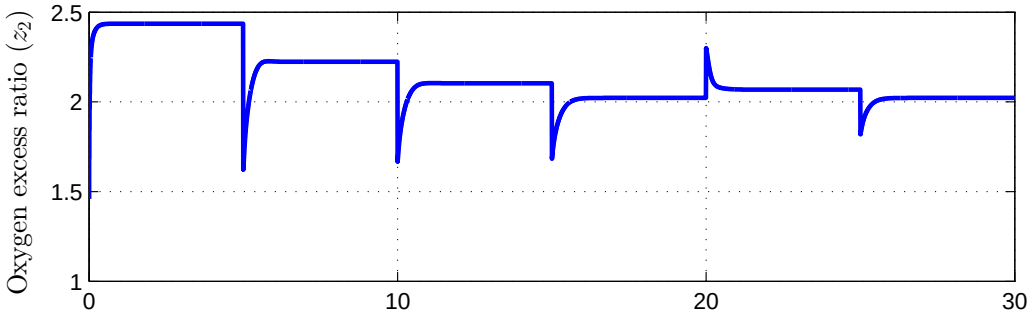

(e) Oxygen excess ratio

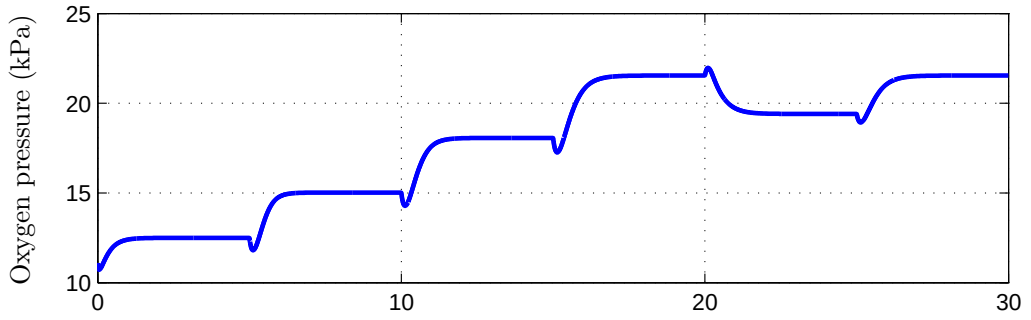

(f) Oxygen pressure

Figure 2.5: Dynamic simulation results of the fuel-cell system model for a series of input stack-current changes.

2.8 Summary

This chapter presents the main concepts about PEMFC systems, showing the expressions corresponding to the fuel-cell voltage and efficiency. Also, different approaches for modelling are presented. Accordingly, a review of PEMFC model has been done. Fuel-cell models may be classified into one of three categories: fuel-cell performance models, steady-state fuel-cell system models or dynamic fuel-cell system models. Among these models, a model widely used in the literature for control purposes is described in detail. Using this model, the influence of the auxiliary equipment in the system efficiency is analyzed and the model is also used to study the optimal operation of a PEMFC system, finding an optimal compressor voltage for each current load that maximizes the net output power. Similarly, this dynamic model is used as a base model in the other chapters of this thesis.

Chapter 3

Advanced Control Strategies for PEMFC Air Supply Systems

“ Acquire wisdom from the story of those who have already passed. ”

Uthman ibn Affan

3.1 Introduction

As discussed in the previous chapter, the control objective is to adjust the Oxygen Excess Ratio (OER) at a given setpoint in order to prevent oxygen starvation and damage of the fuel-cell stack. Accordingly, this chapter presents two advanced control strategies based on artificial intelligence and sliding mode control techniques. Firstly, a hybrid fuzzy PID (HFPID) controller is developed which consists of three parts: a fuzzy-logic controller (FLC), a fuzzy-based self-tuned PID (FSTPID) controller and a fuzzy supervisor. Secondly, a twisting controller based on sliding mode control is designed. Then, the designed control strategies are applied to the model of the PEMFC air supply system and the simulation results for stack-current changes, model uncertainties, and comparative study are presented in detail in Section 3.5. This chapter has been the subject of several papers [Baroud et al., 2015, Baroud et al., 2017b]. At the end of this chapter, a comparative study of both two controllers performances is presented.

3.2 Control problem formulation

In this section, the control objective and the PEMFC air supply system model are remembered. The control objective is to define the compressor motor input voltage, v_{cm}, in order to maintain $z_2 = 2.05$ and achieve the desired fuel-cell system net power under variable load operation, (I_{st}), which is considered as an external disturbance to the fuel-cell system. The resulting control problem is defined as follows (Figure 3.1):

$$\begin{cases} \dot{x}_1 &= c_1 \left(x_4 - \chi - c_2\right) - \dfrac{c_3 x_1 \alpha}{c_4 x_1 + c_5 x_2 + c_6} - c_7 w, \\ \dot{x}_2 &= c_8 \left(x_4 - \chi - c_2\right) - \dfrac{c_3 x_2 \alpha}{c_4 x_1 + c_5 x_2 + c_6}, \\ \dot{x}_3 &= -c_9 x_3 - \dfrac{c_{10}}{x_3} \left[\left(\dfrac{x_4}{c_{11}} \right)^{c_{12}} - 1 \right] y_3 + c_{13} u, \\ \dot{x}_4 &= c_{14} \left[1 + c_{15} \left[\left(\frac{x_4}{c_{11}} \right)^{c_{12}} - 1 \right] \right] \times \left[y_3 - c_{16} \left(x_4 - \chi - c_2 \right) \right], \end{cases} \tag{3.1}$$

where

$$\begin{cases} x &= \begin{bmatrix} p_{O_2} & p_{N_2} & \omega_{cp} & p_{sm} \end{bmatrix}^T, \\ u &= v_{cm}, \\ w &= I_{st}, \\ y &= \begin{bmatrix} y_1 & y_2 & y_3 \end{bmatrix}^T = \begin{bmatrix} p_{sm} & V_{st} & W_{cp} \end{bmatrix}^T, \\ z &= \begin{bmatrix} z_1 & z_2 \end{bmatrix}^T = \begin{bmatrix} P_{net} & \lambda_{O_2} \end{bmatrix}^T \end{cases} \tag{3.2}$$

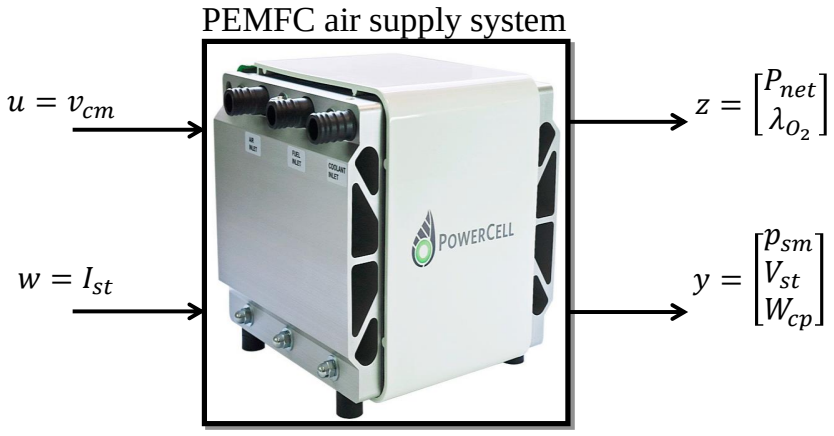

Figure 3.1: Model setup scheme.

Next, a brief survey of existing control methods for PEMFC air supply system will be presented.

3.3 Review on PEMFC air supply system control

During recent years, many control strategies have been proposed for PEMFC air supply system to maintain optimal OER, and thus maximization of system net power. It can be cited, among others, linear control methods based on model linearization such as Linear Quadratic Regulator (LQR), proportional integral (PI) plus dynamic feed-forward controller are proposed in [Pukrushpan et al., 2004b] and [Niknezhadi et al., 2011]. These controllers attain good transient regulation but loss robustness facing the variation of the fuel-cell system parameters. Kunusch et al. [Kunusch et al., 2009] were the first use the super-twisting algorithm, based on the second order sliding mode (SOSM) control, for the PEMFC air supply system. Matraji et al. [Matraji et al., 2013] have proposed adaptive SOSM control strategy, which is based on two cascade adaptive SOSM controllers. The use of adaptive controllers gives better results than fixed parameters super-twisting control. Although the controllers based on SOSM control strategy has been validated experimentally. Different topologies of fuzzy-logic control (FLC) are proposed. In [Ou et al., 2015], feed-forward fuzzy PID is developed to adapt PID parameters to regulate air flow rate using on-line fuzzy logic optimization loop. Beirami et al. [Beirami et al., 2015] have proposed an optimal PID plus fuzzy controller. The controller parameters are optimized using a self-adaptive differential algorithm. An efficient controller combines conventional PID and fuzzy logic is addressed in [Baroud et al., 2016a].

Feroldi et al. [Basualdo et al., 2012] have reported a control architecture based on Adaptive Predictive Control with Robust Filter (APCWRF). The APCWRF is designed for controlling the compressor motor voltage. The objectives of this control strategy are to regulate both the fuel-cell voltage and OER in the cathode. Works [Chang and Moura, 2009, Almeida and Simoes, 2005] have used optimal control technique to control the air supply PEMFC-based systems. Gain scheduled Linear Parameter-Varying (LPV) control and fault tolerant unfalsified control are presented in [Bianchi et al., 2014, Bianchi et al., 2015], respectively. All these control strategies are applied for the regulation of the OER in the PEMFC with different degrees of success.

However, these controllers impose certain limitations on the tracking performance and none of them consider uncertainties of system parameters. These drawbacks are addressed in this chapter. In the following two sections, two types of controllers for z_2 regulation

are developed. The first is considered as a novel combining method based on conventional PID and fuzzy-logic controllers. This proposal bears two major advantages: the strengths of both PID and fuzzy-logic controllers are benefited while the hybrid controller suitably performs with uncertainties of nominal parameters of the PEMFC-based system. The second is based on the SOSM control and use the twisting algorithm. This controller is capable of avoiding chattering effects, converging to the reference in finite time under load variations and parametric uncertainties.

3.4 Hybrid fuzzy PID controller design

The proposed control scheme is separated into three parts: a fuzzy logic controller, a fuzzy-based self-tuned PID controller and a fuzzy supervisor. The fuzzy supervisor, based on fuzzy rules, and depending on the error between the current value of OER and its setpoint value, is used to determine signals that have the greatest effect over the control system. To fully understand the design method of this controller, it is better to present mainly the following sub-controllers:

- PID controller,
- Fuzzy logic controller,
- Fuzzy-based self-tuned PID controller.

3.4.1 PID controller

The PID control scheme, shown in Figure 3.2, is widely used in industrial process control due to its simple structure and to its robust performance for both linear and nonlinear systems. The mathematical expression of this controller is given by

$$u_{PID}(t) = k_p e(t) + k_i \int e(t)dt + k_d \frac{de(t)}{dt}, \tag{3.3}$$

where $e\,(t)$ is the feedback error, that is defined in the case of this paper as the difference between the current value of $z_2\,(t)$ and its setpoint value, i.e.,

$$e(t) = z_2(t) - z_{2,opt}, \tag{3.4}$$

and the parameters k_p, k_i and k_d are known as proportional gain, integral gain and derivative gain, respectively.

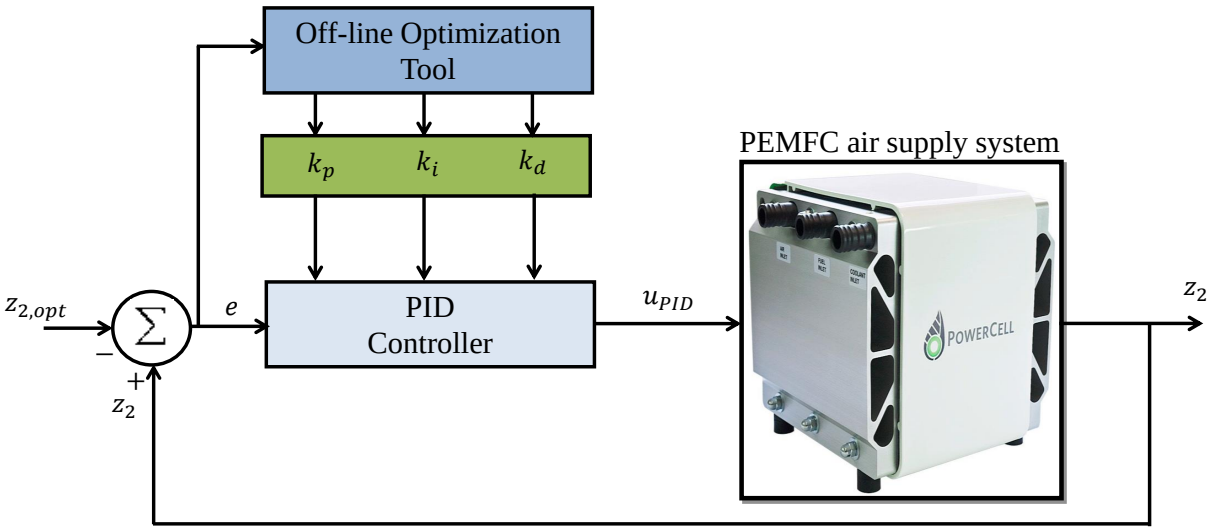

Figure 3.2: Structure of PID controller.

The three PID gains design, k_p, k_i and k_d, is not easy task due to the complexity of the PEMFC system model. Therefore, to obtain the corresponding PID parameters an optimization tool in Matlab is needed [O'Dwyer, 2009]. This command is called `fminsearch`, which finds the minimum of the quadratic cost function specified by

$$\int_0^{T_f} (z_2(t) - z_{2,opt})^2. \tag{3.5}$$

3.4.2 Fuzzy Logic controller

Fuzzy logic was firstly proposed by Lotfi A. Zadeh in 1965 to control plants that were difficult to model [Zadeh, 1965]. The application of fuzzy logic in control problems was firstly introduced by Mamdani in 1974 [Mamdani, 1974]. Fuzzy logic is one of the most versatile control techniques due to its simplicity, efficiency and robustness against the system dynamics variation. The fuzzy logic controller synthesize does not require the precise information of system. It has been successfully used in the PEMFC systems with better performance with respect to the PID controller counterpart [Sinthipsomboon et al., 2012,Fereidouni et al., 2015]. There are three main parts in the fuzzy logic controller (FLC) as shown in Figure 3.3:

- Fuzzification interface converts a crisp input to a fuzzy value by using fuzzy sets,
- Rule base and inference system generates a result for each suitable rule, then combines the results of the rules,

- Defuzzification interface converts the combined result back into a specific control output value.

For the fuzzification and defuzzification interfaces, this controller considers five membership functions, which are justified by the required precision of the closed-loop system.

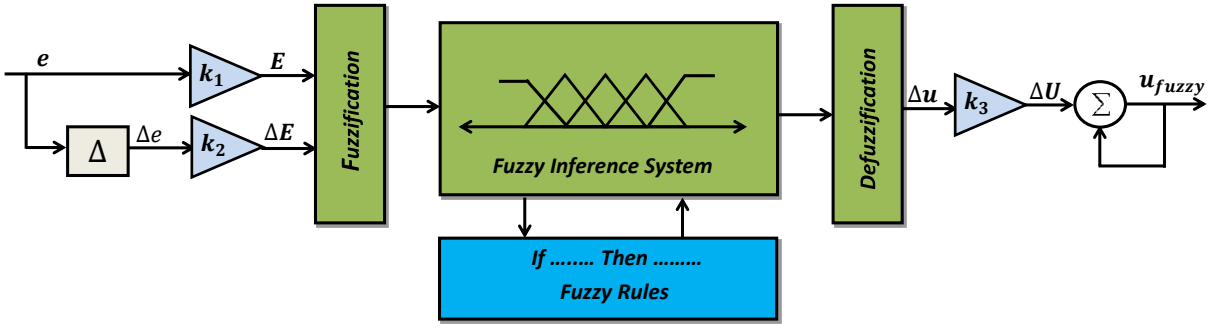

Figure 3.3: Structure of fuzzy controller.

In Figure 3.3, variables $e, \Delta e, E$ and ΔE indicate error, derivative of error, normalized error and normalized derivative of error, respectively, while the parameters k_1, k_2 and k_3 are input and output scaling factors, which have an important effect on the system dynamic behaviour. The scaling factors k_1, k_2 and k_3 may be selected, based on control experience and a lot of simulations, among other advanced meta-heuristics approaches [Bouallègue et al., 2015]. In Table 3.1, the fuzzy linguistic variables are NB, N, Z, P and PB, which represent negative big, negative, zero, positive and positive big, respectively. The basic form of the fuzzy control rules is: "if the error E is Z and the error derivation ΔE is Z, then the fuzzy control output Δu is Z".

Table 3.1: Linear rule base for FLC.

Δu		E				
		NB	**N**	**Z**	**P**	**PB**
ΔE	**NB**	NB	NB	N	N	Z
	N	NB	N	N	Z	P
	Z	N	N	Z	P	P
	P	N	Z	P	P	PB
	PB	Z	P	P	PB	PB

The membership functions of the FLC inputs and output are respectively shown in Figures 3.4(a) and 3.4(b).

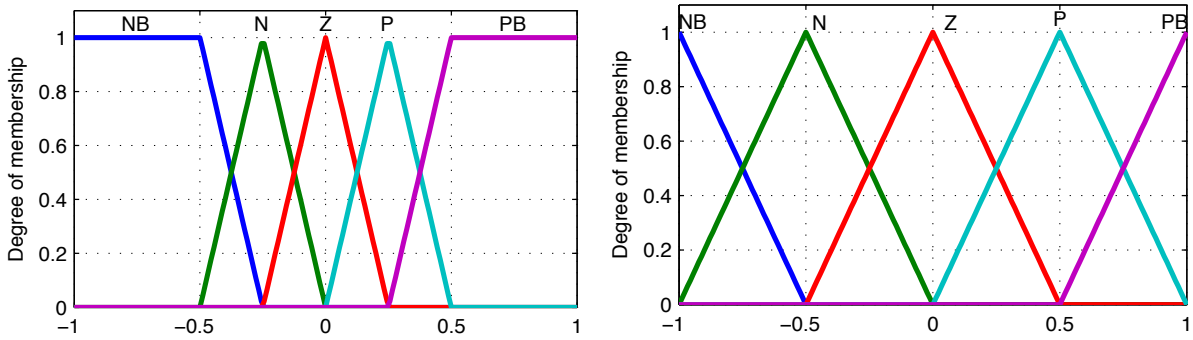

(a) E and ΔE (b) Δu

Figure 3.4: Membership functions of the FLC.

3.4.3 Fuzzy-based Self-Tuned PID controller

The coefficients of the classical PID controller are not always tuned for the nonlinear plant with unpredictable parameter variations. Hence, it is necessary to automatically tune the PID parameters. The fuzzy-based self-tuned PID (FSTPID) controller is designed such that the three-term control k_p, k_i and k_d are tuned by using a fuzzy tuner [Baroud et al., 2015, Zulfatman and Rahmat, 2009]. The OER control scheme that will be considered in this subsection is shown in Figure 3.5. The output of the FSTPID controller is given by

$$u_{FSTPID}(t) = k_p e(t) + k_i \int e(t)dt + k_d \frac{de(t)}{dt}. \tag{3.6}$$

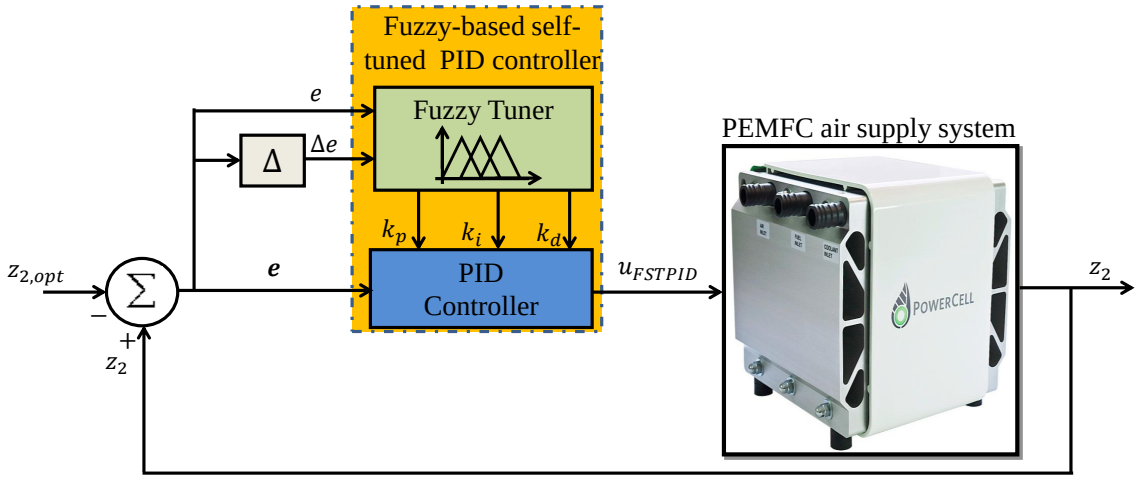

Figure 3.5: Fuzzy self-tuning PID controller structure.

Further details about the fuzzy tuner are shown in Figure 3.6. In that figure, there are two inputs to the fuzzy inference: e and Δe, and three outputs: k_p, k_i and k_d. In Figure 3.6, variables $e, \Delta e, E$ and ΔE indicate error, derivative of error, normalized error and normalized derivative of error, respectively, while the parameters k_1, k_2 and k_3, k_4 and k_5 are input/output scaling factors.

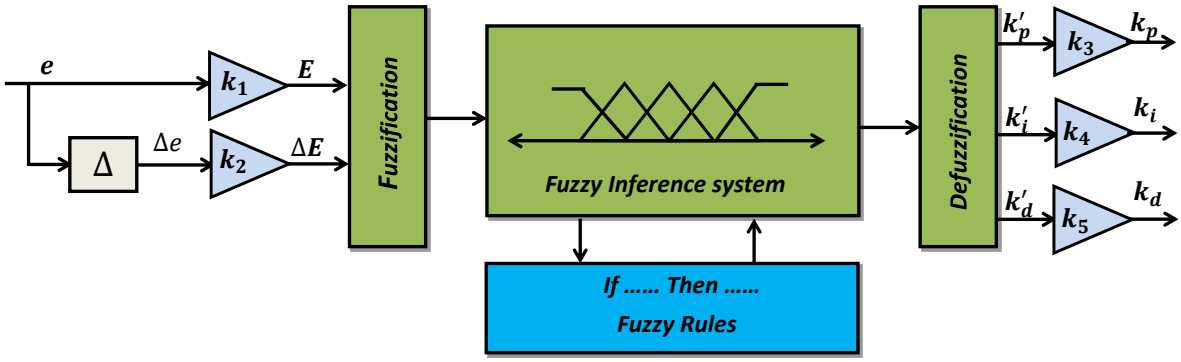

Figure 3.6: Structure of the fuzzy tuner.

In order to determine the domain of each PID parameter, several simulations of the closed-loop system were carried out. Therefore, domains for those parameters were defined as $k_p \in [0, 1000]$, $k_i \in [0, 400]$ and $k_d \in [0, 1]$. Thus, they can be scaled over the fuzzy interval $[0, 1]$ as follows:

$$k'_p = \frac{k_p - k_p^{\min}}{k_p^{\max} - k_p^{\min}} = \frac{k_p}{k_3}, \tag{3.7a}$$

$$k'_i = \frac{k_i - k_i^{\min}}{k_i^{\max} - k_i^{\min}} = \frac{k_i}{k_4}, \tag{3.7b}$$

$$k'_d = \frac{k_d - k_d^{\min}}{k_d^{\max} - k_d^{\min}} = \frac{k_d}{k_5}, \tag{3.7c}$$

with $k_3 = 1000$, $k_4 = 400$ and $k_5 = 1$, while the fuzzy interval for E and ΔE is $[-1, 1]$.

The fuzzy subsets of inputs and outputs are negative, zero and positive. The membership functions of inputs and outputs are respectively depicted in Figures 3.7(a) and 3.7(b). As shown in Tables (3.2, 3.3 and 3.4), the columns represent the normalized feedback error E and the rows represent the normalized derivative of error ΔE. Each pair $(E, \Delta E)$ determines the output parameters corresponding to k'_p, k'_i and k'_d.

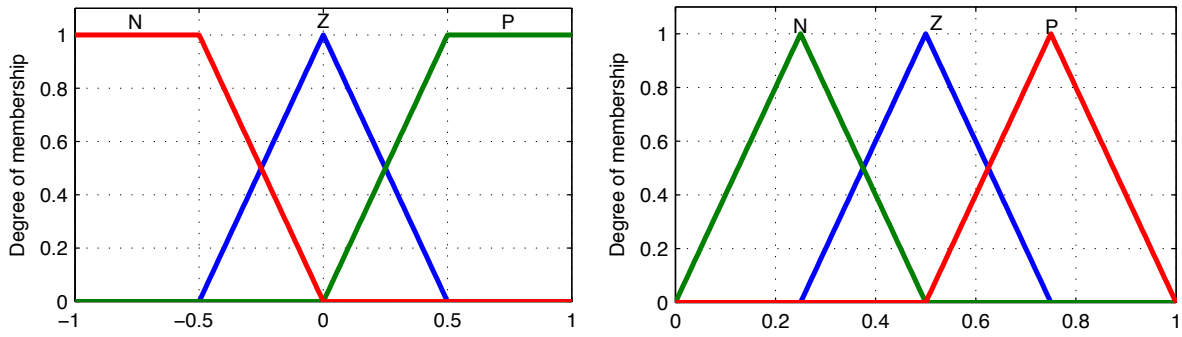

(a) E and ΔE (b) k'_p, k'_i and k'_d

Figure 3.7: Membership functions of fuzzy tuner.

Table 3.2: Fuzzy rules for FSTPID -proportional action-

k'_p		E		
		N	**Z**	**P**
ΔE	**N**	Z	Z	P
	Z	P	Z	Z
	P	P	Z	N

Table 3.3: Fuzzy rules for FSTPID -integral action-

k'_i		E		
		N	**Z**	**P**
ΔE	**N**	N	N	N
	Z	Z	Z	N
	P	P	P	P

Table 3.4: Fuzzy rules for FSTPID -deravative action-

k'_d		E		
		N	**Z**	**P**
ΔE	**N**	N	N	N
	Z	Z	N	N
	P	P	N	N

The fuzzy tuner utilized in this controller considers product-sum as the inference method, centre of gravity as the defuzzification method and triangular-shaped as the membership functions for the inputs and outputs. In addition, the relation between the inputs and the outputs of the fuzzy tuner is calculated by [Ou et al., 2015] as follows:

$$k'_p = \frac{\sum_{k=1}^{m} \mu_{k'_{pk}}(C_p)\, C_{pk}}{\sum_{k=1}^{m} \mu_{k'_{pk}}(C_p)}, \tag{3.8}$$

where C_{pk} is the central value of fuzzy set at the $k-th$ rule and $\mu_{k'_{pk}}$ is the output membership value. The same result can be calculated for both k'_i and k'_d.

Once the sub-controllers are designed, the design of the HFPID can be completed, without difficulty. This controller derives its strength from the advantages of both fuzzy and PID controllers together. In addition, the gain adjustment of PID with a fuzzy tuner is included to ameliorate the controller. The control scheme in Figure 3.8 consists of three parts: a fuzzy-based self-tuned PID controller, a fuzzy controller, and a fuzzy supervisor. Based on the fuzzy rules and depending on the error between the current value of OER and its setpoint value, the fuzzy supervisor determines, in a suitable way, when and how to switch the controller. If the output value of the system is far away from the setpoint, the fuzzy controller has the largest effect on the control system. Similarly, when the output value is near the setpoint value, the fuzzy-based self-tuned PID controller has, in turn, the largest effect over the system rather than the fuzzy controller. Notice that the fuzzy-based self-tuned PID controller has better accuracy near the setpoint.

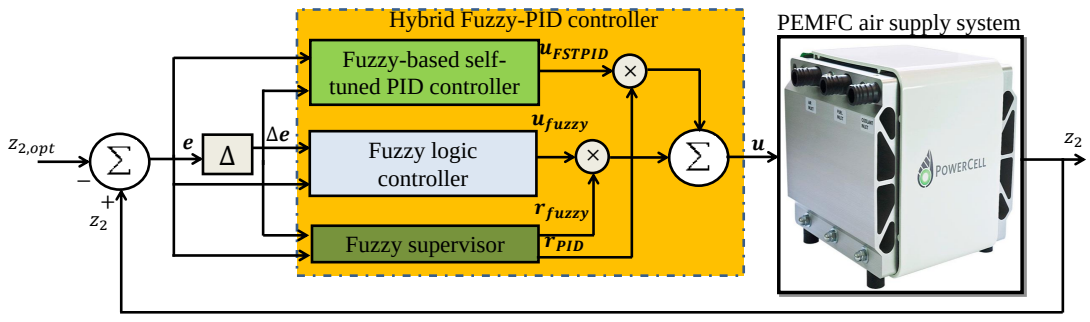

Figure 3.8: Proposed hybrid fuzzy PID controller structure.

As shown in Figure 3.8, the inputs of the fuzzy supervisor are e and Δe, and the fuzzy linguistic variables of input are N, Z and P. The output of the fuzzy supervisor is the

fuzzy control coefficient r_{fuzzy}, and the fuzzy linguistic variables related to the output are P and PB. The fuzzy inference rules are shown in Table 3.5. The membership functions of inputs and output are shown in Figures 3.9(a) and 3.9(b), respectively.

The output of the HFPID controller is given by the following expression:

$$u(t) = r_{PID} \times u_{FSTPID}(t) + r_{fuzzy} \times u_{fuzzy}(t). \tag{3.9}$$

where r_{PID} and r_{fuzzy} are the adjustment coefficients of both PID and fuzzy control law. Moreover, $r_{PID} + r_{fuzzy} = 1$.

Table 3.5: Linear rule base for fuzzy supervisor

r_{fuzzy}		E		
		N	**Z**	**P**
ΔE	**N**	P	P	P
	Z	PB	P	PB
	P	P	P	P

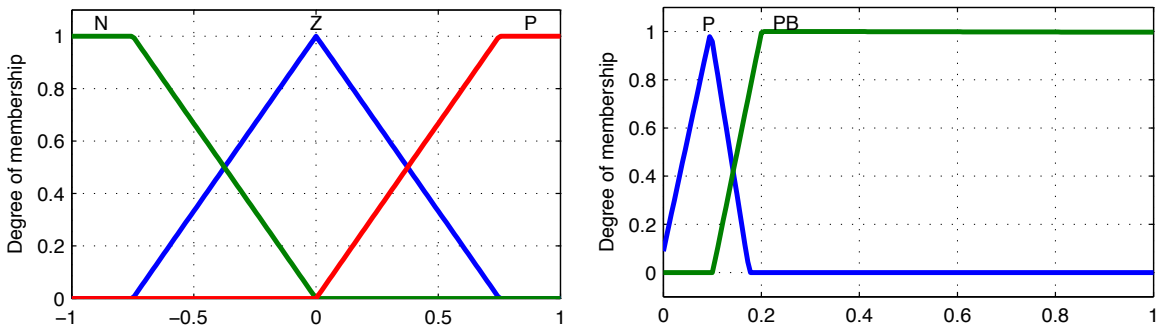

(a) E and ΔE (b) r_{fuzzy}

Figure 3.9: Membership functions of the fuzzy supervisor.

Based on the proposed control structure of Figure 3.8, the design procedure of the hybrid fuzzy PID controller can be outlined as follows:

- Step 1: Design the fuzzy logic controller as in Subsection 3.4.2.
- Step 2: Design the fuzzy-based self-tuned PID controller as in Subsection 3.4.3.
- Step 3: Design the fuzzy supervisor using e and Δe.
- Step 4: Calculate the global control $u(t)$ from (3.13).

Remark 1 *Concerning the stability issue, it has been said in [Zimmermann, 2001] that the stability analysis appears something unrelated for fuzzy controllers. They are implicitly supposed robust since they are based on the human experience. And when the PID controller is placed within the loop, the stability feature should be related to the PID controllers. This analysis is deeply discussed in [Ang et al., 2005].*

3.5 HFPID controller simulation results

To verify the performance, the robustness and the efficiency of the proposed control strategy, detailed simulations are performed and analysed. Simulations are divided into three groups: performance results, sensibility analysis and comparative study. The numerical parameters used in the simulation are given in Table A.3 in Appendix A. The main aim of the design of these controllers is to regulate the OER at a setpoint value, which is assumed equal to 2.05. With this setpoint, it can be assured that the PEMFC air supply system works within the range of its maximum net power for each load variation while the oxygen starvation is avoided.

The performance indices of the PEMFC air supply control system include the Integral Squared Error (ISE)

$$ISE = \int_0^{t_f} \mid e\left(t\right) \mid^2 dt, \tag{3.10}$$

the Integral Absolute Error (IAE)

$$IAE = \int_0^{t_f} \mid e\left(t\right) \mid dt, \tag{3.11}$$

and the Integral Time-weighted Absolute Error (ITAE)

$$ITAE = \int_0^{t_f} t \mid e\left(t\right) \mid dt. \tag{3.12}$$

3.5.1 Performance results

This subsection shows a comparison study between the control strategies presented previously, i.e., PID, fuzzy logic, fuzzy-based self-tuned PID and the hybrid fuzzy PID. The dynamic behaviour of z_2 under different stack-current variation (see Figure 3.10), using PID, FLC, FSTPID and HFPID control strategies is shown in Figure 3.11. The stack current rises up from 150 A to 200 A at t=5 s. Next, after 5 s, it increases by 50 A. This increment stopped when the stack current reaches 300 A. After 20 s, the current falls to 270 A. Finally, at time t=25 s, it increases again from 270 A to 300 A (Figure 3.10). It can

be seen from Figure 3.11 that all the applied control strategies adjust z_2 at the setpoint with a satisfactory tracking performance.

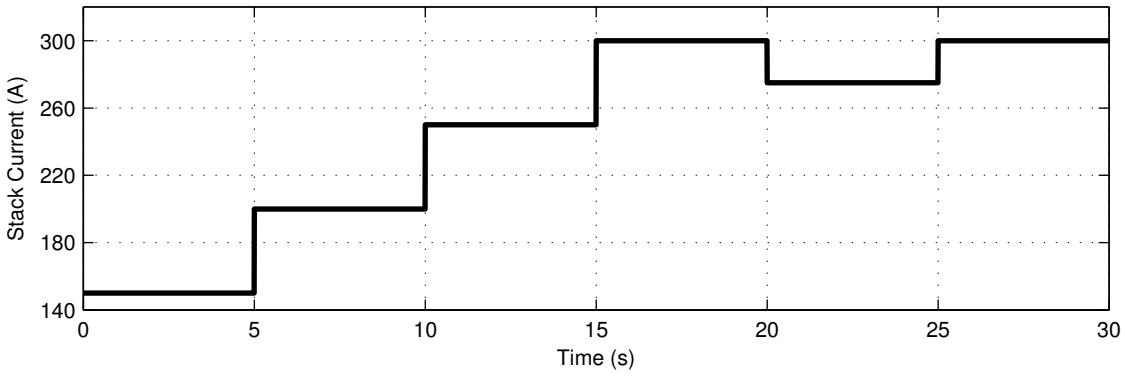

Figure 3.10: Stack-current variation.

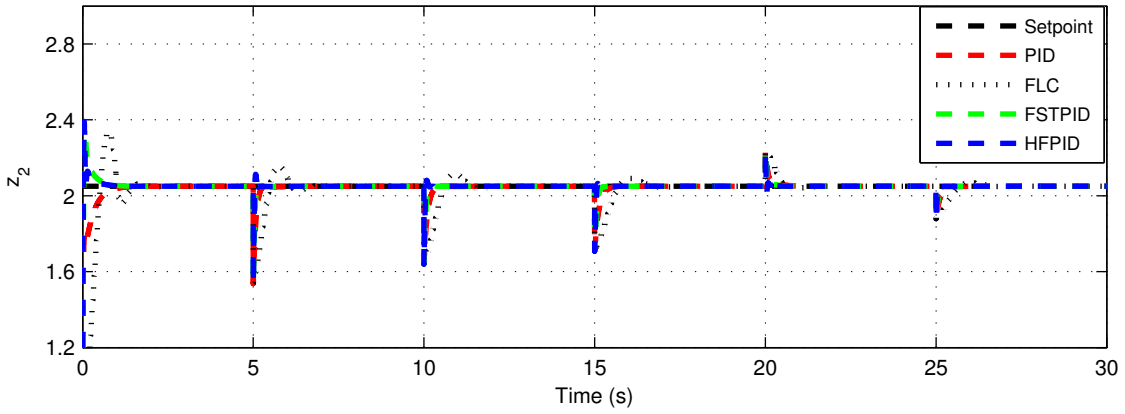

Figure 3.11: Response of OER for different control strategies.

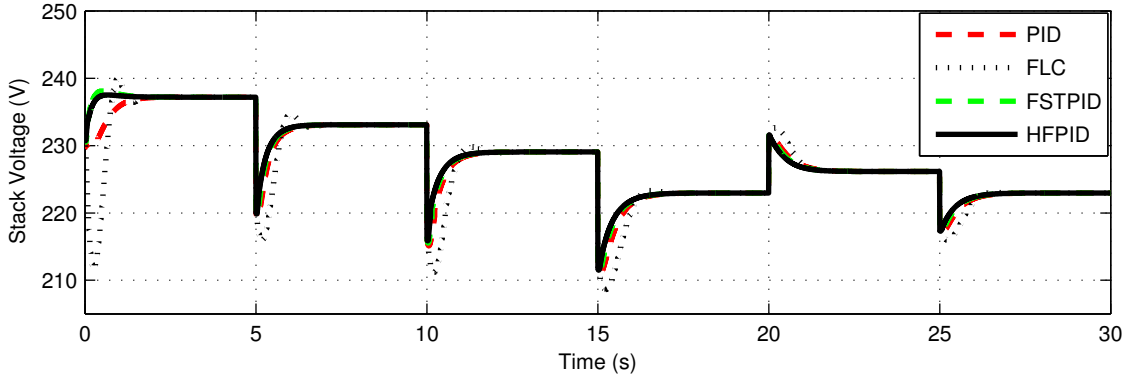

Figure 3.12: Stack-voltage variation for different control strategies.

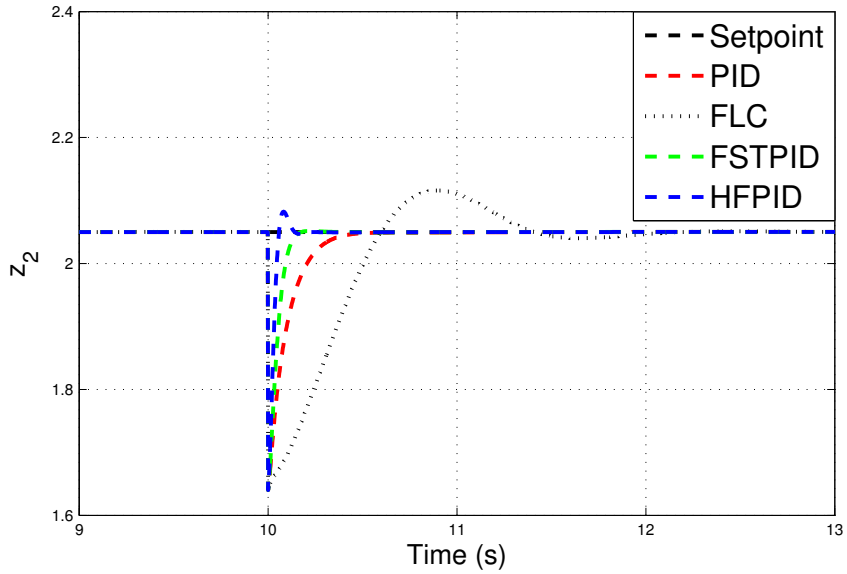

(a) Variation at t=10 s

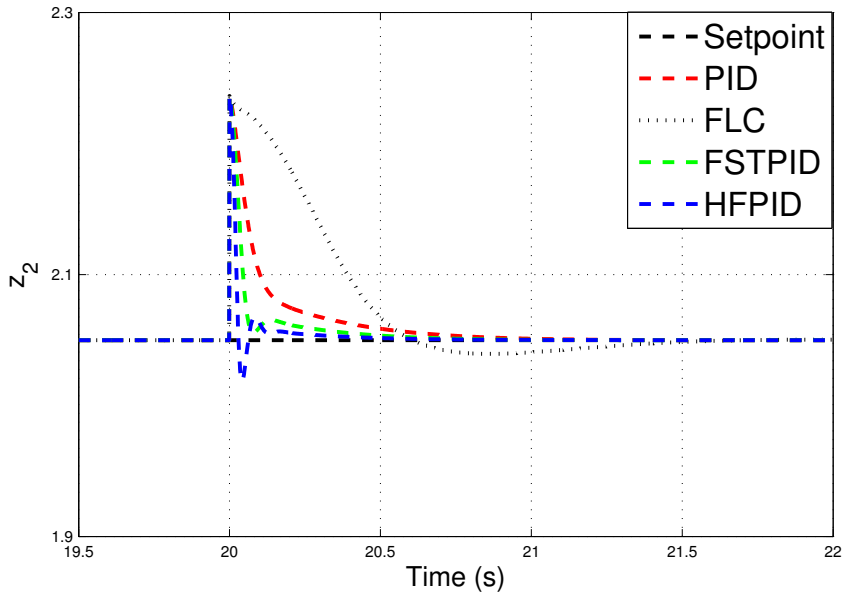

(b) Variation at t=20 s

Figure 3.13: Zoomed plot of OER variations.

Figures 3.13(a) and 3.13(b) present the zoomed plot of z_2 when the stack current is increased from 200 A to 270 A (at t=10 s) and when the stack current is decreased from 300 A to 250 A (at t=20 s), respectively. In the former case, the OER decreases, as shown in Figure 3.13(a), due to the depletion of the oxygen at the cathode side. This fact caused an important drop of the stack voltage, as shown in Figure 3.12. An inverse case is shown in Figure 3.13(b) at t=20 s. According to the zoomed plot of z_2 (Figures 3.13(a) and

Table 3.6: Performance index comparison and time-domain specifications.

Controllers	ISE	IAE	ITAE	Overshoot (%)	Rise Time (s)	Settling Time (5%) (s)
PID	0.0627	0.2903	2.2741	9.037	0.55	0.14
FLC	0.5045	1.1047	8.0201	13.95	0.6	0.43
FSTPID	0.036	0.1577	1.1548	13.65	0.17	0.07
HFPID	0.0249	0.1005	0.6781	15.1	0.06	0.04

3.13(b)), it is found that the HFPID controller exhibits a faster time response compared to the other control strategies. As it can be seen in Figure 3.11 and Table 3.6, that the HFPID controller reduces the rise time and the settling time of tuning z_2 during the transient step changes of w with respect to the FL and FSTPID controllers. The results in Table 3.6 show also, in terms of several performance indices including: the Integral Squared Error (ISE), the Integral Absolute Error (IAE) and the Integral Time-weighted Absolute Error (ITAE), that the proposed control strategy performs much better than the FL and FSTPID control strategies.

To further show the effectiveness of the proposed control strategy (HFPID) on the PEMFC systems, changes of $z_{2,opt}$ are considered, rising up from 2.05 to 3 at t=12 s and then, falling to 2.05 at t=22 s. Simulation results show in Figure 3.14 that z_2 suitably and accurately tracks $z_{2,opt}$ in the presence of $w\,(t)$ variation.

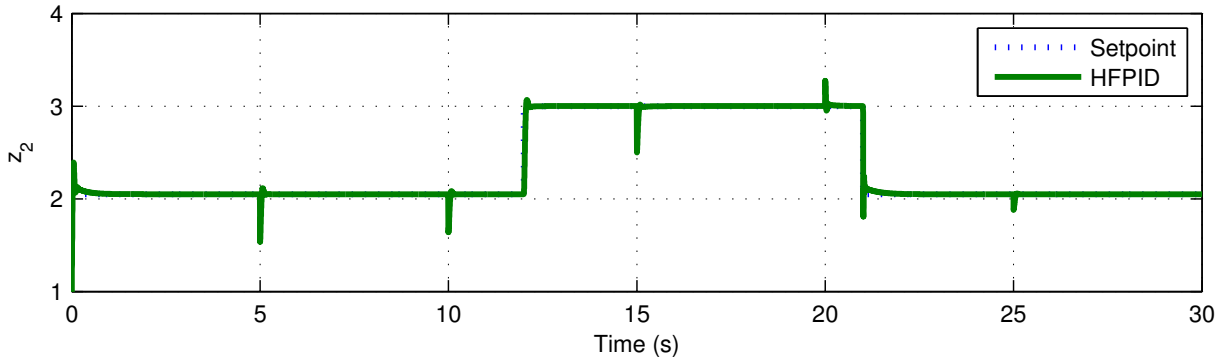

Figure 3.14: Regulation of OER with changing reference.

The behaviour of the compressor motor input voltage (u) is depicted in Figure 3.15(a). Figures 3.15(b) and 3.15(c) exhibit the control action of the fuzzy logic controller u_{fuzzy} and the control action of the fuzzy-based self-tuned PID controller u_{FSTPID}, respectively.

Figure 3.16 shows the adjustment of the coefficients r_{fuzzy} and r_{PID}. This figure shows that the r_{fuzzy} increases when the current value of z_2 is so far away from $z_{2,opt}$, and decreases when that value is near $z_{2,opt}$. Similarly, the value of r_{PID} in the steady-state response, which is equal to 0.92, is greater than the value of r_{fuzzy}, which is equal to 0.1.

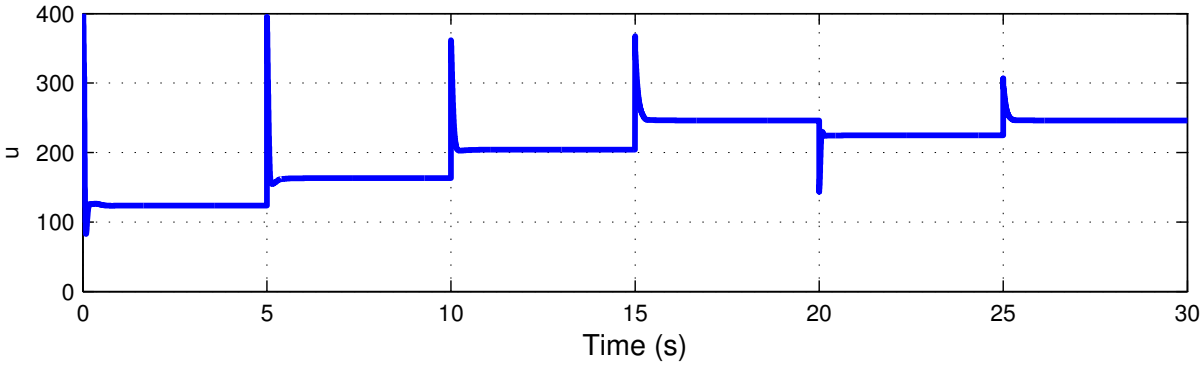

(a) Compressor motor voltage

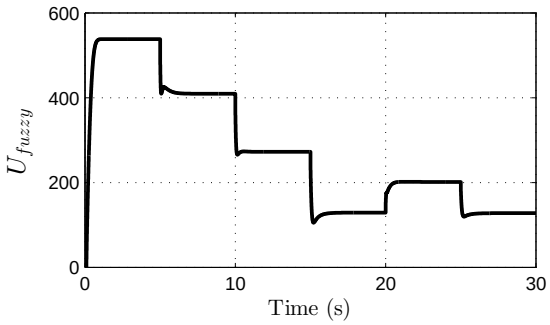

(b) Fuzzy-logic control

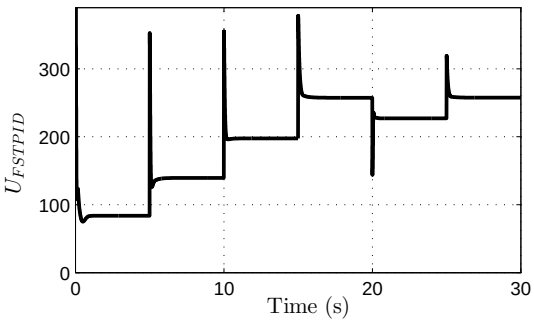

(c) PID control

Figure 3.15: Control signal components.

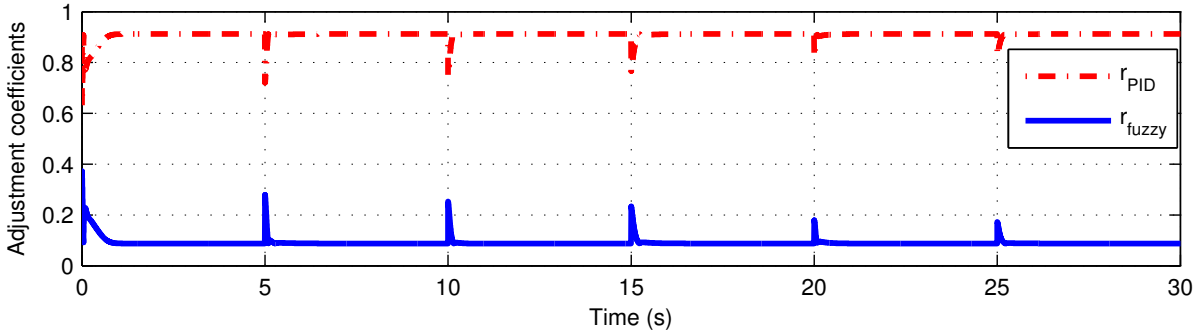

Figure 3.16: Output of the fuzzy supervisor.

3.5.2 Sensibility analysis

In order to test the robustness of the HFPID controller in the presence of uncertainty, a small variation can be applied to the combined inertia of the compressor and the motor (J_{cp}), which is related to the capacity of the air to be supplied from the compressor. This uncertainty appears at the time interval $t = [10, 20]\, s$, as shown in Figure 3.17(b). It can be seen from Figure 3.17(a) that the HFPID controller exhibits a proper effect over this uncertainty. The zoomed plot is shown in Figure 3.17(c), where the transient response of z_2 can be seen at t=15 s.

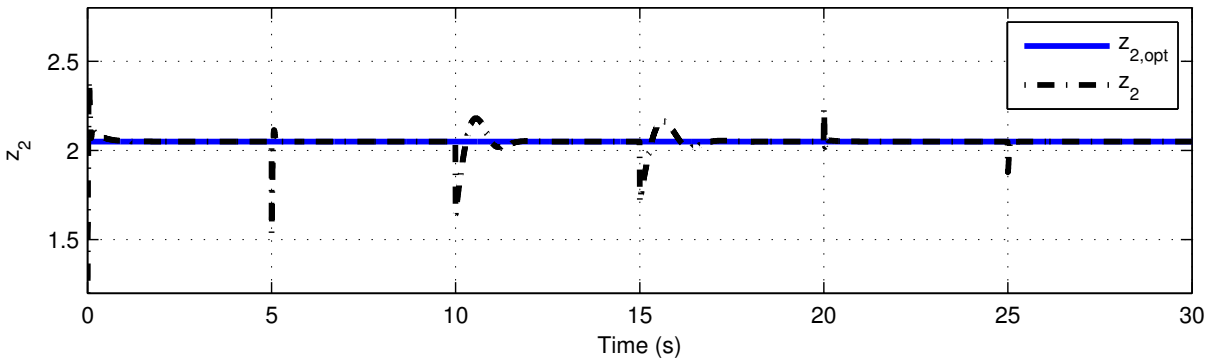

(a) z_2 considering compressor motor inertia variation

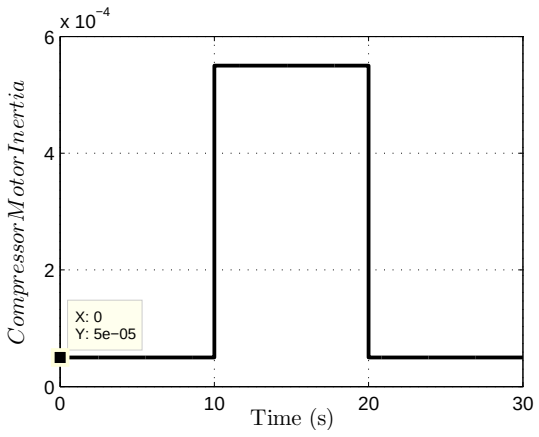

(b) Compressor motor inertia variation

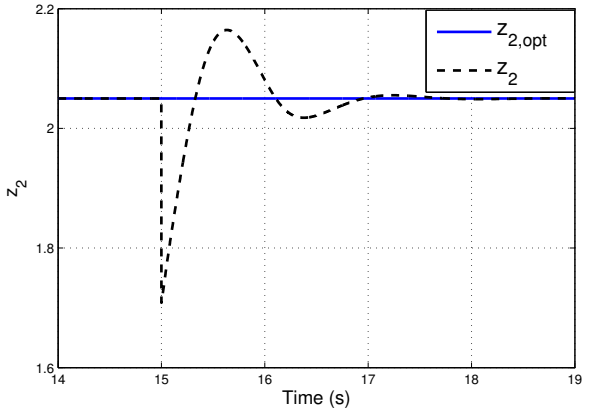

(c) Zoomed plot of z_2 at t=15 s

Figure 3.17: Sensibility analysis.

3.5.3 Comparative study

In this subsection, it is compared the performance of the controller proposed in this study with one of the new controllers published in the literature for the same control objective. The work in [Ou et al., 2015] adopted an adaptive PID controller to regulate z_2 around a

reference value $z_{2,r}$, which is taken equal to 2.4. The parameters of the PID controller are tuned by using an on-line fuzzy logic optimization loop. Simulation are performed taking into account the same stack-current profile adopted in [Ou et al., 2015], which is shown in Figure 3.18(b). Figure 3.18(a) exhibits the dynamic behaviour of z_2, which has a proper transient response despite of the existence of large load variations. Figure 3.18(c) shows the zoomed plot of z_2 at t=15 s, where the proposed control strategy has improved greatly the transient response of z_2 compared to the control strategy presented in [Ou et al., 2015]. The rising time of z_2 for the controller adopted in [Ou et al., 2015] is approximately 150 ms reduced to 60 ms in the control scheme proposed in this chapter (see Figure 3.18(c)).

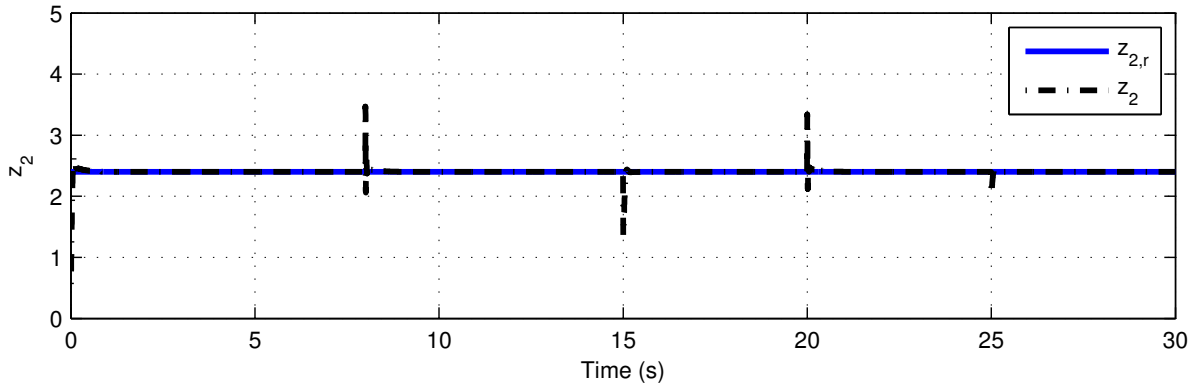

(a) z_2 variation using HFPID

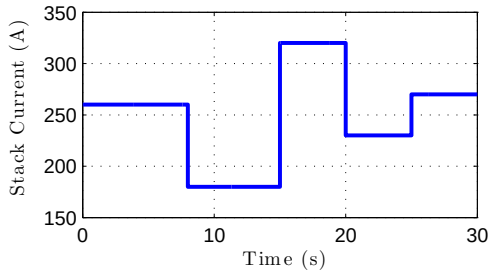

(b) $I_{st}\,(t)$ variation

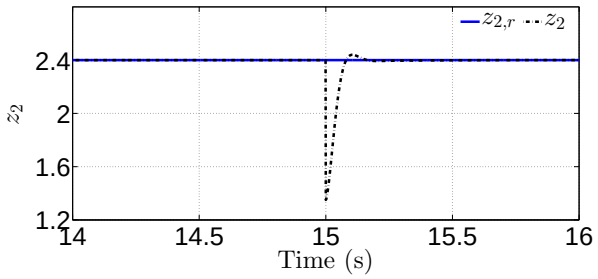

(c) Zoomed plot of z_2 variation at t=15 s

Figure 3.18: Comparative study.

3.6 Twisting controller design

In this section, the PEMFC air supply system performance is evaluated under a SOSM twisting controller [Utkin et al., 2017, Azar and Zhu, 2016, Asif et al., 2002], which is known by its robustness against both parameter uncertainties and disturbances. The twisting controller parameters are tuned through an off-line tuning procedure. A static

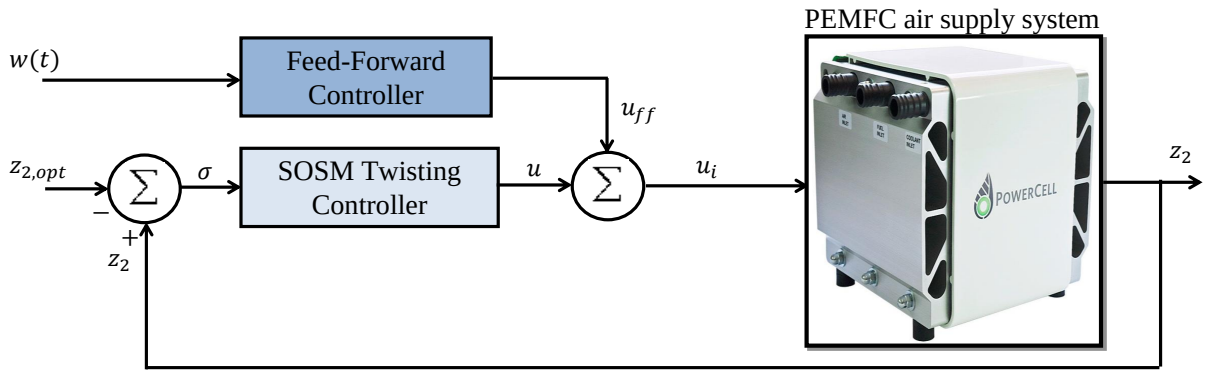

Figure 3.19: SOSM twisting control system.

feed-forward controller, $u_{ff}(t)$, was combined with the twisting controller to enhance the dynamic and the steady-state performance of OER regulation. The structure of the closed-loop OER control scheme that will be considered in this section is shown in Figure 3.19.

The overall control is defined as

$$u_i(t) = u(t) + u_{ff}(t), \tag{3.13}$$

where $u(t)$ corresponds to the SOSM twisting control action calculated below and $u_{ff}(t)$ corresponds to the static feed-forward control action, which is computed as a function of stack current as follows,

$$u_{ff}(t) = -1.36 \times 10^{-3} \times w^2(t) + 1.17 \times w(t) + 14.3 \tag{3.14}$$

Define the corresponding regulation-error variable as

$$\sigma(t) = z_2(t) - z_{2,opt}, \tag{3.15}$$

which will be driven to zero in finite time and will be kept at zero thereafter by a suitable twisting controller. Collecting (2.40) in a unique state-space representation, yields the form

$$\begin{aligned} \dot{x}(t) &= f(x(t)) + gu(t) + \varphi w(t), \\ &= \begin{bmatrix} f_1(x_1, x_2, x_4) \\ f_2(x_1, x_2, x_4) \\ f_3(x_3, x_4) \\ f_4(x_1, x_2, x_3, x_4) \end{bmatrix} + \begin{bmatrix} 0 \\ 0 \\ c_{13} \\ 0 \end{bmatrix} u(t) + \begin{bmatrix} -c_7 \\ 0 \\ 0 \\ 0 \end{bmatrix} w(t), \end{aligned} \tag{3.16}$$

where $f_i : \mathbb{R}^4 \mapsto \mathbb{R}^4$, $i = \{1, \ldots, 4\}$, are smooth state maps. Considering the regulation error variable (3.15) as the sliding variable, the control problem for the PEMFC air supply system can be mathematically formulated as follows:

$$\begin{cases} \dot{x}\,(t) = f(x(t)) + gu\,(t) + \varphi w\,(t)\,, \\ \sigma\,(t) \in \mathbb{R}, \end{cases} \tag{3.17}$$

with a bounded control action $u\,(t) \in \mathbb{R}$, the measurable disturbance $w\,(t) \in \mathbb{R}$ is a piecewise constant function and $\sigma\,(t)$ is a smooth function.
Note that the sliding variable expressed in (3.15) can be rewritten as

$$\sigma\,(t) = \frac{c_{23}}{c_{24}w(t)}\Lambda x(t) - \frac{c_{23}}{c_{24}w(t)}c_2 - z_{2,opt}, \tag{3.18}$$

being $\Lambda = [-1 \quad -1 \quad 0 \quad 1]$. Differentiating twice the sliding variable with respect to time, the following expressions are obtained:

$$\begin{aligned} \dot{\sigma}\,(t) &= \frac{c_{23}}{c_{24}w(t)}\Lambda\dot{x}\,(t) \\ &= \frac{c_{23}}{c_{24}w(t)}\Lambda\left(f(x(t)) + gu\,(t) + \varphi w\,(t)\right) \\ &= \frac{c_{23}}{c_{24}w(t)}\Lambda\left(f(x(t)) + \varphi w\,(t)\right) \end{aligned} \tag{3.19}$$

$$\begin{aligned} \ddot{\sigma}\,(t) &= \frac{\partial\dot{\sigma}\,(t)}{\partial t} + \frac{\partial\dot{\sigma}}{\partial x}\dot{x}(t) \\ &= \frac{c_{23}}{c_{24}w(t)}\Lambda\Big[\frac{\partial f\,(x(t))}{\partial x}(f(x(t)) + gu(t) + \varphi w\,(t))\Big] \\ &= \Psi\,(x(t), w\,(t)) + \Phi(x(t))u(t), \end{aligned} \tag{3.20}$$

with

$$\begin{aligned} \Psi\,(x(t), w\,(t)) &= \frac{c_{23}}{c_{24}w(t)}\Lambda\Big[\frac{\partial f\,(x(t))}{\partial x}(f(x(t)) + \varphi w\,(t))\Big] \\ \Phi(x(t)) &= \frac{c_{23}}{c_{24}w(t)}\Lambda\frac{\partial f\,(x(t))}{\partial x}g \\ &= \frac{c_{23}}{c_{24}w(t)}\frac{\partial f_4}{\partial x_3}. \end{aligned} \tag{3.21}$$

Functions $\Psi\,(x(t), w\,(t))$ and $\Phi(x(t))$ can be bounded as follows:

$$|\Psi\,(x(t), w\,(t))| \leq \Theta, \tag{3.22}$$

$$0 < B_m \leq \Phi(x(t)) \leq B_M. \tag{3.23}$$

The bounding values Θ, B_m and B_M were computed by means of a numerical study of functions $\Psi\left(x(t), w\left(t\right)\right)$ and $\Phi(x(t))$. After calcuation, the following bounding values can be obtained:

$$\Theta = 3 \times 10^5, \quad B_m = 450, \quad B_M = 475. \tag{3.24}$$

Once bounds in (3.24) have been determined, the stabilisation problem of system (3.17) with sliding variable dynamics (3.20) can be solved through the stabilisation of the following equivalent differential inclusion by applying twisting algorithm:

$$\ddot{\sigma}(t) \in [-\Theta,\ \Theta] + [B_m,\ B_M]u(t). \tag{3.25}$$

The algorithm structure and the chosen parameters for the PEMFC air supply system controller are recalled below. The resultant control law related to the twisting algorithm is defined by [Shtessel et al., 2014]

$$u(t) = -(r_1 sign(\sigma(t)) + r_2 sign(\dot{\sigma}(t))), \tag{3.26}$$

where r_1 and r_2 are design parameters that were derived from the corresponding sufficient conditions for finite-time convergence of the algorithm [Kunusch et al., 2012].

Theorem 3.1 *(Taken from [Shtessel et al., 2014]) Let r_1 and r_2 satisfy the conditions*

$$\begin{cases} r_1 > r_2 > 0, \\ (r_1 + r_2)B_m - \Theta > (r_1 - r_2)B_M + \Theta, \\ (r_1 - r_2)B_m > \Theta. \end{cases} \tag{3.27}$$

The controller in (3.26) guarantees the appearance of second-order sliding-mode $\sigma(t) = \dot{\sigma}(t) = 0$ attracting the trajectory of the sliding variable dynamics (3.19) in finite time.

Proof 3.1 *The proof of convergence follows from [Shtessel et al., 2014].*

Through the set of parameters that satisfy (3.27), the control parameters are chosen as:

$$r_1 = 750, \qquad r_2 = 0.1. \tag{3.28}$$

3.7 Twisting controller simulation results

To verify the performance and the efficiency of the twisting controller, simulations are performed and analyzed. Simulations are divided into two tets: performance results and comparative study with the aforementioned controller (Section 3.4). It is important to remember that the main aim of the controller design is to regulate the OER at a setpoint value, which is assumed equal to 2.05.

3.7.1 Performance results

The dynamic behaviour of z_2 under different stack-current variation (see Figure 3.20(a)), using the twisting control strategy is shown in Figure 3.20(b). It can be seen from Figure 3.20(b) that the twisting control strategy adjust z_2 at the setpoint with a satisfactory tracking performance. At t=10 s, the stack current increases from 200 A to 250 A and gives decrease in the OER, as shown in Figure 3.20(b). The decrease in the OER is also due to the depletion of the oxygen in the cathode channel. Moreover, this decrease leads to a significant drop in the stack voltage, as shown in Figure 3.20(c).

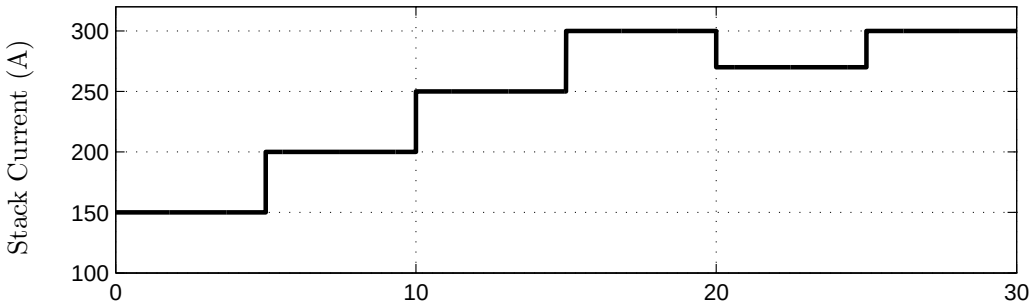

(a) Stack-current variation

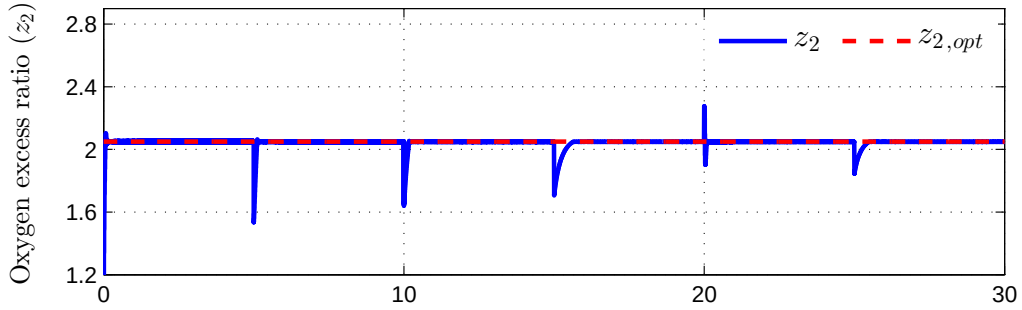

(b) Response of OER for Twisting controller strategy

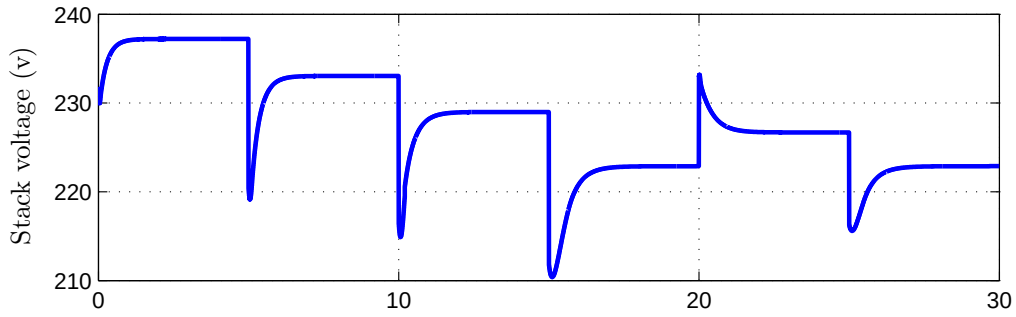

(c) Fuel-cell stack voltage

Figure 3.20: Performance results: Twisting controller.

3.7.2 Comparative study

Here, a comparative between the two controllers, twisting and HFPID, will be given for the purpose of selecting the suitable controller for the sensorless control in the next chapter. Figure 3.21 presents the dynamics of z_2 when two types of controllers are used. Both controllers achieve the control objective with a response time less than 50 ms without overshoot. It can conclude from these results that the twisting controller maintain good performance despite the stack-current changes. Moreover, the implementation of the twisting controller is well validated experimentally [Kunusch et al., 2012].

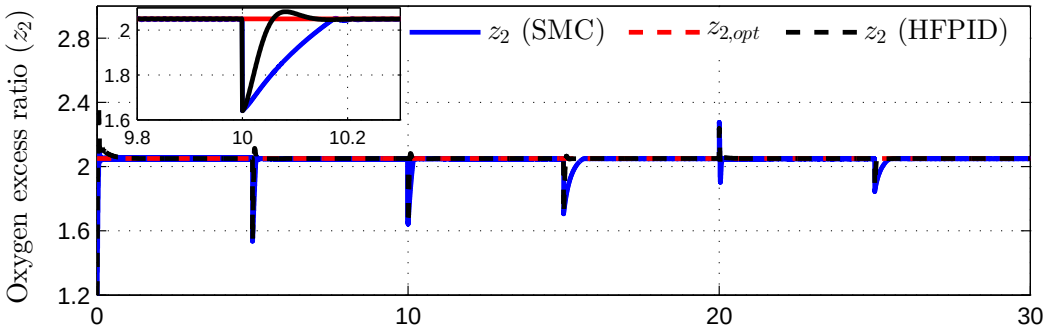

Figure 3.21: Response of OER for Twisting and HFDPID controllers.

3.8 Summary

In this chapter, two controllers are designed to regulate the OER during fast current transitions and uncertainties in the system parameters. The first proposed control strategy, known as hybrid fuzzy PID control, separated into three parts: fuzzy control, fuzzy-based self-tuned PID control and fuzzy supervisor. The second proposed control strategy, known as SOSM twisting control, used an off-line tuning procedure to tune the controller parameters. Then, the proposed controllers have been verified through extensive computer simulations, based on the four state-space model presented in Chapter 2. Subsequently, highly satisfactory simulation results using HFPID and SOSM twisting controllers confirm the simplicity, feasibility and robustness of the solutions.

In conclusion, the SOSM twisting controller is relatively simple to design compared to the hybrid fuzzy PID controller. This represents a major advantage for the SOSM twisting controller. In the next chapter, the applicability of the SOSM twisting controller will be confirmed in a sensorless control scheme.

Chapter 4

Observer-Based Output-Feedback Control for PEMFC Air Supply Systems

> *A hopeless man sees difficulties in every chance, but a hopeful person sees chances in every difficulty.*
>
> Ali ibn Abi-Talib

4.1 Introduction

All control strategies proposed in Chapter 3 require the knowledge of the precise value of Oxygen Excess Ratio (OER). Unfortunately, it depends on internal variables such as the partial pressures of both oxygen and nitrogen in the cathode channel and the air pressure in the supply manifold. This means they should be measured by using additional sensors that increase both the cost and the overall system complexity, while decrease the accuracy of the PEMFC system. For these reasons, the estimation of the observable states using only the measurements of available states become a cheaper and attractive solution.

In this chapter, an algebraic observer-based output-feedback controller is proposed for a PEMFC air supply systems, based on algebraic observer and sliding-mode control approaches. At first, an algebraic estimation approach is used to reconstruct the OER through estimation of their relevant states in real time, from the measurement of the supply manifold air pressure, based on a robust differentiation method. Afterwards, the

SOSM twisting controller presented in Chapter 3 is adopted to control the estimated OER. The performance of the proposed algebraic-observer based output-feedback controller is analyzed through simulations for different stack-current variations, for parameters uncertainties, and for noise rejection. Results are shown that the proposed approach properly estimates and regulates in finite time the OER.

4.2 Review on PEMFC system observation

Over the last decades, several studies have focused on the observer design for fuel-cell systems. Here, some available results are recalled: Liu et al. have reported in [Liu et al., 2015], a nonlinear observer to estimate the hydrogen partial pressure from the measurements of the stack voltage, stack current, anode pressure and anode inlet pressure. Gorgun et al. have presented in [Görgün et al., 2006], an algorithm for estimating humidity by exploiting its effect on cell resistive voltage drop. Kunusch et al. have presented in [Kunusch et al., 2013], an integrated observation and identification approach to estimate the hydrogen input flow at the stack anode and the water transport across the membrane in PEMFC systems. Observers and parameter identification algorithms adopted in this work are based on the Generalized Super-Twisting algorithm. Several approaches of Kalman Filter (KF) in [Pukrushpan et al., 2002a, Vepa, 2012], are used to estimate the states of the PEMFC from a linearized model. Other researches have considered Luenberger and adaptive observers types to estimate the PEMFC system states. However, all the above works lack robustness in the presence of disturbance and parameters uncertainties.

A variety of sliding mode observers have used in PEMFC state estimation due to its robustness with respect to matched modeling errors and its insensitivity to external disturbance [Kim, 2012, Rakhtala et al., 2014, Pilloni et al., 2015, Liu et al., 2014]. Kim has estimated both oxygen and hydrogen pressures in PEMFC system by sliding mode observers in [Kim, 2012]. Authors in [Rakhtala et al., 2014] have presented a finite-time High-Order Sliding Mode observer to estimate some key states in the PEMFC air supply system. Pilloni et al. [Pilloni et al., 2015] have proposed high-order sliding-mode approach to the observer design, which is able to reconstruct in finite time the whole state of the PEMFC system. Moreover, Pilloni et al. [Pilloni et al., 2015] observer does not require the implementation of any differentiator. Counter to the work of Baroud et al. [Baroud et al., 2017a], the nonlinear observer requires a first sliding mode differentiator to estimate the OER. More recently, authors in [Liu et al., 2014] have proposed an adaptive algebraic observer for PEMFC system based on high-order sliding-mode differentiator. The pro-

posed adaptive differentiators estimate the time derivatives of output variables in finite time without any knowledge of the upper bounds of their higher-order time derivative. Moreover, the proposed observer in [Liu et al., 2014] was successfully implemented on a Hardware In the Loop (HIL) test bench. All these sliding-mode observers are applied for the estimation of the OER in the PEMFC system with various degrees of success.

The main contribution of this chapter is to design an algebraic observer-based output-feedback controller in order to estimate and regulate the OER in a PEMFC air supply system. Hence, the robustness and the accuracy of the differentiation method are important elements to the observer design. A robust differentiation method taken from [Fliess and Sira-Ramirez, 2004] is adopted to estimate, in finite time, the time derivatives of output variable. The proposed observer estimates the partial pressures of both oxygen and nitrogen in finite time from the measurement of the supply manifold pressure. Then, the design of twisting controller in order to use as closed-loop control strategy. This controller was proposed in Chapter 3, where an off-line tuning procedure was used to tuned the controller parameters.

4.3 Problem statement

The main control objective for the PEMFC air supply system is to regulate the OER (z_2), which is defined through the following expression:

$$z_2 = \frac{c_{23}\left(y_1 - \chi - c_2\right)}{c_{24} w}, \tag{4.1}$$

However, the z_2 expression depends on the internal variables that are the air pressure in the supply manifold and the partial pressures of both oxygen and nitrogen in the cathode channel. Fortunately, the expression of $z_2(t)$ is related to the unkown sum of the partial pressures of both oxygen and nitrogen, $\chi(t)$. So, to compute $z_2(t)$ it is required to estimate only $\chi(t)$. For this purpose, an algebraic finite-time converging observer will be designed, which maintains the condition

$$e(t) = \hat{\chi}(t) - \chi(t) = 0 \qquad \forall \quad t \geq T, \quad T \in \mathbb{R}^+ \tag{4.2}$$

where T is a positive constant, which is chosen to improve the precision of the estimated derivative, $\hat{\dot{y}}_1(t)$. The estimate value of OER, $\hat{z}_2(t)$, can be obtained for some finite time $T > 0$ according to

$$\hat{z}_2(t) = \frac{c_{23}\left(y_1(t) - \hat{\chi}(t) - c_2\right)}{c_{24} w(t)}. \tag{4.3}$$

4.4 Algebraic observer design

In this section, an algebraic observer is developed for estimating the OER from the measurement of supply manifold pressure. The proposed observer is known for its low computational time, and its finite-time convergence and its robustness against measurement noise compared to other observers presented in the literature [Liu et al., 2014]. However, before designing the observer, the algebraic observability of the PEMFC air supply system should be verified. Then, the implementation of the algebraic observer needs an exact numerical differentiation.

4.4.1 Algebraic observability

The algebraic obserability definition is illustrated as follows.

Definition 4.1 *Consider the nonlinear system described by the following dynamic equations,*

$$\dot{x}(t) = f(x(t), u(t), y(t)) = h(x(t)), \tag{4.4}$$

where $f(\bullet, \bullet) \in \mathbb{R}^n$ and $h(\bullet) \in \mathbb{R}^p$ are assumed to be continuously differentiable. $x(t) \in \mathbb{R}^n$ represents the system state vector, $u(t) \in \mathbb{R}^m$ is the control input vector and $y(t) \in \mathbb{R}^p$ is the output vector. system (4.4) is said to be algebraically observable if there exists two positive integers μ and v such that

$$x(t) = \phi(y, \dot{y}, \ddot{y}, \cdots, y^{(\mu)}, u, \dot{u}, \ddot{u}, \cdots, u^{(v)}), \tag{4.5}$$

where $\phi(\bullet) \in \mathbb{R}^n$ is a differentiable vector valued nonlinearity of the inputs, the outputs and their time derivatives [Liu et al., 2014].

In order to verify the algebraic observability of the PEMFC air supply system, let us consider the model of the PEMFC air supply system (2.40) with the outputs (2.43). The variable $\chi = x_1 + x_2$, that is defined in Chapter 2, follows from (2.40d) that

$$\chi = \frac{\dot{y}_1}{c_{14}c_{16}\left[1 + c_{15}\left[\left(\frac{y_1}{c_{11}}\right)^{c_{12}} - 1\right]\right]} - \frac{y_3}{c_{16}} + y_1 - c_2 = \phi_1\left(y_1, \dot{y}_1, y_3\right). \tag{4.6}$$

The time derivative of χ is

$$\begin{aligned}\dot{\chi} &= \frac{\ddot{y}_1}{c_{14}c_{16}\left[1 + c_{15}\left[\left(\frac{y_1}{c_{11}}\right)^{c_{12}} - 1\right]\right]} - \frac{c_{15}c_{12}y_1^{(c_{12}-1)}(\dot{y}_1)^2}{c_{11}^{c_{12}}c_{14}c_{16}\left[1 + c_{15}\left[\left(\frac{y_1}{c_{11}}\right)^{c_{12}} - 1\right]\right]^2} - \frac{\dot{y}_3}{c_{16}} + \dot{y}_1 \\ &= \phi_2\left(y_1, \dot{y}_1, \ddot{y}_1, \dot{y}_3\right).\end{aligned} \tag{4.7}$$

Then in view of (4.6) and (4.7), the system can be rewritten as

$$\begin{aligned} x_1 &= \frac{1}{c_4 - c_5}\left[\frac{c_3\left(\phi_1 - c_2\right)\alpha}{\left(c_1 + c_8\right)\left(y_1 - \phi_1\right) - \phi_2 - c_7 w} + c_2 c_5 - c_6 - c_5\phi_1\right], \\ &= \phi_3\left(y_1, \dot{y}_1, \ddot{y}_1, y_3, \dot{y}_3\right), \\ x_2 &= \chi - x_1 = \phi_4\left(y_1, \dot{y}_1, \ddot{y}_1, y_3, \dot{y}_3\right), \\ x_3 &= \frac{y_3}{c_{17}} = \phi_5\left(y_3\right), \\ x_4 &= y_1 = \phi_6\left(y_1\right). \end{aligned} \tag{4.8}$$

It can be seen from (4.8) that all PEMFC system states have been expressed in terms of output variables and their time derivatives up to some finite number, i.e. $\dot{y}_1$, $\ddot{y}_1$ and $\dot{y}_2$. for that reason, the system (2.40) is algebraically observable according to the definition of algebraic observability (see Definition 4.1).

It is worth to remember that the variable $z_2(t)$ is related to the unkown sum of the partial pressures of oxygen and nitrogen at the cathode channel (i.e., the expression $\chi = x_1 + x_2$). So, to minimize the cost of calculation and avoid the reconstruction of whole system state, it is required to estimate only $\chi(t)$ from (4.6). Moreover, the value of $\chi(t)$ can be calculated using only the first derivative of the supply manifold pressure $y_1(t) = x_4(t)$ in (2.40d) and the measured output $y_3(t)$ in (2.21). As considered in Chapter 2, the supply manifold pressure is measurable and its time derivative will be estimated by employing robust numerical differentiation method in next subsection [Fliess and Sira-Ramirez, 2004].

4.4.2 Numerical differentiator

The work reported in [Baroud et al., 2016b] provides the robust computation of the output derivative $y_1(t)$ based on the truncated Taylor expansion of $y_1(t)$ around t as follows:

$$y_1(t') = y_1^{(0)}(t) + y_1^{(1)}(t)(t' - t). \tag{4.9}$$

This identification procedure consists in several algebraic manipulations on the operational Laplace domain [Fliess and Sira-Ramirez, 2004]. From [Mboup et al., 2007], the first-order derivative estimation of the supply manifold pressure is given as follows:

$$\hat{\dot{y}}_1(t) = \int_0^T \frac{6}{T^3}\left(2T - 3\tau\right) Y\left(t - \tau\right) d\tau, \tag{4.10}$$

where $Y(t)$ represents the noisy supply manifold pressure measurement. One can obtain robustly $\hat{\chi}(t)$ from (2.40d) and (4.10) as follows:

$$\hat{\chi}(t) = \frac{1}{c_{16}} \left(\frac{\hat{\dot{y}}_1(t)}{c_{14}\left(1 + \left(c_{15}\left(\frac{y_1(t)}{c_{11}}\right)^{c_{12}} - 1\right)\right)} - y_3(t) \right) + y_1(t) - c_2. \tag{4.11}$$

Depending on the response time of the system, a relevant sliding time window, T, is chosen in order to obtain an accurate value of $\dot{y}_1(t)$, and thus the estimated states $\hat{\chi}(t)$ reach the real states, $\chi(t) = x_1(t) + x_2(t)$, i.e.,

$$\hat{\chi}(t) = \chi(t). \tag{4.12}$$

Finally, $\hat{z}_2(t)$ is estimated using the expression provided by the algebraic observer ($\hat{\chi}(t)$) and the nominal PEMFC parameters, defined in Table A.2 in the Appendix A, according to the following expression:

$$\hat{z}_2(t) = \frac{c_{23}\left(y_1(t) - \hat{\chi}(t) - c_2\right)}{c_{24} w(t)}. \tag{4.13}$$

4.5 Observer-based output-feedback control for PEMFC air supply system

It is important to notice that the algabraic observer converges in finite time, then the seperation principle of observation and control can be simply fixed as in [Pilloni et al., 2015]. Thus, the feedback controller using the estimated OER (4.13) can be designed separately from the algebraic observer.

The proposed observer/controller is schematically shown in Figure 4.1, where the overall control for the PEMFC air supply system controller are recalled from Chapter 3 and is defined as

$$u_i(t) \;=\; u(t) + u_{ff}(t), \tag{4.14}$$

where $u_{ff}(t)$ corresponds to the static feed-forward control action, which is computed as a function of stack current as follows:

$$u_{ff}(t) \;= -1.36 \times 10^{-3} \times w^2\,(t) + \;1.17 \times w\,(t) + \;14.3, \tag{4.15}$$

and $u(t)$ corresponds to the SOSM twisting control action and is given by

$$u(t) \;= -(r_1 sign(\hat{\sigma}(t)) + r_2 sign(\dot{\hat{\sigma}}(t))), \tag{4.16}$$

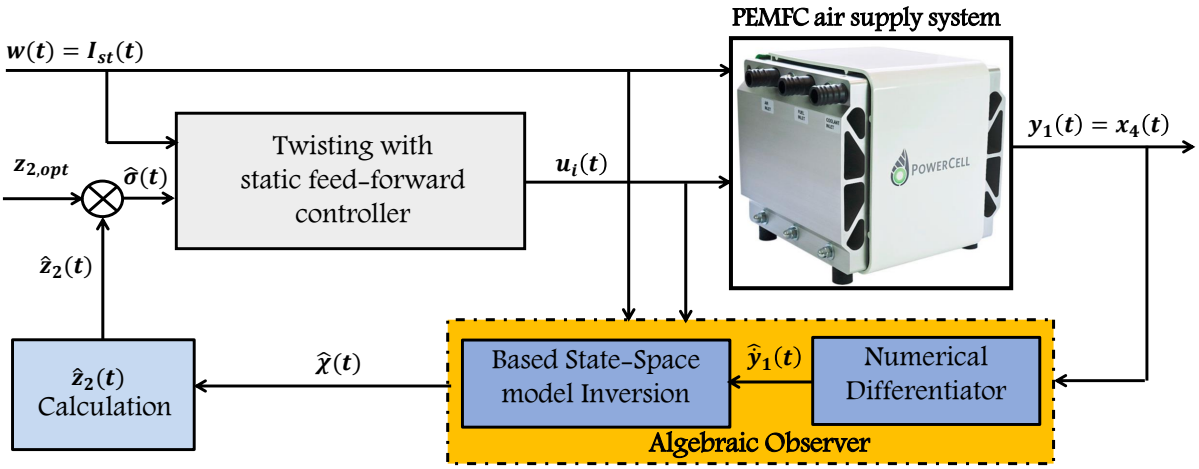

Figure 4.1: Algebraic observer-based output-feedback control for PEMFC air supply system.

where r_1 and r_2 are design parameters that were derived from the corresponding sufficient conditions for finite-time convergence of the algorithm [Kunusch et al., 2012]. Therefore, through the set of parameters that satisfy (3.27), the control parameters are chosen as:

$$r_1 = 750, \qquad r_2 = 0.1, \tag{4.17}$$

and the variable $\hat{\sigma}(t)$ correspond to the sliding variable is defined as follows,

$$\hat{\sigma}(t) = \hat{z}_2(t) - z_{2,opt}. \tag{4.18}$$

Note that the derivative of the sliding variable, $\dot{\hat{\sigma}}(t)$, is estimated also through an algebraic differentiator similar to $\dot{\hat{y}}_1(t)$ in (4.10).

Remark 2 *It is worth to remark that the algebraic observer is able to reconstruct the OER in finite time. Therefore, the separation principle is automatically satisfied and the twisting controller and the algebraic observer can be separately designed. Moreover, the stability of the closed-loop system is guaranteed because the differential inclusion (3.25) is satisfied due to the twisting algorithm [Kunusch et al., 2012].*

4.6 Simulation results

The proposed observer-based control strategy is applied to the model of the PEMFC air supply system in (2.40). To assess the performance, the effectiveness and the robustness of the proposed observer-based control strategy, detailed simulations are peformed and

analysed. Simulation are divided into four tests: nominal performance, parameters uncertainties, noise rejection and comparative study. The numerical parameters for simulation are based on a fuel-cell prototype vehicle, which corresponds to a 75 kW high-pressure FC stack fed by a 14 kW turbo compressoor used in a Ford P2000 FC electric vehicle. The numerical parameters are given in Table A.2 in the Appendix A. All the simulation have been performed using the Matlab/Simulink environnement. The initial values of the states are

$$x(0) = \left[\begin{array}{cccc} 11004\,\text{Pa} & 83813\,\text{Pa} & 5200\,\text{rad/s} & 149000\,\text{Pa} \end{array} \right]^T. \tag{4.19}$$

Note that the main aim of the proposed observer-based control scheme is to estimate/regulate the OER, $\hat{z}_2(t)$, at an optimal setpoint value by means of compressor motor voltage $v_{cm}(t)$. With this optimal setpoint, which is set equal to 2.05, it can be assured that the PEMFC air supply system achieves the maximum net power during stack-current variation while the oxygen starvation is avoided.

The stack current, i.e. the load is shown in Figure 4.2, steps up from 100 A to 150 A at t=5 s. Next, after 5 s, it rises up by 50 A. This increment stopped when the stack current reaches 250 A. After 20 s, the current decreases to 220 A. Finally, at time t=25 s, it increases again from 220 A to 250 A. This stack-current behaviour is adopted for all simulation tests.

4.6.1 Test 1. Nominal performance

This test focuses on the performance of the closed-loop system by showing the actual and the estimated value of OER. No parameters uncertainties and no noise in the supply manifold pressure are considered in this test.

Figure 4.3(b) shows that the value of OER is estimated in finite time by the proposed algebraic observer. Figure 4.3(a) presents both the real and estimated values of oxygen and nitrogen partial pressures. These partial pressures are properly estimated based on the algebraic observer. In the beginning of the estimation, the proposed observer reached the real value of $\chi(t)$ in less than 30 ms. The real and the estimated values of OER are shown in Figure 4.3(b). As can be seen from Figure 4.3(c), the estimation error is acceptably low in spite of having a stack-current variation. The dynamic behaviour of actual and estimated OER under different stack-current variation are illustrated in Figure 4.3(b). In conclusion, the proposed observer-based control scheme adjusts $\hat{z}_2(t)$ suitably and accurately at the setpoint $z_{2,opt}$ in the presence of $I_{st}(t)$ variation.

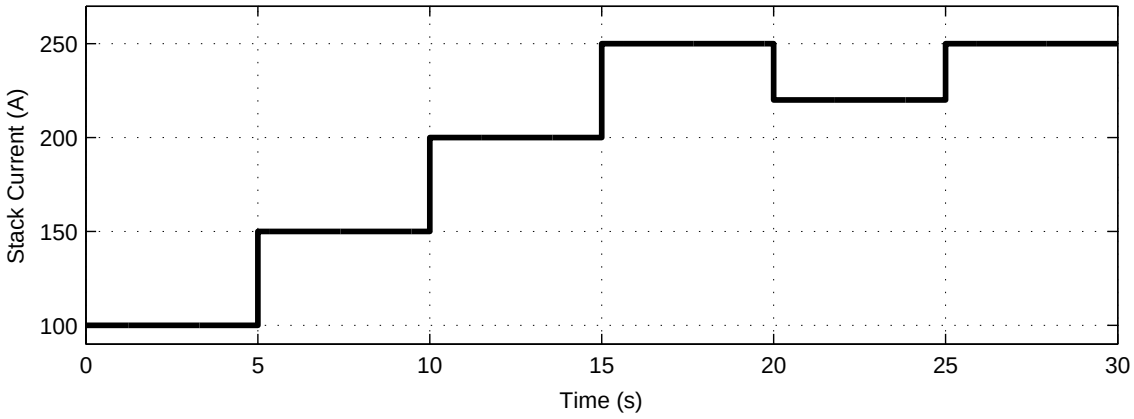

Figure 4.2: Stack-current variation.

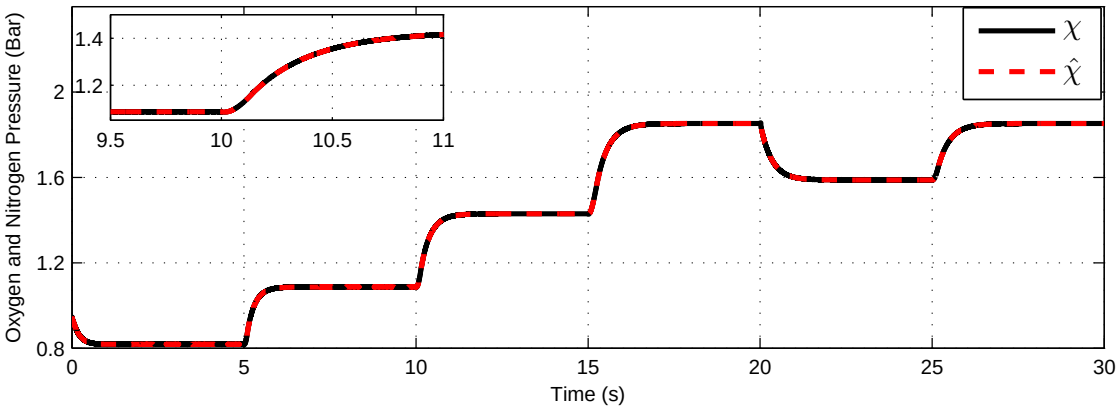

(a) Real and estimated values of oxygen and nitrogen partial pressures

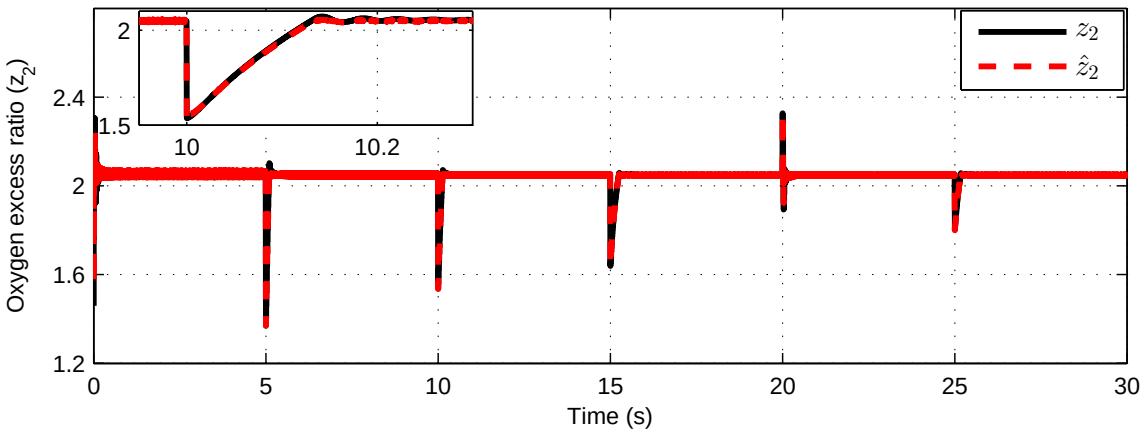

(b) Real and estimated values of OER

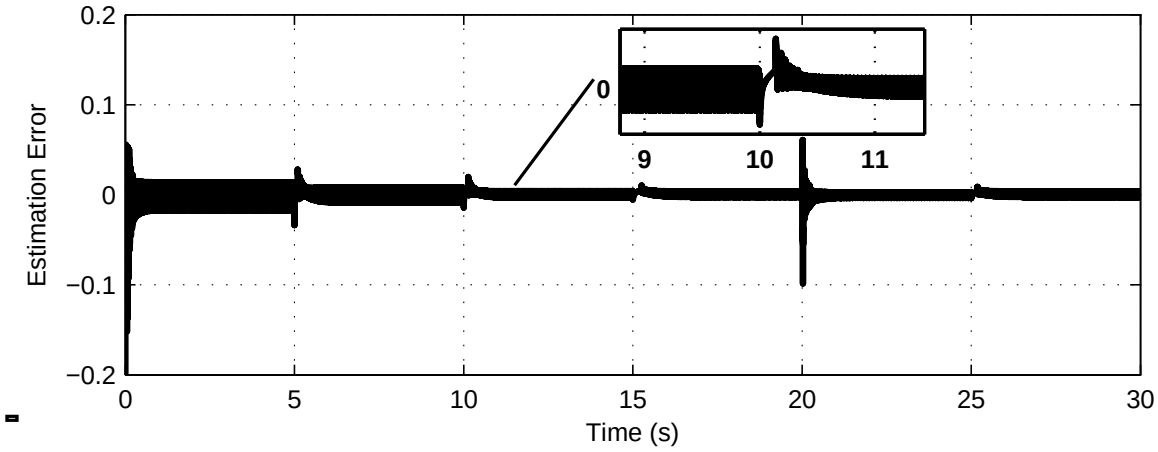

(c) Estimation error $(z_2 - \hat{z}_2)$

Figure 4.3: Test 1: Performance results.

Table 4.1: Variation of system parameters

Parameter	**Nominal value**	**Variation**
Stack Temperature T_{st} [K]	353.15	+10 %
Atmospheric temperature T_{atm} [K]	298.15	+10 %
Supply manifold volume V_{sm} [m^3]	0.02	−10 %
Supply manifold outlet orifice constant $k_{sm,out}$ [kg/(s Pa)]	0.3629×10^5	+5 %
Compressor inertia J_{cp} [kg m^{-2}]	5×10^{-5}	+10 %

4.6.2 Test 2. Parameters uncertainties

This test focuses on the effect of some parameter uncertainties in the performance of the algebraic observer-based output-feedback controller. The variation of system parameters is listed in Table 4.1 [Kunusch et al., 2012].

Figure 4.4(a) shows the real and the estimated values of oxygen and nitrogen partial pressures. Figure 4.4(a) indicates the favorable robust performance of the proposed observer-based control scheme in the face of the parameters uncertainties and disturbance variation. In addition, Figure 4.4(b) shows that the OER is estimated and regulated with sufficient accuracy. The proposed observer-based control remains the estimation error $(z_2 - \hat{z}_2)$, shown in Figure 4.4(c), into an acceptable range during this test. The outputs, stack voltage and net power of the PEMFC air supply system are depicted in Figures (4.4(d), 4.4(e)), respectively. It can be seen from these figures that, during a positive stack-current

step, the stack voltage drops due to the decreasing of oxygen concentration in the cathode channel. This fact, in turn, causes an important increase in the net power.

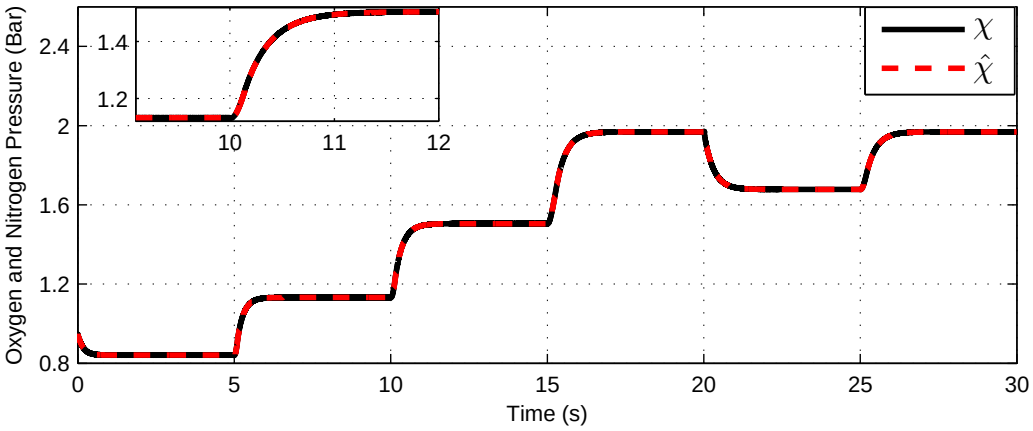

(a) Real and estimated values of oxygen and nitrogen partial pressures

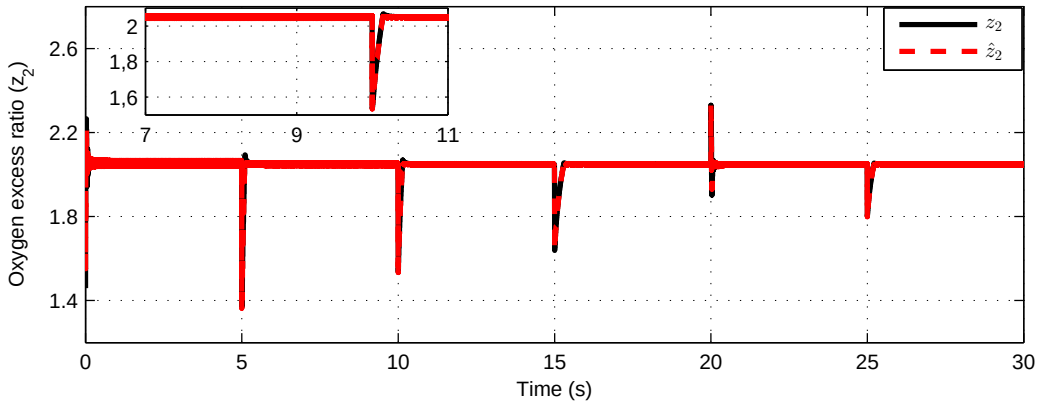

(b) Real and estimated values of OER

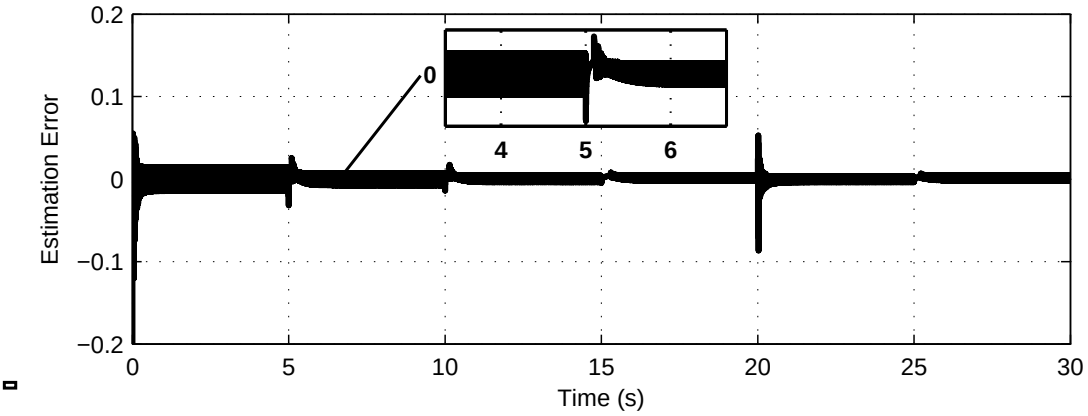

(c) Estimation error ($z_2 - \hat{z}_2$)

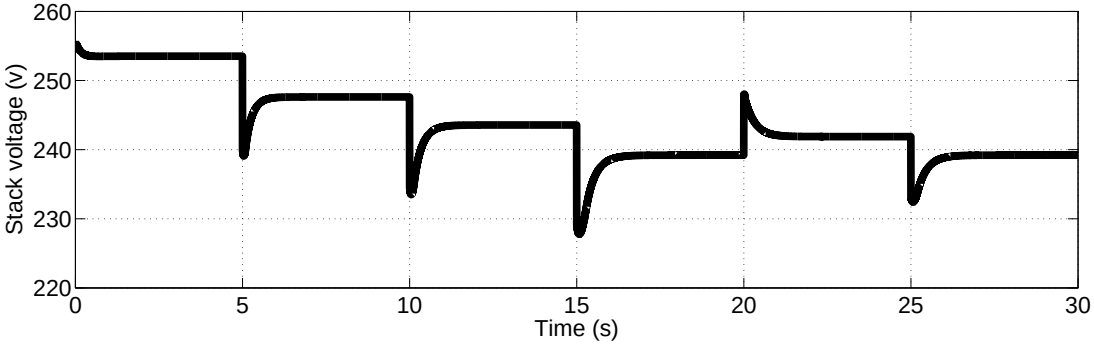

(d) Output stack voltage

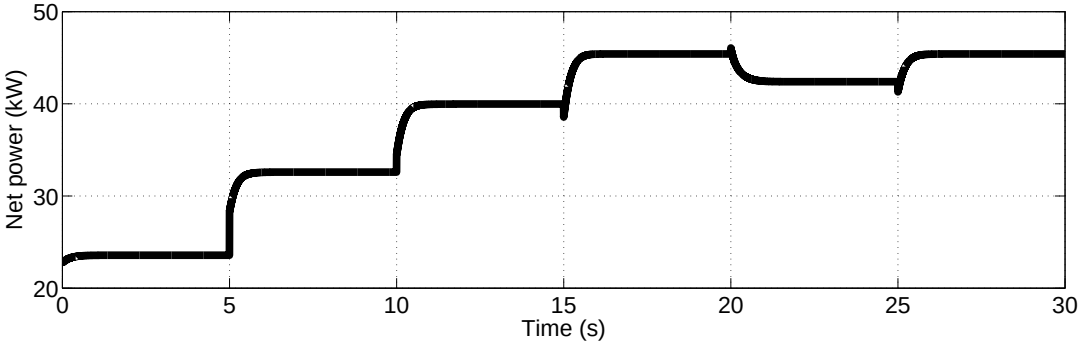

(e) Output net power

Figure 4.4: Test 2: Parameters uncertainties.

4.6.3 Test 3. Noise rejection

In this test, some simulations were carried out to test the robustness of the proposed observer-based control scheme in the presence of noise in the supply manifold pressure $y_1(t)$. Let $Y(t) = y_1(t) + \xi(t)$ be the real measurement of $y_1(t)$, where $\xi(t)$ is a noisy signal with mean $\mu = 3.11 \times 10^{-3}$ and variance $\sigma^2 = 4.00948$.

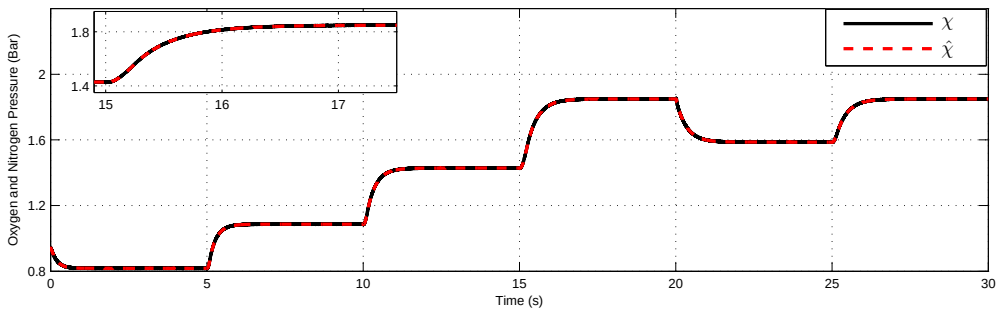

(a) Real and estimated values of oxygen and nitrogen partial pressures

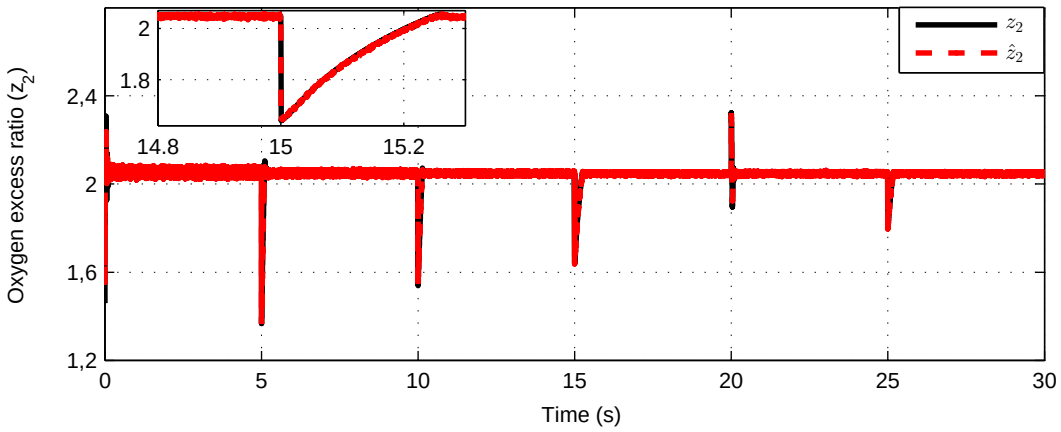

(b) Real and estimated values of OER

Figure 4.5: Test 3: Noise rejection.

The simulation results are shown in Figures 4.5(a) and 4.5(b). The real and estimated values of the OER are depicted in Figure 4.5(b). In that figure, it is possible to look that the proposed observer-based control scheme both estimates and regulates the OER well enough in spite of the noise in the measurement of the supply manifold pressure.

4.6.4 Test 4. Comparative results

Here, a comparative study between the proposed observer-based control scheme and one of the recent observer-based control architectures published in the literature for the same control objective. The authors in [Pilloni et al., 2015] have presented an observer-based control scheme for estimating and regulating the OER of PEMFC air supply system around an optimal value, $z_{2,opt} = 2.06$. Firstly, the nonlinear observer design is based on high-order sliding algorithms. Secondly, the control loop, which uses the observed OER ($\hat{z}_2$), is also based on the HOSM and its parameters are tuned by using local linearization and frequency domain arguments.

Simulations of the observer-based control scheme are performed including the same stack-current demand adopted in [Pilloni et al., 2015], which is shown in Figure 4.6(a). Figure 4.6(b) shows the actual and the estimated profiles of oxygen and nitrogen partial pressures. According to Figure 4.6(b), it can be seen the precision of the algebraic observer. Figure 4.6(c) presents the actual and the estimated value of OER. Suitable transient response and proper estimation are shown despite large load variations. Figure 4.6(c) exhibits also the zoomed plot of z_2 at t=35 s, where the proposed observer-based con-

troller has improved greatly the transient response of $\hat{z}_2$ compared to the observer-based control strategy presented in [Pilloni et al., 2015] (see Figure 4.6(d)).

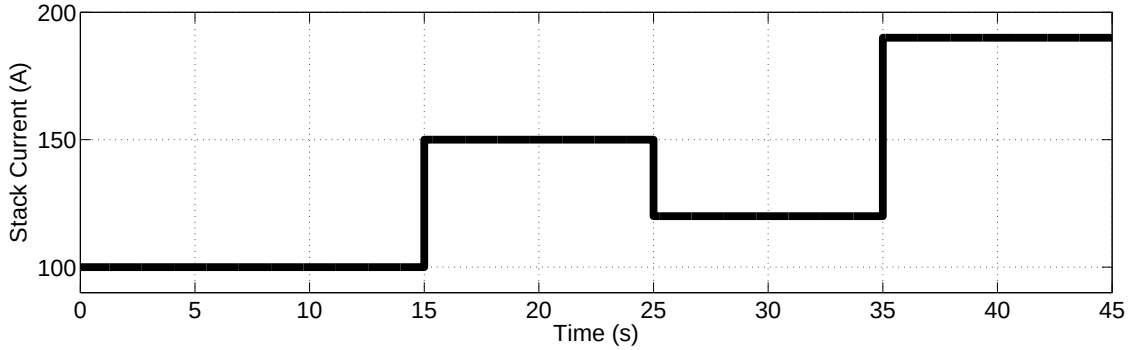

(a) Pilloni et al. [Pilloni et al., 2015] stack-current variation

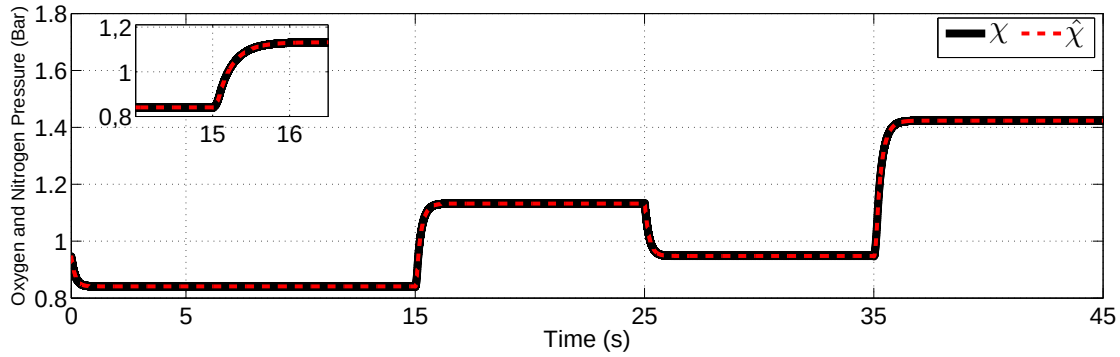

(b) Real and estimated values of oxygen and nitrogen partial pressures

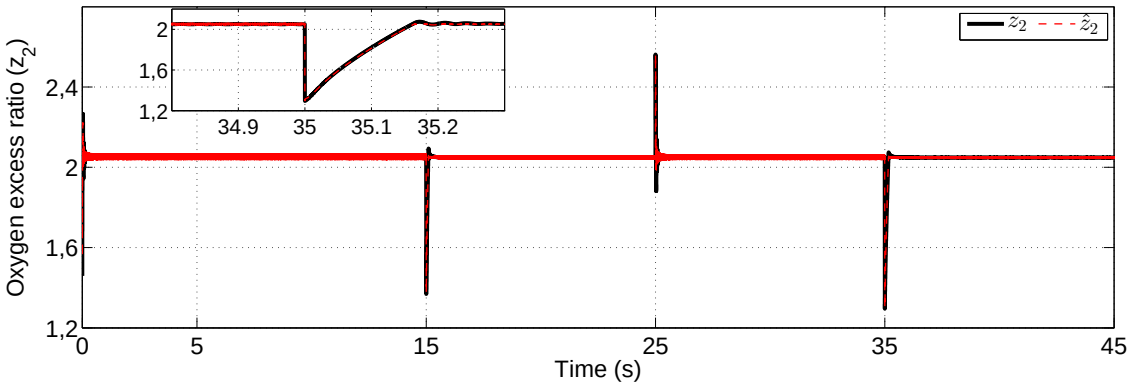

(c) Real and estimated values of OER

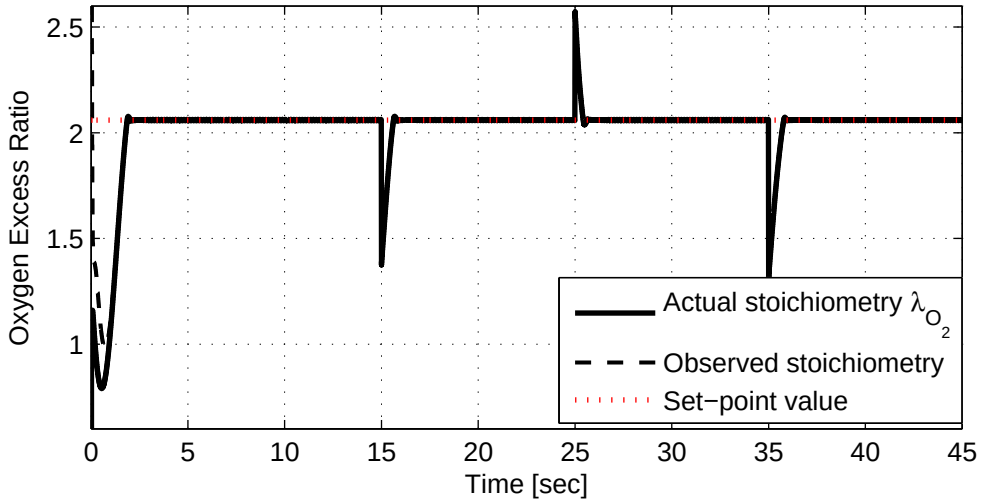

(d) Real and estimated values of OER (Pilloni et al. [Pilloni et al., 2015])

Figure 4.6: Test 4: Comparative results.

4.7 Summary

In this chapter, an algebraic observer-based output-feedback controller has been designed for regulating the OER of a PEMFC air supply system at an optimal setpoint value. The algebraic observer design provides a finite-time converging OER reconstruction based on a robust differentiation method. The proposed controller, which uses the estimated OER, is based on one of the second-order sliding-mode variety algorithms. This chapter adopted the twisting algorithm depending only on few parameters, which were calculated during an off-line tuning procedure. Four simulation tests have shown that the designed algebraic observer-based output-feedback controller is robust to external disturbances, parameters uncertainties and measurement noise.

Concluding Remarks

This thesis work has been interested in the control of the fuel-cell systems for transportation applications. This study was focused on the PEMFC air supply system. The control objective is to regulate fast and efficiently the oxygen depleted in the cathode channel in order to avoid both oxygen starvation and saturation phenomena.

The first part of this thesis discussed controller design for PEMFC air supply system based on both fuzzy-logic and Second-Order Sliding-Mode (SOSM) algorithms. A reduced control-oriented PEMFC system model was proposed, which presents cathode mass flow dynamics. Based on this model, two efficient controllers were proposed based on fuzzy-logic and Second-Order Sliding-Mode (SOSM) algorithms, respectively. The first one is separated into three parts: fuzzy control, fuzzy-based self-tuned PID control, and fuzzy supervisor. The second one was simple since its parameters can be calculated by an off-line tuning procedure. Satisfactory simulation results were obtained for both of the proposed controllers.

The second part of the thesis was focused on the algebraic-observer-based output-feedback controller design, which is based on both algebraic differentiation and sliding-mode control approaches. At first, an algebraic estimation approach is used to reconstruct the OER based on a robust differentiation method. The proposed observer is known by its finite-time convergence and low computational time compared to other observers presented in the literature. Then, the SOSM twisting controller presented in the first part of the thesis was adopted. The performance of the proposed algebraic-observer-based output-feedback controller is analysed through simulations. Results show that the proposed approach properly estimates and regulates the OER in finite time.

Future researchs

The thesis work has discussed the theoretical contributions to control and observation in the PEMFC air supply system. This thesis may be extended in the future in the following aspects:

- The model used in this work considered that sufficient hydrogen is available and both temperature and humidity of input reactant flows are well regulated. It would be interesting to work on a complete model, which takes into account all the dynamics within the fuel-cell system.
- The optimal value of the oxygen excess ratio varies with different operating charges and may change depending on fuel-cell system age and environmental conditions. In the future works, extremum-seeking or other maximum-finding methods will be used to search online for the optimum oxygen excess ratio levels.
- The algebraic-observer-based output-feedback controller design will be integrated and evaluated in real fuel-cell system test bench.

Appendix A

PEMFC System Model Parameters

A.1 PEMFC steady-state model parameters

For the activation loss, the expressions of v_0 and v_a are expressed as follows [Pukrushpan et al., 2004c]:

$$\begin{aligned} v_0 &= 0.279 - 8.5 \times 10^{-4} \left(T_{fc} - 298.15\right) \\ &\quad + 1.308 \times 10^{-5} T_{fc} \left[ln\left(\frac{\chi}{1.01325}\right) + \frac{1}{2}\left(\frac{0.1173 \times \chi}{1.01325}\right)\right], \\ v_a &= \left(-1.618 \times 10^{-5} T_{fc} + 1.618 \times 10^{-2}\right)\left(\frac{x_1}{0.1173} + c_2\right)^2 \\ &\quad + \left(1.8 \times 10^{-4} T_{fc} + 0.166\right)\left(\frac{x_1}{0.1173} + c_2\right) + \left(-5.8 \times 10^{-4} T_{fc} + 0.5736\right) \end{aligned} \tag{A.1}$$

where $\chi = x_1 + x_2$ and $c_2 = p_{sat}\left(T_{fc}\right)$.

For the concentration loss, the expression of b_2 is given according to [Pukrushpan et al., 2004c] as follows:

$$b_2 = \begin{cases} \left(7.16 \times 10^{-4} T_{fc} - 0.622\right)\left(\frac{x_1}{0.1173} + c_2\right) \\ \qquad\qquad \left(+1.45 \times 10^{-3} T_{fc} + 1.68\right) \quad \text{for} \quad \left(\frac{x_1}{0.1173} + c_2\right) < 2\, atm \\ \left(8.66 \times 10^{-5} T_{fc} - 0.068\right)\left(\frac{x_1}{0.1173} + c_2\right) \\ \qquad\qquad \left(-1.6 \times 10^{-4} T_{fc} + 0.54\right) \quad \text{for} \quad \left(\frac{x_1}{0.1173} + c_2\right) \geq 2\, atm. \end{cases} \tag{A.2}$$

Table A.1: Steady-state model parameters

Parameter	**Description**	**Value**	**Unit**
R	Universal gas constant	8.3145	$\mathrm{J/(mol\,K)}$
F	Faraday number	96485	$\mathrm{C\,mol^{-1}}$
T_{fc}	Stack temperature	353.15	K
ΔG^0	Changes on the Gibbs free energy	-237.2	$\mathrm{kJ\ mol^{-1}}$
$\bar{\alpha}$	Change transfer coefficient	0.06	–
i_0	Exchange current density	$0.04\ \times 10^{-3}$	A
A_{fc}	Active-cell area	0.028	$\mathrm{mm^{-2}}$
t_m	Membrane thickness	$125{\times}10^{-6}$	$\mathrm{m^{-1}}$
λ_m	Membrane water content mass	14	–
b_1	Empirical constant for activation loss	10	–
b_3	Empirical constant for concentration loss	2	–
i_{max}	Maximal cell current density	2.2	A
n	Number of cells in fuel-cell stack	381	–

A.2 Dynamic model parameters

Table A.2: Constants of the PEMFC system model

Constants	
$c_1 = \frac{RT_{fc}k_{sm,out}}{M_{O_2}V_{ca}}\left(\frac{x_{O_2,atm}}{1+\omega_{atm}}\right)$	$c_{13} = \frac{\eta_{cm}k_t}{J_{cp}R_{cm}}$
$c_2 = p_{sat}$	$c_{14} = \frac{RT_{atm}\gamma}{M_{a,atm}V_{sm}}$
$c_3 = \frac{RT_{fc}}{V_{ca}}$	$c_{15} = \frac{1}{\eta_{cp}}$
$c_4 = M_{O_2}$	$c_{16} = k_{sm,out}$
$c_5 = M_{N_2}$	$c_{17} = \frac{C_D A_T}{\sqrt{RT_{fc}}}\sqrt{\frac{2\gamma}{\gamma-1}}$
$c_6 = M_v p_{sat}$	$c_{18} = \frac{1}{\gamma}$
$c_7 = \frac{RT_{fc}n}{2FV_{ca}}$	$c_{19} = \left(\frac{2}{\gamma+1}\right)^{\frac{\gamma}{\gamma-1}}$
$c_8 = \frac{RT_{fc}k_{sm,out}}{M_{N_2}V_{ca}}\left(\frac{1-x_{O_2,atm}}{1+\omega_{atm}}\right)$	$c_{20} = \frac{C_D A_T}{\sqrt{RT_{fc}}}\gamma^{0.5}\left(\frac{2}{\gamma+1}\right)^{\frac{\gamma+1}{2\gamma-2}}$
$c_9 = \frac{\eta_{cm}k_t k_v}{J_{cp}R_{cm}}$	$c_{21} = \frac{1}{R_{cm}}$
$c_{10} = \frac{C_p T_{atm}}{J_{cp}\eta_{cp}}$	$c_{22} = k_v$
$c_{11} = p_{atm}$	$c_{23} = k_{sm,out}\left(\frac{x_{O_2,atm}}{1+\omega_{atm}}\right)$
$c_{12} = \frac{\gamma-1}{\gamma}$	$c_{24} = \frac{nM_{O_2}}{2F}$

Table A.3: Dynamic model parameters

Parameter	Description	Value	Unit
η_{cp}	Motor mechanical efficiency	0.98	%
η_{cm}	Compressor efficiency	0.8	%
J_{cp}	Compressor inertia	5×10^{-5}	$\mathrm{kg\,m^2}$
R_{cm}	Compressor motor resistance	0.82	Ω
k_t	Motor parameter	0.0153	$(\mathrm{N\,m})/\mathrm{A}$
k_v	Motor parameter	0.0153	$\mathrm{V}/(\mathrm{rad/s})$
$M_{a,atm}$	Air molar mass	29×10^{-3}	$\mathrm{kg\,mol^{-1}}$
M_{O_2}	Oxygen molar mass	32×10^{-3}	$\mathrm{kg\,mol^{-1}}$
M_{N_2}	Nitrogen molar mass	28×10^{-3}	$\mathrm{kg\,mol^{-1}}$
M_v	Vapor molar mass	18×10^{-3}	$\mathrm{kg\,mol^{-1}}$
$y_{O_2,atm}$	Oxygen mole fraction	0.21	–
V_{ca}	Cathode volume	0.01	$\mathrm{m^3}$
$k_{sm,out}$	Supply manifold outlet orifice constant	0.3629×10^{-5}	$\mathrm{kg}/(\mathrm{s\,Pa})$
V_{sm}	Supply manifold volume	0.02	$\mathrm{m^3}$
T_{fc}	Fuel-cell temperature	353.15	K
T_{atm}	Atmospheric temperature	298.15	K
p_{atm}	Atmospheric pressure	101325	Pa
$p_{sat}(T_{fc})$	Saturation pressure at stack temperature	42666	Pa
$p_{sat}(T_{atm})$	Saturation pressure at atmospheric temperature	2811.9	Pa
C_p	Constant pressure Specific heat of air	1004	$\mathrm{J}/(\mathrm{mol\,K})$
C_D	Cathode outlet throttle discharge coefficient	0.0124	–
γ	Ratio of specific heat of air	1.4	–
A_T	Cathode outlet throttle area	0.002	$\mathrm{m^2}$
ϕ_{atm}	Average ambient air relative humidity	0.5	–

References

[Almeida and Simoes, 2005] Almeida, P. and Simoes, M. (2005). Neural optimal control of PEM fuel cells with parametric CMAC networks. *IEEE Transactions on Industry Applications*, 41(1), pp 237–245.

[Amphlett et al., 1995] Amphlett, J. C., Baumert, R. M., Mann, R. F., Peppley, B. A., Roberge, P. R., and Harris, T. J. (1995). Performance modeling of the ballard mark IV solid polymer electrolyte fuel cell i. mechanistic model development. *Journal of the Electrochemical Society*, 142(1), pp 1–8.

[Andrew, 1996] Andrew, L. (1996). Hydrogen generation from natural gas for the fuel cell systems of tomorrow. *Journal of Power Sources*, 61(1), pp 113 – 124.

[Ang et al., 2005] Ang, K., Chong, G., and Li, Y. (2005). PID control system analysis, design, and technology. *IEEE Transactions on Control Systems Technology*, 13(4), pp 559–576.

[Asif et al., 2002] Asif, Š., Karel, J., and Nadira, Š. (2002). *Sliding Modes Applications in Power Electronics and Electrical Drives*. Springer Berlin Heidelberg, Berlin, Heidelberg.

[Azar and Zhu, 2016] Azar, A. and Zhu, Q. (2016). *Advances and applications in sliding mode control systems*. Springer.

[Bagotsky, 2012] Bagotsky, V. (2012). *Fuel Cells: Problems and Solutions*. Electrochemical Society series. Wiley. `https://books.google.dz/books?id=ijSlsr7BN94C`.

[Barbir, 2012] Barbir, F. (2012). *PEM fuel cells: theory and practice*. Academic Press.

[Baroud and Benalia, 2014] Baroud, Z. and Benalia, A. (2014). Steady-State Modeling and Performance Analysis of PEM Fuel Cell. In *The First Day of Automatic Theory and its Applications (JEAA)*, pages 1–6, Laghouat, Algeria.

[Baroud et al., 2016a] Baroud, Z., Benalia, A., and Ocampo-Martinez, C. (2016a). Air flow regulation in fuel cells: An efficient design of hybrid fuzzy-PID control. *Electrotehnica, Electronica, Automatica (EEA)*, 64(4), pp 28 – 32.

[Baroud et al., 2017a] Baroud, Z., Benalia, A., and Ocampo-Martinez, C. (2017a). Nonlinear observer design for PEM Fuel-Cell Systems using First-Order Sliding Mode Techniques. In *2nd International Conference on Automatic Control, Telecommunications and Signals (ICATS 2017)*, pages 1–6, Annaba, Algeria. `http://www.iri.upc.edu/download/scidoc/1929`.

[Baroud et al., 2015] Baroud, Z., Benmiloud, M., and Benalia, A. (2015). Fuzzy self-tuning PID controller for air supply on a PEM fuel cell system. In *4th International Conference on Electrical Engineering (ICEE)*, pages 1–4.

[Baroud et al., 2017b] Baroud, Z., Benmiloud, M., Benalia, A., and Ocampo-Martinez, C. (2017b). Novel hybrid fuzzy-PID control scheme for air supply in PEM fuel-cell-based systems. *International journal of hydrogen energy*, 42(15), pp 10435–10447.

[Baroud et al., 2016b] Baroud, Z., Gazzam, N., Benalia, A., and Ocampo-Martinez, C. (2016b). Algebraic observer design for PEM fuel cell system. In *Modelling, Identification and Control (ICMIC), 2016 8th International Conference on*, pages 966–970, Algiers, Algeria. IEEE.

[Basualdo et al., 2012] Basualdo, M., Feroldi, D., and Outbib, R. (2012). *PEM fuel cells with bio-ethanol processor systems*, volume 10. Springer.

[Beirami et al., 2015] Beirami, H., Shabestari, A., and Zerafat, M. (2015). Optimal PID plus fuzzy controller design for a PEM fuel cell air feed system using the self-adaptive differential evolution algorithm. *International Journal of Hydrogen Energy*, 40(30), pp 9422 – 9434.

[Bessarabov, 2011] Bessarabov, D. (2011). Gas permeability of proton–exchange–membranes. *PEM Fuel Cell Diagnostic Tools*, pages 443–473.

[Bianchi et al., 2014] Bianchi, F., Kunusch, C., Ocampo-Martinez, C., and Sánchez-Peña, R. (2014). A gain-scheduled LPV control for oxygen stoichiometry regulation in PEM fuel cell systems. *IEEE Transactions on Control Systems Technology*, 22(5), pp 1837–1844.

[Bianchi et al., 2015] Bianchi, F., Kunusch, C., Ocampo-Martinez, C., and Sánchez-Peña, R. (2015). Fault-tolerant unfalsified control for PEM fuel cell systems. *IEEE Transactions on Energy Conversion*, 30(1), pp 307–315.

[Bouallègue et al., 2015] Bouallègue, S., Toumi, F., Haggège, J., and Siarry, P. (2015). Advanced metaheuristics-based approach for fuzzy control systems tuning. In Quanmin, Z. and Ahmad, A., editors, *Complex System Modelling and Control Through Intelligent Soft Computations*, pages 627–653. Springer International Publishing.

[Chang and Moura, 2009] Chang, Y. and Moura, S. (2009). Air flow control in fuel cell systems: An extremum seeking approach. In *American Control Conference*, pages 1052–1059.

[Ehsani et al., 2017] Ehsani, M., Gao, Y., and Emadi, A. (2017). *Modern electric, hybrid electric, and fuel cell vehicles: fundamentals, theory, and design*. CRC press.

[Fereidouni et al., 2015] Fereidouni, A., Masoum, M., and Moghbel, M. (2015). A new adaptive configuration of PID type fuzzy logic controller. *ISA transactions*, 56, pp 222–240.

[Fergus et al., 2016] Fergus, J., Hui, R., Li, X., Wilkinson, D. P., and Zhang, J. (2016). *Solid oxide fuel cells: materials properties and performance*. CRC press.

[Fliess and Sira-Ramirez, 2004] Fliess, M. and Sira-Ramirez, H. J. (2004). Control via state estimations of some nonlinear systems. In *IFAC Symposium on Nonlinear Control Systems (NOLCOS)*, pages 1121–1126, Stuttgart, Germany.

[Fuel Cell Norway ANS., 2006] Fuel Cell Norway ANS. (2006). The History of Fuel Cells. `http://www.fuelcell.no/principle_history_eng.htm`.

[FuelCellToday., 2017a] FuelCellToday. (2017a). History. `http://www.fuelcelltoday.com/history`.

[FuelCellToday., 2017b] FuelCellToday. (2017b). Stationary. `http://www.fuelcelltoday.com/applications/stationary`.

[Gold, 2017] Gold, S. (2017). Low-temperature fuel cell technology for green energy. In *Handbook of Climate Change Mitigation*, pages 1657–1702. Springer.

[Görgün et al., 2006] Görgün, H., Arcak, M., and Barbir, F. (2006). An algorithm for estimation of membrane water content in PEM fuel cells. *Journal of power sources*, 157(1), pp 389–394.

[Gruber et al., 2008] Gruber, J., Bordons, C., and Dorado, F. (2008). Nonlinear control of the air feed of a fuel cell. In *American Control Conference*, pages 1121–1126.

[Haddad, 2009] Haddad, A. (2009). *Modèle dynamique non linèaire de la pile à combustible du type PEM: application à la régulation de l'humidité dans la membrane électrolytique*. PhD thesis, Sciences de l'ingénieur Belfort-Montbéliard 2009. `http://www.theses.fr/2009BELF0111/document`.

[Jurado, 2004] Jurado, F. (2004). Modeling SOFC plants on the distribution system using identification algorithms. *Journal of power sources*, 129(2), pp 205–215.

[Kang, 2015] Kang, S. (2015). Quasi-three dimensional dynamic modeling of a proton exchange membrane fuel cell with consideration of two-phase water transport through a gas diffusion layer. *Energy*, 90, pp 1388–1400.

[Kim, 2012] Kim, E. (2012). Observer based nonlinear state feedback control of PEM fuel cell systems. *Journal of Electrical Engineering & Technology*, 7(6), pp 891–897.

[Kunusch et al., 2013] Kunusch, C., Moreno, J. A., and Angulo, M. T. (2013). Identification and observation in the anode line of PEM fuel cell stacks. In *Decision and Control (CDC), 2013 IEEE 52nd Annual Conference on*, pages 1665–1670, Firenze, Italy. IEEE.

[Kunusch et al., 2012] Kunusch, C., Puleston, P., and Mayosky, M. (2012). *Sliding-Mode control of PEM fuel cells*. Springer Science & Business Media.

[Kunusch et al., 2009] Kunusch, C., Puleston, P., Mayosky, M., and Riera, J. (2009). Sliding mode strategy for PEM fuel cells stacks breathing control using a super-twisting algorithm. *IEEE Transactions on Control Systems Technology*, 17(1), pp 167–174.

[Lachaize, 2004] Lachaize, J. (2004). *Étude des stratégies et des structures de commande pour le pilotage des systèmes énergétiques à Pile à Combustible (PAC) destinés à la traction*. PhD thesis, Systèmes automatiques Toulouse, INPT. `http://www.theses.fr/2004INPT028H/document`.

[Laghrouche et al., 2013] Laghrouche, S., Matraji, I., Ahmed, F., Jemei, S., and Wack, M. (2013). Load governor based on constrained extremum seeking for PEM fuel cell oxygen starvation and compressor surge protection. *International Journal of Hydrogen Energy*, 38(33), pp 14314–14322.

[Larminie et al., 2003] Larminie, J., Dicks, A., and McDonald, M. (2003). *Fuel cell systems explained*, volume 2. Wiley New York.

[Liu, 2014] Liu, J. (2014). *Contributions to Adaptative Higher Order Sliding Mode Observers : Application to Fuel Cell an Power Converters.* PhD thesis, Université de Technologie de Belfort-Montbeliard. `https://tel.archives-ouvertes.fr/tel-01488404/file/These_LIU_Jianxing_UTBM.pdf`.

[Liu et al., 2014] Liu, J., Laghrouche, S., Ahmed, Z., and Wack, M. (2014). PEM fuel cell air-feed system observer design for automotive applications: An adaptive numerical differentiation approach. *International Journal of Hydrogen Energy*, 39(30), pp 17210–17221.

[Liu et al., 2015] Liu, J., Lin, W., Laghrouche, S., Alsaadi, F., and Hayat, T. (2015). Nonlinear observer design for PEM fuel cell power systems via second order sliding mode technique. *Neurocomputing*, 168, pp 145–151.

[Liu, 2005] Liu, T. (2005). *Pressure-and Temperature-Sensitive Paints.* Wiley Online Library.

[Liu et al., 2006] Liu, Z., Mao, Z., Wang, C., Zhuge, W., and Zhang, Y. (2006). Numerical simulation of a mini PEMFC stack. *Journal of Power Sources*, 160(2), pp 1111 – 1121.

[Maldonado, 2012] Maldonado, S. (2012). *Experimental characterization of water sorption and transport properties of polymer electrolyte membranes for fuel cells.* PhD thesis, Mécanique et énergtique Université de Lorraine. `http://www.theses.fr/2012LORR0146/document`.

[Mamdani, 1974] Mamdani, E. (1974). Application of fuzzy algorithms for control of simple dynamic plant. *Proceedings of the Institute of Electrical Engineers*, 121, pp 1585–1588(3).

[Mann et al., 2000] Mann, R. F., Amphlett, J. C., Hooper, M. A., Jensen, H. M., Peppley, B. A., and Roberge, P. R. (2000). Development and application of a generalised steady-

state electrochemical model for a pem fuel cell. *Journal of power sources*, 86(1-2), pp 173–180.

[Matraji, 2013] Matraji, I. (2013). *Contribution à la commande non linéaire robuste des systèmes d'alimentation en air des piles à combustible de type PEM*. PhD thesis, Université de Technologie de Belfort-Montbeliard.

[Matraji et al., 2013] Matraji, I., Laghrouche, S., Jemei, S., and Wack, M. (2013). Robust control of the PEM fuel cell air-feed system via sub-optimal second order sliding mode. *Applied Energy*, 104, pp 945–957.

[Mboup et al., 2007] Mboup, M., Join, C., and Fliess, M. (2007). A revised look at numerical differentiation with an application to nonlinear feedback control. In *15th Mediterrean Conference on Control and Automation-MED*, pages 1–6, Greece.

[Meyers and Darling, 2006] Meyers, J. P. and Darling, R. M. (2006). Model of carbon corrosion in pem fuel cells. *Journal of the Electrochemical Society*, 153(8), pp A1432–A1442.

[Niknezhadi et al., 2011] Niknezhadi, A., Allué-Fantova, M., Kunusch, C., and Ocampo-Martínez, C. (2011). Design and implementation of LQR/LQG strategies for oxygen stoichiometry control in PEM fuel cells based systems. *Journal of Power Sources*, 196(9), pp 4277–4282.

[O'Dwyer, 2009] O'Dwyer, A. (2009). *Handbook of PI and PID controller tuning rules*, volume 57. World Scientific.

[O'hayre et al., 2016] O'hayre, R., Cha, S. W., Prinz, F. B., and Colella, W. (2016). *Fuel cell fundamentals*. John Wiley & Sons.

[Ou et al., 2015] Ou, K., Wang, Y., Li, Z., Shen, Y., and Xuan, D. (2015). Feedforward fuzzy-PID control for air flow regulation of PEM fuel cell system. *International Journal of Hydrogen Energy*, 40(35), pp 11686 – 11695.

[Pathapati et al., 2005] Pathapati, P., Xue, X., and Tang, J. (2005). A new dynamic model for predicting transient phenomena in a PEM fuel cell system. *Renewable energy*, 30(1), pp 1–22.

[Pilloni et al., 2015] Pilloni, A., Pisano, A., and Usai, E. (2015). Observer-based air excess ratio control of a PEM fuel cell system via high-order sliding mode. *IEEE Transactions on Industrial Electronics*, 62(8), pp 5236–5246.

[Pukrushpan et al., 2002a] Pukrushpan, J., Peng, H., and Stefanopoulou, A. (2002a). Simulation and analysis of transient fuel cell system performance based on a dynamic reactant flow model. In *ASME 2002 International Mechanical Engineering Congress and Exposition*, pages 637–648, New Orleans, Louisiana, USA. American Society of Mechanical Engineers.

[Pukrushpan et al., 2004a] Pukrushpan, J., Peng, H., and Stefanopoulou, A. (2004a). Control-oriented modeling and analysis for automotive fuel cell systems. *Journal of dynamic systems, measurement, and control*, 126(1), pp 14–25.

[Pukrushpan et al., 2002b] Pukrushpan, J., Stefanopoulou, A., and Peng, H. (2002b). Modeling and control for PEM fuel cell stack system. In *American Control Conference, 2002. Proceedings of the 2002*, volume 4, pages 3117–3122. IEEE.

[Pukrushpan et al., 2004b] Pukrushpan, J., Stefanopoulou, A., and Peng, H. (2004b). Control of fuel cell breathing. *IEEE Control Systems*, 24(2), pp 30–46.

[Pukrushpan et al., 2004c] Pukrushpan, J., Stefanopoulou, A., and Peng, H. (2004c). *Control of fuel cell power systems: principles, modeling, analysis and feedback design*. Springer Science & Business Media.

[Pukrushpan et al., 2005] Pukrushpan, J. T., Stefanopoulou, A. G., Varigonda, S., Pedersen, L. M., Ghosh, S., and Peng, H. (2005). Control of natural gas catalytic partial oxidation for hydrogen generation in fuel cell applications. *IEEE Transactions on Control Systems Technology*, 13(1), pp 3–14.

[Qi et al., 2005] Qi, Y., Huang, B., and Chuang, K. (2005). Dynamic modeling of solid oxide fuel cell: The effect of diffusion and inherent impedance. *Journal of Power Sources*, 150, pp 32–47.

[Rabbani, 2013] Rabbani, R. (2013). *Dynamic Performance of a PEM Fuel Cell System*. PhD thesis, DTU Mechanical Engineering. `http://orbit.dtu.dk/files/72795006/Dynamic_Performance_of_a_PEM_Fuel.pdf`.

[Rakhtala et al., 2014] Rakhtala, S., Noei, A., Ghader, R., and Usai, E. (2014). Design of finite-time high-order sliding mode state observer: A practical insight to PEM fuel cell system. *Journal of Process Control*, 24(1), pp 203–224.

[Santarelli and Torchio, 2007] Santarelli, M. G. and Torchio, M. F. (2007). Experimental analysis of the effects of the operating variables on the performance of a single pemfc. *Energy Conversion and Management*, 48(1), pp 40–51.

[Sheila, 2012] Sheila, S. (2012). *Model-based design and operation of fuel cell systems*. PhD thesis, University College London. `http://discovery.ucl.ac.uk/1344169/1/1344169.pdf`.

[Shtessel et al., 2014] Shtessel, Y., Edwards, C., Fridman, L., and Levant, A. (2014). *Sliding mode control and observation*, volume 10. Springer.

[Sinthipsomboon et al., 2012] Sinthipsomboon, K., Hunsacharoonroj, I., Khedari, J., Pratumsuwan, P., and Pongaen, W. (2012). A hybrid of fuzzy and fuzzy self-tuning pid controller for servo electro-hydraulic system.

[Spiegel, 2011] Spiegel, C. (2011). *PEM fuel cell modeling and simulation using MATLAB*. Academic press.

[Spiegel, 2017] Spiegel, C. (2017). Introduction to Fuel Cell Applications. `http://www.fuelcellstore.com/blog-section/intro-fuel-cell-applications`.

[Steele and Heinzel, 2011] Steele, B. C. and Heinzel, A. (2011). Materials for fuel-cell technologies. In *Materials For Sustainable Energy: A Collection of Peer-Reviewed Research and Review Articles from Nature Publishing Group*, pages 224–231. World Scientific.

[Suh, 2006] Suh, K. (2006). *Modeling, analysis and control of fuel cell hybrid power systems*. PhD thesis, Department of Mechanical Engineering, The University of Michigan. `https://books.google.dz/books?id=ijSlsr7BN94C`.

[Töpler and Lehmann, 2015] Töpler, J. and Lehmann, J. (2015). *Hydrogen and Fuel Cell: Technologies and Market Perspectives*. Springer Berlin Heidelberg. `https://books.google.dz/books?id=OFO-CwAAQBAJ`.

[UniversityofCambridge., 2018] UniversityofCambridge. (2018). History of the technology. `https://www.doitpoms.ac.uk/tlplib/fuel-cells/history.php`.

[Utkin et al., 2017] Utkin, V., Guldner, J., and Shi, J. (2017). *Sliding mode control in electro-mechanical systems*. CRC press.

[Vepa, 2012] Vepa, R. (2012). Adaptive state estimation of a PEM fuel cell. *IEEE Transactions on Energy Conversion*, 27(2), pp 457–467.

[Vielstich et al., 2009] Vielstich, W., Lamm, A., and Gasteiger, H. (2009). *Handbook of fuel cells: fundamentals, technology, and applications*, volume 2. John Wiley & Sons.

[Yerramalla et al., 2003] Yerramalla, S., Davari, A., Feliachi, A., and Biswas, T. (2003). Modeling and simulation of the dynamic behavior of a polymer electrolyte membrane fuel cell. *Journal of power sources*, 124(1), pp 104–113.

[Zadeh, 1965] Zadeh, L. (1965). Fuzzy sets. *Information and Control*, 8(3), pp 338 – 353.

[Zimmermann, 2001] Zimmermann, H. (2001). *Fuzzy set theory and its applications*. Springer Science & Business Media.

[Zulfatman and Rahmat, 2009] Zulfatman, L. and Rahmat, M. (2009). Application of self-tuning fuzzy PID controller on industrial hydraulic actuator using system identification approach. *International Journal on Smart Sensing and Intelligent Systems*, 2(2), pp 246–261.